Indole-3-carbinol modulates microglia homeostasis and prevents light-induced retinal degeneration

I n a u g u r a l – D i s s e r t a t i o n

Zur

Erlangung des Doktorgrades

der Mathematisch-Naturwissenschaftlichen Fakultät

der Universität zu Köln

vorgelegt von

Amir Saeed Khan

Aus Sheikhupura, Pakistan

Köln 2020

Berichterstatter/in: **Prof. Dr. Thomas Langmann**

Prof. Dr. Elena Rugarli

Tag der mündlichen Prüfung: 22.01.2021

For my dear mother

“To be a good experimenter you must have patience towards things, which are not always in your control.”

Nobel laureate Abdus Slam

Table of Contents

Summary

Age-related macular degeneration (AMD) is a retinal degenerative disease and the most common cause of blindness in the elderly. Microglia activation is a hallmark of neurodegenerative diseases including AMD. Pharmacological approaches of microglia-related immunomodulation emerge as a therapeutic option. Aryl hydrocarbon receptor (AhR) plays a significant role in the physiological and pathological mechanisms involved in ocular compartment and AhR is expressed by various immune cells including microglia. Retina-specific AhR knockout mice have been shown to enhance retinal degeneration and dry AMD-like phenotype. Indole-3-carbinol (I3C) is a natural ligand of AhR with potent immunomodulatory properties. Here, we hypothesized that I3C may inhibit microglia reactivity and exert neuroprotective effects in the light damaged murine retina mimicking important immunological aspects of AMD.

The in vitro data showed that I3C significantly reduced LPS-induced pro-inflammatory gene expression of *i-NOS*, *IL-1ß*, *NLRP3*, *IL-6*, and *CCL2* and induced anti-oxidants gene levels of *NQO1*, *HMOX1*, and *CAT1* in BV-2 cells. I3C also reduced LPS-induced i-NOS, IL-1ß, COX2, and P-ERK1/2 protein levels and induced HMOX1 protein in BV-2 cells. Furthermore, I3C also reduced LPS-induced NO secretion, phagocytosis, migration, and enhanced protective phenotype as important functional microglia parameters. siRNA-mediated knockdown of *AhR* partially prevented the previously observed gene regulatory effects in BV-2 microglia cells. I3C reduced PMA plus Zymosan-induced pro-inflammatory gene expression of *IL-1ß*, *NLRP3*, and *IL-6* and enhanced *NQO1*, *HMOX1*, and *CAT1* gene levels in SV-40 cells. Furthermore, I3C reduced microglia-mediated neurotoxic effects in ARPE-19 cells. I3C also reduced LPS-induced pro-inflammatory genes in primary microglia cells and retinal explants. The in vivo experiments showed that I3C treatment significantly diminished light-damage induced *i-NOS*, *IL-1ß*, *NLRP3*, *IL-6*, and *CCL2* gene levels and reduced CCL2, i-NOS, IL-1ß, p-NFkBp65 protein levels in mice. Moreover, I3C increased anti-oxidant NQO1 and HMOX1 protein levels in light exposed retinas. Finally, I3C therapy prevented the accumulation of amoeboid microglia in the sub-retinal space and protected from retinal degeneration. Taken together, the AhR ligand I3C potently reduces microgliosis and light-induced retinal damage, highlighting a potential treatment concept for retinal degeneration in AMD.

Zusammenfassung

Die altersbedingte Makuladegeneration (AMD) ist eine degenerative Netzhauterkrankung und einer der häufigsten Ursachen für Blindheit bei älteren Menschen. Die Aktivierung von Mikrogliazellen ist ein Kennzeichen für neurodegenerative Erkrankungen einschließlich AMD. Immonomudulation durch Einwirkung auf Mikrogliazellen erwiesen sich als vielversprechende therapeutische Option. AhR spielen innerhalb physiologischer und pathologischer Mechanismen des Auges eine bedeutsame Rolle und werden zudem von verschiedenen Immunzellen einschließlich Mikrogliazellen exprimiert. Es wurde nachgewiesen, dass Retina-spezifische AhR-Knockout-Mäuse unter Netzhautdegeneration und den trockenen AMD-ähnlichen Phänotyp leiden. Indole-3-carbinol (I3C) ist ein natürlicher Ligand des AhR mit starken immunmodulatorischen Eigenschaften. Hier stellten wir die Hypothese auf, dass I3C die Mikroglia-Reaktivität hemmt und neuroprotektive Effekte im Mausmodel der lichtinduzierten Netzhautdegeneration ausübt. Die In-vitro-Daten zeigten, dass I3C die LPS-induzierte proinflammatorische Genexpression von *i-NOS*, *IL-1ß*, *NLRP3*, *IL-6*, und *CCL2* signifikant reduziert und gleichermaßen die Genexpression von antioxidativen *NQO1*, *HMOX1* und *CAT1* in BV-2-Mikroglia-Zellkulturen induziert. I3C reduzierte auch die LPS-induzierten Proteinlevel von i-NOS, IL-1ß, COX2, und P-ERK1/2 und induzierte das HMOX1-Protein in BV-2-Zellen. Darüber hinaus reduzierte I3C auch die LPS-induzierte Stickoxid-Sekretion, Phagozytose und Mikrogliazellen-Zellmigration und induzierte den schützenden Microglia-zellphänotypen, welche wichtige funktionelle Parameter darstellen. siRNA-vermittelter Knockdown von *AhR* verhinderte teilweise die zuvor beobachteten genregulatorischen Effekte welche BV-2-Mikroglia-Zellkulturen observiert wurden. I3C reduzierte die PMA plus Zymosan-induzierte proinflammatorische Genexpression von *IL-1ß*, *NLRP3* und *IL-6* und erhöhte die Genexpression von *NQO1*, *HMOX1* und *CAT1* in humanen SV-40-Mikrogliazellen. Darüber hinaus reduzierte I3C die durch Mikroglia-vermittelten neurotoxischen Wirkungen auf ARPE-19-Zellen. I3C reduzierte ebenfalls die LPS-induzierte proinflammatorische Genexpression in primären Mikroglia-Zellen und Netzhautexplantaten. In-vivo-Experimente zeigten, dass die I3C-Behandlung die, durch Lichtschäden in Mäuseretina induzierten, *i-NOS*, *IL-1ß*, *NLRP3*, *IL-6*, und *CCL2* Genlevel signifikant verringerte und die Proteinlevel von CCL2, i-NOS, IL-1ß, und p-NFkBp65 in verringerte. Darüber hinaus erhöhte I3C die Proteinlevel von antioxidativen NQO1 und HMOX1 in lichtexponierten Netzhäuten. Schlussendlich

verhinderte die I3C-Therapie die Ansammlung von amöboidalen Mikroglia im subretinalen Raum und schützte die Retina vor Netzhautdegeneration. Zusammengenommen reduziert der AhR-Ligand I3C äußerst wirksam die Mikrogliose und lichtinduzierte Netzhautschäden und zeigt ein mögliches Behandlungskonzept für die Netzhautdegeneration bei AMD auf.

List of Figures

List of Tables

List of Abbreviations

AhR	Aryl hydrocarbon receptor
AhRR	Aryl hydrocarbon receptor repressor
AMD	Age-related macular degeneration
ANOVA	Analysis of variance
ARNT	Aryl hydrocarbon receptor nuclear translocator
BDNF	Brain derived neurotrophic factor
BRB	Blood retinal barrier
BM	Bruch's membrane
CAT1	Catalase1
CCL2	Chemokine (C-C motif) ligand 2
cDNA	Complementary DNA
CNS	Central nervous system
CNV	Choroidal neovascularization
COX2	Cyclooxygenase2
CSF1R	Colony stimulating factor-1 receptor
CX3CR1	C-X3-C motif chemokine receptor 1
DIM	3,3′-Diindolylmethane
DMEM	Dulbecco’s modified eagle’s medium
DNA	Deoxyribonucleic acid
DER	Dioxin response elements
EAE	Experimental autoimmune encephalomyelitis
ERK1	Extracellular signal regulated protein kinase
GA	Geographic atrophy
GCL	Ganglion cell layer
GDNF	Glial cell-line derived neurotrophic factor
HMOX1	Heme oxygenase 1
IBA 1	Ionized calcium-binding adapter molecule 1
IL-1β	Interleukin-1β
IL-6	Interleukin-6
INL	Inner nuclear layer
IPL	Inner plexiform layer
IRF8	Interferon regulatory factor 8

IS	Inner segment
I3C	Indole-3-carbinol
i-NOS	Inducible nitric oxide synthase
kDa	Kilo Dalton
LPS	Lipopolysaccharide
MAPK	mitogen-activated protein kinase
NF-κB	Nuclear factor kappa-light-chain-enhancer of B cells
NQO1	NAD(P)H dehydrogenase [quinone] 1
NLRP3	NLR family pyrin domain containing 3
NO	Nitric oxide
ONL	Outer nuclear layer
OPL	Outer plexiform layer
OS	Outer segment
PMA	Phorbol 12-myristate 13-acetate
qRT-PCR	Quantitative real time polymerase chain reaction
RGC	Retinal ganglion cells
RPE	Retinal pigment epithelium
RNA	Ribonucleic acid
SD-OCT	Spectral domain-optical coherence tomography
SEM	Standard error of the mean
SOCS	Suppressor of cytokine signaling
TBE	Tris/Borate/EDTA
TBS	Tris buffers saline
TLR	Toll-like receptor
TRITC	Tetramethylrhodamine
RPMI	Roswell Park Memorial Institute
siRNA	Small interfering RNA
TED	Thyroid eye disease
XRE	Xenobiotic response elements

1 Introduction

1.1. The retina

The eye is a photo-sensory organ in the body, which transmits visual information to its receptive tissue known as the retina (Lamb et al., 2007; Lamb, 2013). The retina is a concave hemispherical sheet, which is around 200 µM in thickness and resides in the posterior part of the eye (Figure.1A). It is an important part of the central nervous system and shares many similarities with the brain (Erskine and Herreral, 2015). The retina permits the perception of colors and shapes via complex molecular signaling pathways, which are further amplified and transmitted to the midbrain and thalamus via the optic nerve (Sung and Chuang, 2010). The retina is a highly conserved photo-sensory tissue, which is organized into different cell layers with more than 60 heterogeneous cell types (Masland, 2001, 2012). These distinct circuits work together and produce morphologically and functionally different pathways to encode visual information (Hoon et al., 2014). The retinal cell types are highly organized into different layers (Figure. 1B). The major cell layers are the ganglion cell layer (GCL), the inner nuclear layer (INL), and the outer nuclear layer (ONL). The retinal ganglion layer (RGL) is the innermost layer of the retina with retinal ganglion cells (RGC) and this layer is present near to the vitreous humor of the eye. The INL comprises the nuclei of horizontal, bipolar, and most amacrine cells, whereas the ONL comprises of photoreceptor nuclei. The outer plexiform layer (OPL) divides ONL and INL, whereas the inner plexiform layer (IPL) divides the INL and GCL (Lee et al., 2010).

Retinal photoreceptor cells have two basic subtypes known as rods and cones. These cells have a unique morphology with an outer segment (OS), a connecting cilium, the inner segment (IS), the nucleus, the axon, and the synaptic terminal (Brzezinski and Reh, 2015). Rods are extremely sensitive photoreceptor and responsible for the detection of low and dim light. Rods are capable of even detecting a single photon. Cones are less sensitive and responsible for the detection of bright light (Molday and Moritz, 2015). Furthermore, neural retina is replenished with blood by retinal blood vessels and endothelial tight junctions control transport across these vessels. These tight junctions are part of the inner blood-retinal barrier (Ambati et al., 2013). The outer segments of photoreceptor cells are adjacent to retinal pigment epithelium (RPE) which is a highly organized monolayer of hexagonal cells overlying to the photoreceptors. The RPE is responsible for the transepithelial transport, phagocytosis of photoreceptors OS, absorption of light, and protection against photo-oxidation

(Alexander et al., 2015). The RPE cells are equipped with tight junctions and maintain the integrity of the retina (Obert et al., 2017).

Posterior to RPE is a thick Bruch's membrane (BM) that comprises of a collagenous extracellular matrix. RPE and BM form the outer blood-retinal barrier, which blocks the entry of macromolecules and immune cells from the choroid (Bhutto and Lutty, 2012). The choroid is located behind to the BM and comprises of blood vessels known as choriocapillaris that provide the nutrients and oxygen to the RPE, outer retina, and optic nerve (Ambati et al., 2013).

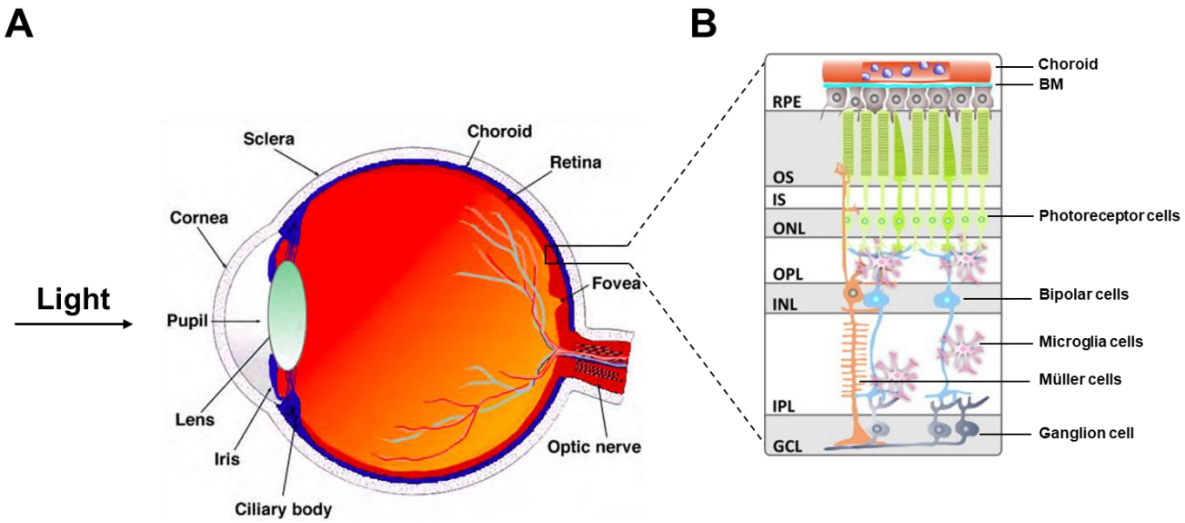

Figure 1 Schematic overview of the human eye and structure of the retina.
(A) Human eye with its major anatomical structures and light sensitive retina, which lies in the posterior part of the eye. **(B)** Different retinal layers and cell types present in the retina. The cells are arranged and distributed in different layers: GCL: ganglion cell layer, IPL: inner plexiform layer, INL: inner nuclear layer, OPL: outer plexiform layer, ONL: outer nuclear layer, IS: inner segment, and OS: outer segment. Retinal cells include ganglion cells (gray), Müller cells (orange), microglia cells (pink), bipolar cells (blue), and photoreceptor cells (green). Figures are modified from Karlstetter et al and Toomey et al. (Karlstetter et al., 2015; Toomey et al., 2018).

In the eye, light passes through the cornea, which refracts the light. The lens is present behind the cornea and responsible for the inverting images top to bottom and right to left. Both cornea and lens are important for light transmission. Light passes through different retinal layers and is absorbed by the OS of the photoreceptor cells (Erskine and Herreral, 2015). Rod cells are responsible for scotopic vision, whereas cone cells are responsible for photopic vision (Zele and Cao, 2015). Cone cells are abundantly present in the macula. There are three different types of cone cells: S-cones, M-cones

and L-cones, which are sensitive to short-wavelength (437nm for blue color), medium-wavelength (533nm for green color) and longer wavelength (564nm for red color) of light (Wässle, 2004). Encoded visual information is incorporated into different layers of the retina before its transmission to the brain (Masland, 2011). The RPE is responsible for absorption of light and inhibits the light to backscatter in the retina. It is noteworthy that connectivity of retinal cells is well defined and intercellular communication is important to maintain homeostasis (Hoon et al., 2014).

1.2. Age-related macular degeneration

Age-related macular degeneration (AMD) is an age dependent chronic degeneration of the central retina and is one of the leading causes of blindness in the Western society. It is estimated that there are around 196 million patients with AMD in 2020, which is expected to increase to 288 million in 2040 (Wong et al., 2014). The macula is the most affected part of the retina in AMD (Ambati and Fowler, 2012). Other cells and tissues affected with AMD include photoreceptors, RPE, BM, and blood supply to the eye (choriocapillaris and choroidal endothelial cells) (Malek and Lad, 2014). Patients with AMD are classified into 2 groups, early or intermediate AMD and late AMD is categorized as either geographic atrophy (GA) which is also known as dry AMD or neovascular (exudative) which is also known as wet AMD (Figure. 2) (Ramkumar et al., 2010; García-Layana et al., 2017).

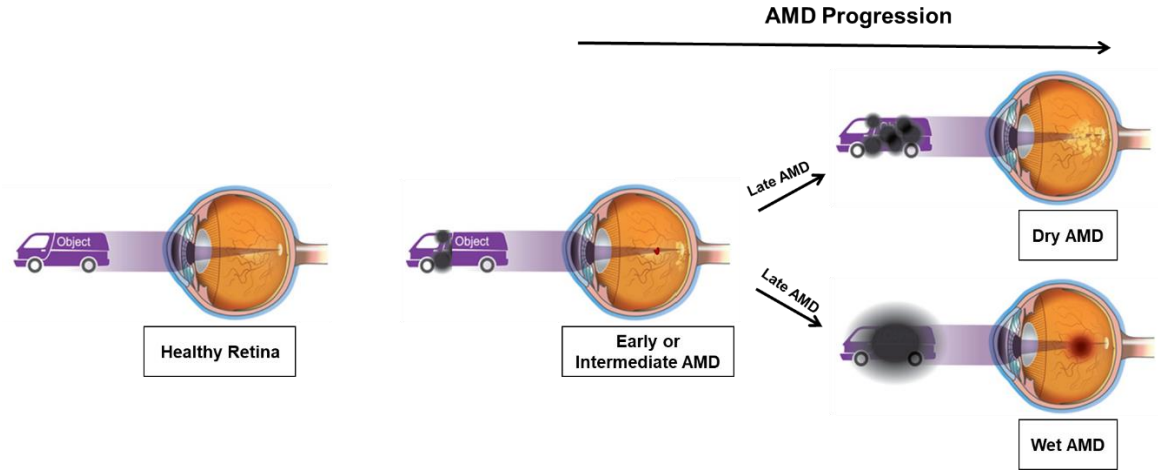

Figure 2 Symptoms and progression of AMD.
Individuals with healthy retina can clearly visualize the full object, whereas individuals with early or intermediate AMD partially visualize the object with small black dots. Early or intermediate stages of AMD progress into late AMD (dry and wet) in a time

dependent manner. Patients with dry or wet AMD experience the central vision loss and are unable to visualize the full object. Figure is modified from https://www.webrn-maculardegeneration.com/macular-degeneration stages.html.

The major hallmark of early and intermediate AMD is drusen formation, pigmentary variation, and partial vision loss (Figure. 3) (Michalska-Małecka et al., 2015). Drusen formation is an accumulation of extracellular lipids, lipoproteins, cell debri, and is located between BM and basal lamina of RPE (Abdelsalam et al., 1999; Bowes Rickman et al., 2013). Drusen formation can vary in size, border, and thickness. It is noteworthy that drusen formation in the retina increases with age and small drusen particles are correlated with old age (Luibl et al., 2006). Histopathological analysis of donor eyes further highlighted the different forms of drusen below the RPE, which were not clearly identified with fundus examination. These distributions of deposits are in the form of basal laminar deposits (BLamD), basal linear deposits (BLinD), and focal nodular forms. BLamD comprises amorphous material of long spacing collagen with granules and membrane debri present between RPE and its plasma membrane. BLinD comprises diffuse and amorphous accumulations present between the BM and RPE. Focal nodular form consists of small dome shaped deposits present within the BM. These forms of drusen are associated with AMD (Gehrs et al., 2006; Malek and Lad, 2014). Intermediate drusen particles are associated with early or intermediate AMD. Patients with early or intermediate AMD struggle to see in the dim light. Moreover, normal life activities are not easily performed (Slakter and Stur, 2005; Mitchell and Bradley, 2006; Owsley and McGwin, 2008).

GA or dry AMD is most prevalent and characterized with drusen, pigment changes, and vision loss (Bowes Rickman et al., 2013). Drusen may be soft or hard, and accumulates between RPE and BM (Figure. 3). This results in RPE dysfunction, loss of photoreceptors, and ultimately evolves into GA (Figure. 3). Pathogenic mechanisms underlying GA are still unclear (Bowes Rickman et al., 2013). Neovascular or wet AMD is less frequent and characterized by growth of leaky blood vessels into choroid, which is also known as choroidal neovascularization (CNV). Neovascular AMD causes bleeding, sprouting of new blood vessels, plasma exudation, hemorrhage, fibrosis, edema formation, and pigment epithelium detachment (PED) (Figure. 3). PED highlights the separation of RPE and BM in the retina (Figure. 3) (Gehrs et al., 2006; Toomey et al., 2018). CNV damages the retinal architecture and causes 90% of vision

loss in patients. Furthermore, most of the vision loss occurs in the late stage of AMD and patients in this stage are incapable of performing daily activities and report the worst medical conditions (Hassell et al., 2006; Malek and Lad, 2014; Taylor et al., 2016).

To date, the Food and Drug Administration (FDA) has not approved any drug to halt the development and progression of GA. Routine eye examination of patients with CNV are executed and treated with anti-vascular endothelial growth factor (VEGF) therapy in the form of intravitreal injections (FDA approved). Even though these injections inhibit the blood vessel growth, a complete recovery is not possible. The therapeutic options for AMD are far from satisfactory (Ambati and Fowler, 2012).

Both late forms of AMD are not mutually exclusive. GA eventually develops CNV and the neovascular form of AMD is often observed at the periphery of GA affected eyes (Sunness et al., 1999). Furthermore, long-term treatment with anti-VEGF agents is correlated with the development of GA (Martin et al., 2012).

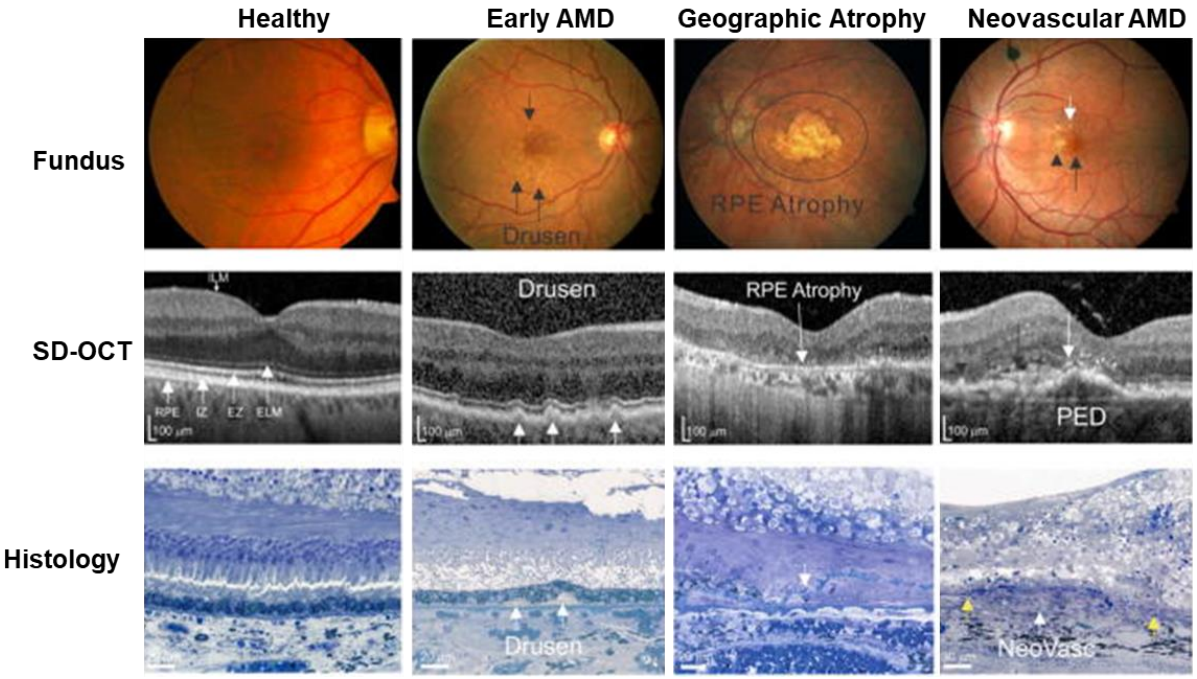

Figure 3 Images of fundus, SD-OCT, and tissue staining of healthy retina and AMD affected retinas.
Healthy retina shows the normal color of fundus with normal retinal structure and layers (SD-OCT). Healthy retina has no drusen like deposit in subretinal (SR) space or sub-RPE. Early AMD shows fundus pigmentation and drusen deposit (white arrows) in SD-OCT and in the histology image. GA shows the yellow drusen in fundus, SD-OCT image with RPE atrophy, and histology image shows the absence of RPE. Neovascular AMD shows the change in fundus color and thinned layer of subretinal fluid in SD-OCT

image. Furthermore, pigment epithelial detachment (PED) with hyperreflective foci in SD-OCT image and a neovascular complex (NeoVAsc) are present in between the two free ends of Bruch's membrane. ELM, external limiting membrane; EZ, ellipsoid zone; IZ, interdigitation zone; and SD-OCT, Spectral domain-optical coherence tomography. Image is modified from Toomey et al. (Toomey et al., 2018).

AMD is a complex, heterogeneous, and multifactorial disease with risk factors, such as ageing, smoking, obesity, and a diet consistent with high levels of fat (Heesterbeek et al., 2020b). Epidemiological studies have shown that AMD development and progression are related to these risk factors (Seddon et al., 2011). The retina is also affected by ageing like other organs of the body. Phagocytic and waste clearance capacity of RPE reduce with age (Keeling et al., 2018). Therefore, the risk of acquiring AMD increases with age. For example, the risk of acquiring an earlier stage of AMD increases with every 5 years of age until 85 years. Furthermore, the risk of acquiring late stage AMD is 20 times more likely at the age of 85 compared to 65-69 years of age (Chen et al., 2008). Age was the most important factor for early and late AMD in risk factors analysis (Lambert et al., 2016). Smoking is consistently reported as a risk factor for AMD (Thornton et al., 2005). Cigarette smoke and the basic ingredients of tobacco have a negative impact on AMD, due to reduction in a blood flow, high-density lipoprotein, increase in platelet aggregates, oxidative stress, and inflammatory markers (Klein et al., 1998; Malek and Lad, 2014; Myers et al., 2014). Smoking also increases 2-4 fold risk to acquire any form of AMD (Heesterbeek et al., 2020). Furthermore, nicotine enhanced the lesion size and severity in a CNV animal model (Suñer et al., 2004). Data from three continents showed that current smokers are at greater risk for AMD as compared to the past-smoker or non-smoker (Tomany et al., 2004).

Obesity and diet with high glycemic index induce progression of AMD (Chiu and Taylor, 2011). However, a healthy diet consistent with vegetables, fruits, and physical activity can slow down such progression (Carneiro and Andrade, 2017).

Additionally, environmental factors such as sunlight, artificial light, UV light, visible light, ionizing radiations, chemotherapeutic agents, and environmental toxins, enhance the oxidative stress in the retina (Saccà et al., 2014). A retina with long-term oxidative stress changes in oxygen and nutrients supply, maintenance of photoreceptors and choriocapillaris, and waste product clearance in retina. These events upregulate the formation of lipofuscin, which triggers the RPE dysfunction and photoreceptor cell

death (Golestaneh et al., 2017; Cho et al., 2019). Furthermore, oxidative stress also enhances CNV (Dong et al., 2009).

The pathological mechanisms underlying AMD are still elusive. However, several known pathological factors are key players in AMD development and progression. Such known factors are inflammation, retinal lipid alteration, complement dysregulation, and pro-angiogenic signaling (Kauppinen et al., 2016; Schnichels et al., 2020). With confronting threats such as microbes or foreign particles, cells induce short term-inflammation in response to these signals. Such inflammation is advantageous whereas long-term inflammation is detrimental which leads to chronic disease state. These inflammatory stimuli evoke the innate immune response (Ambati et al., 2013).

1.3. Microglia

In 1856, a famous German pathologist Rudolf Virchow coined the term “glia” (Greek for “glue”) and mentioned the non-neuronal compartments of the central nervous system (CNS) as glia (Sousa et al., 2017). Later, in 1919, a Spanish scientist, Pio del Río Hortega described microglia as the “third element” of CNS and performing the phagocytic function with plasticity and heterogeneity (Sousa et al., 2017). Initially, microglia were thought to be derived from neuroectoderm. Now, it is firmly proved that microglia are primary immune cells and arise from primitive myeloid progenitors in the extra embryonic yolk sac (Ginhoux et al., 2013).

1.3.1. Microglia in the central nervous system (CNS)

Microglia comprise 5-20% of total glial cells in the CNS (Yang et al., 2010). At present, microglia are multifunctional innate immune cells of the CNS. They are specialized macrophages of CNS and are supplemented with memory-like function and respond in a context dependent manner (Prinz et al., 2019). Furthermore, microglia play a significant role in host’s defense against pathogens, regulating homeostasis, and CNS disorders (Hickman et al., 2018).

1.3.1.1. Microglia as sentinels in CNS

Microglia cells are distributed throughout the CNS before the blood-brain barrier is established (Ginhoux et al., 2013). Microglia are specialized multitasking immune cells and act as sentinels in CNS for the maintenance of its homeostasis (Sousa et al., 2017; Yin et al., 2017). In a physiological state, localization and numbers of microglia are firmly controlled which is disrupted in disease state (Tay et al., 2017). After an injury, microglia migrate to the site of injury in minutes. However, microglia transform to amoeboid shape in hours to days (Prinz et al., 2019). Pio del Río Hortega mentioned the transformation of microglia in earlier studies. Microglia transformation includes a number of changes, such as in gene expression, morphology, migration, proliferation, metabolism, phagocytosis, and death (Benmamar-Badel et al., 2020). Microglia perform several functions including immune surveillance, sensing the invading pathogens, and dead cells. Furthermore, microglia eliminate these threats to protect the CNS (Casano and Peri, 2015).

Murine microglia are equipped with a number of receptors known as sensome which enable the microglia to recognize the invading pathogens, cytokine, chemokines, metabolites, misfolded proteins, extracellular matrix, and change in pH (Hickman et al., 2018). These murine microglia sensome consists of different receptors like purinergic (P2rx4, P2rx7, P2ry12, P2ry13 and P2ry6), chemokine (Ccr5, Cx3cr1, Cxcr4 and Cxcr2), Fc (Fcer1g and Fcgr3), interferon-induced transmembrane proteins (Ifitm2, Ifitm3 and Ifitm6), Toll-like receptor (Tlr2 and Tlr7), and siglecs (Siglech and Siglec3/Cd33) (Prinz et al., 2019).

1.3.1.2. Microglia in brain homeostasis

In a developing brain or early postnatal brain, microglia act differently compared to the adult brain (Lenz and Nelson, 2018). In the prenatal brain, microglia control the growth of dopaminergic axons in the forebrain and regulate the positioning of cortical interneurons (Squarzoni et al., 2014). In developing and early postnatal days of the mouse brain, microglia become highly mobile and activated. In such state, microglia are amoeboid and more proliferative (Figure. 4). Furthermore, expression profiling has shown that microglia are responsible for the phagocytosis and synaptic remodeling (Figure. 4). During late postnatal and adulthood, microglia become more homeostatic (Figure. 4) (Lawson et al., 1990; Matcovitch-Natan et al., 2016; Prinz et al., 2019).

Microglia and neurons arise at the same time during development, but microglia are responsible for controlling neuronal fates and numbers (Mazaheri et al., 2014, 2017; Frost and Schafer, 2016). In young mice, microglia organize and form the neuronal architecture by engulfing the neurons in the hippocampus (Sierra et al., 2010). Microglia lacking CX3C chemokine receptor 1 (CX3CR1) have been shown to cause the neuronal death that highlights the importance of microglia in the maintenance of neurogenesis in the developing brain (Paolicelli and Ferretti, 2017). Furthermore, colony stimulating factor 1 receptor (CSF1R) knockout mice showed absence of microglia and abnormalities in brain structure (Erblich et al., 2011). This study emphasized the importance of microglia in the normal brain development. In adult brain scans, microglia remove the dead cells and pathogens that may reside in the region. Microglia are heterogeneously distributed in the brain of adult mice where these cells act as sensors for the microenvironment (Lawson et al., 1990; Stratoulias et al., 2019).

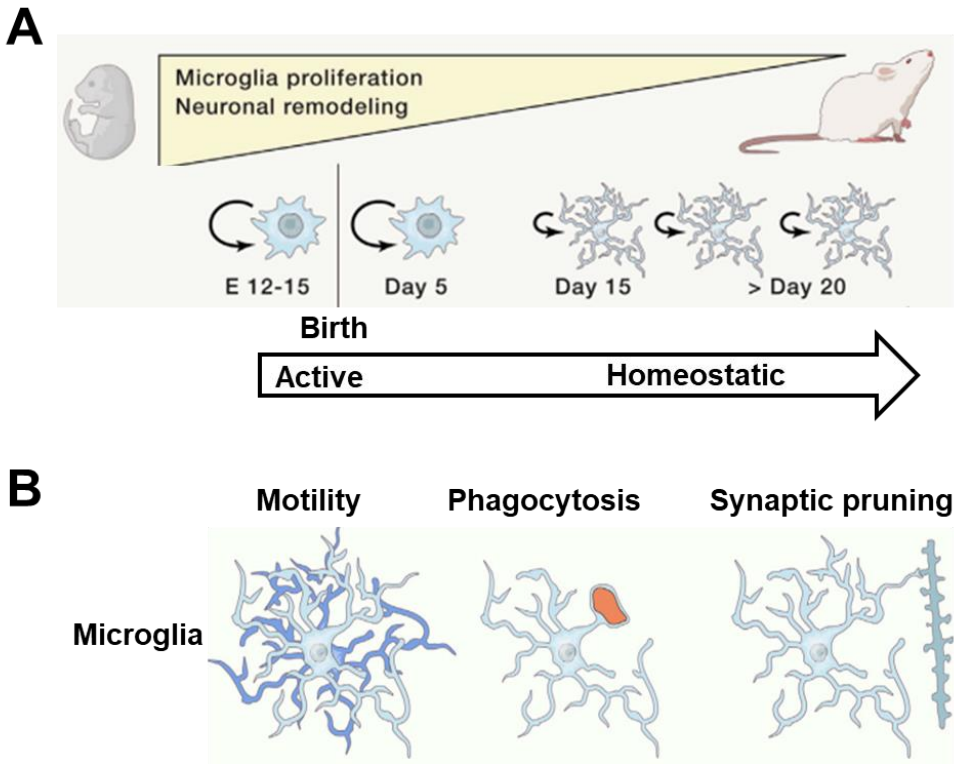

Figure 4 Functions of microglia during development and adulthood.
(A) Morphology and proliferation of microglia. Microglia are activated during embryonic and early postnatal development. Microglia are in a homeostatic state during late postnatal and adulthood. **(B)** During embryonic and prenatal development microglia are motile. In postnatal development, microglia become more ramified and phagocytose the dead cells and are responsible for the synapse pruning. Figure is modified from Prinz et al. (Prinz et al., 2019).

1.3.2. Self-renewal ability of microglia

Microglia are autonomous cells that have the ability of self-renewal (Ajami et al., 2007) and their population in the CNS including the retina is maintained throughout life (Réu et al., 2017; Tay et al., 2017). Animal studies have shown that CSF1R, interleukin-34 (IL-34), and interferon regulatory factor-8 (IRF-8) are important factors for microglia development. The reduction in these factors also diminishes microglia population (Ginhoux and Prinz, 2015). CSF1R inhibitors are used to deplete microglia in the brain. However, microglia are re-established from surviving microglia, which were expressing nestin (Elmore et al., 2014). In the retina, microglia were repopulated after the elimination of all resident microglia and repopulated microglia were not expressing nestin. Furthermore, repopulated microglia were divided into two categories: the majority, of center-emerging and the minority, of periphery-emerging microglia. The majority center-emerging microglia originated from resident microglia of the optic nerve whereas the minority periphery-emerging microglia originated from macrophages in the ciliary body or iris. Repopulated retina microglia showed no changes at gene levels compared to retinal resident microglia (Huang et al., 2018b).

1.3.3. Microglia in the healthy retina

Microglia are important innate immune cells of the retina and these cells have similar morphology and homeostatic functions as in the brain (Guttenplan et al., 2018; Silverman and Wong, 2018). During retinal development, microglia are localized in the ganglion cell layer (GCL) and inner plexiform layer, where these cells phagocytose the cell debri (Bodeutsch and Thanos, 2000). Following the development stage, microglia migrate to inner and outer plexiform layers (IPL, OPL). Microglia then scan the retina and keep active surveillance with their filopodia like fine cellular processes (Karlstetter et al., 2015). In such a state, microglia with long processes also interact with other retinal cells to control microglia and maintain retinal homeostasis, architecture and integrity (Rashid et al., 2019). For this, microglia express different cell surface proteins to assist crosstalk with other cells. These surface proteins control microglia activation in a healthy retina (Langmann, 2007). For example, the CD200 receptor (CD200R) is an inhibitory receptor and expressed by microglia (Walker and Lue, 2013). The ligand for CD200R is CD200, a membrane glycoprotein expressed by a variety of retinal cells, including the ganglion, photoreceptor, and RPE (Rashid et al., 2019). Importantly,

CD200R deficient mice increased pro-inflammatory markers in an experimental model of uveoretinitis and CNV. Furthermore, CD200R-CD200 interaction is important for the control of tissue damage due to microglia activation (Copland et al., 2007; Horie et al., 2013).

Another important regulator of microglia is C-X3-C motif chemokine ligand 1 (CX3CL1 or fractalkine) released by healthy retinal neurons and endothelial cells. CX3CL1 binds to CX3CR1 expressed by microglia (Karlstetter et al., 2015). Several studies highlighted the importance of CX3CL1-CX3CR1 to inhibit the retinal degeneration. For example, transplantation of CX3CR1-expressing mesenchymal stem cells in sub-retinal (SR) space reduced microglia activation and retinal degeneration (Huang et al., 2013). In CX3CR1 knockout (-/-) model, the velocity of retinal microglia is reduced compared to animals with preserved CX3CR1 (Liang et al., 2009). In retinal microglia depletion studies, microglia efficiently repopulated in the retina (Huang et al., 2018b). This repopulation is also regulated through CX3CL1-CX3CR1 signaling. Interestingly, repopulated microglia restore important surveillance functions of microglia such as movement and morphological changes to retinal injury. However, CX3CR1 deficient mice exhibited abnormal microglia repopulation (Zhang et al., 2018). Deletion of CX3CR1 enhanced the microglia activation and photoreceptor demise in retinal degeneration 10 (rd10) mouse model. Interestingly, overexpression of CX3CL1 reduced photoreceptor death in rd10 mice (Wang et al., 2019). Hence, CX3CL1-CX3CR1 signaling controls microglia activation and phagocytosis. In addition, CX3CL1-CX3CR1 signaling also regulates neuronal activity and synaptic integrity in the retina (Wang et al., 2016).

Sialic acids covalently attached to cell membrane proteins, lipids and form polysialic acid chains (PSA). These chains are present on the healthy neuronal glycocalyx and interact with sialic acid binding immunoglobulin-like lectin 11 (Siglec11) which is a cell surface receptor of microglia (Linnartz-Gerlach et al., 2014). Interactions between the PSA and Siglec11 prevent microglia activation and control the retinal degeneration (Karlstetter et al., 2015).

Microglia also interact with Müller cells in the retina and Müller cells are rich sources of extracellular ATP that control the microglia activity. Microglia and Müller cells interactions regulate retinal inflammation (Wang & Wong, 2014). Microglia release neurotrophic factor, fibroblast growth factor, leukemia inhibitory factor, and glial cell

line-derived neurotrophic factor. These factors could modulate the photoreceptor demise and retinal stress (Kumar et al., 2013). Microglia crosstalk with different cell types in the retina and microglia become highly sensitive to the microenvironment. Such a high sensitivity of microglia requires inhibitory pathways to control the unnecessary microglia activation. For this, RPE releases inhibitory factors, which inhibit the unnecessary infiltration of phagocyte into SR space (Chen and Xu, 2015). However, physiological functions of microglia are dysregulated in retinal diseases (Ramirez et al., 2017).

1.3.4. Microglia in the diseased retina

Microglia activation is a distinctive feature of many retinal diseases. Furthermore, microglia morphology and migration capacity are altered in an activation state. In chronic retinal diseases, microglia are pathologically activated for the long-term. Pro-inflammatory responses are orchestrated by microglia cells and are highly upregulated, which eventually results in tissue damage and degeneration (Karlstetter et al., 2015; Rashid et al., 2019).

1.3.4.1. Microglia in age-related macular degeneration

There is overwhelming evidence to indicate the involvement of inflammation and dysregulation of innate immunity in AMD. Dysregulation of innate immunity is linked with complement factors, inflammasome, and microglia (Ambati et al., 2013; Fritsche et al., 2014; Rashid et al., 2019). Complement fragments (C3a and Ba) and cytokines are upregulated in aqueous humor of wet AMD patients (Schick et al., 2017). Dysregulation of the complement system activation contributes to AMD development and progression (Natoli et al., 2017). Activation of complement system also enhanced drusen deposition in the retina. Moreover, complement factors were also found in the drusen of AMD donors (Nozaki et al., 2006). Furthermore, drusen from AMD donors acts as pro-inflammatory agent to activate inflammasome (Mariathasan et al., 2006; Doyle et al., 2012). Inflammasome activation was also observed in ocular tissue of patients with GA and CNV (Gao et al., 2015). Resident microglia maintain a ramified structure in a resting state (Figure. 5). In transient damage, microglia act as sensors to detect damage-associated patterns (DAMPs) (Kigerl et al., 2014). Thus, they

transform their morphology to amoeboid and migrate to the site of damage (Figure.5). Microglia release pro-inflammatory cytokines, chemokines, and upregulate the reactive oxygen species (ROS) levels (Jurgens and Johnson, 2012) Furthermore, microglia enhance their phagocytic capacity to eliminate the damage (Fu et al., 2014). In such disease states, microglia strive to establish the cellular homeostasis with minimal damage to the retinal tissue (Chen and Xu, 2015). However, persistent damage due to neurodegenerative diseases causes microglia failing to resolve the damage and become pathologically active (McMenamin et al., 2019). In such a state in AMD, activated microglia in SR space release cytokines, chemokines, and phagocytose the healthy photoreceptor cells (Xu et al., 2009; Zhao et al., 2015). Activated microglia also upregulate the surface molecules and major histocompatibility complex (MHC) class I and II antigens (Jurgens and Johnson, 2012). Transcriptomic profiling of AMD patients showed the upregulation of different cytokines (Spindler et al., 2018; Sato et al., 2019). It is also possible that the increase of activated-microglia numbers in SR space is due to release of different chemoattractants (Rathnasamy et al., 2019). For example, chemokine (C-C motif) ligand 2 (CCL2) is released by activated microglia and caused microglia accumulation in SR (Raoul et al., 2010). CCL2 knockout mice have been shown to reduce the microglia accumulation in SR (Levy et al., 2015). CCL2 levels were upregulated in the serum of AMD patients compared to healthy control (Anand et al., 2012). Furthermore, CCL2 levels enhanced the recruitment of monocyte in ocular fluid in AMD patients (Sennlaub et al., 2013; Fauser et al., 2015). Drusen acts as also prominent chemoattractant molecule and enhanced activated microglia were identified in the SR space in association with age-related deposition (Indaram et al., 2015).

Activated microglia also have deleterious effects on neighboring cell types including RPE and photoreceptors (Madeira et al., 2018; Fletcher, 2020). Activated microglia enhanced the photoreceptor cell death in light-induced retinal degeneration model (Figure.5) (Scholz et al., 2015b; Akhtar-Schäfer et al., 2018). Similar to AMD, microglia activation with damaging effects were also found in other degenerative diseases of the eye, such as retinitis pigmentosa (RP) and diabetic retinopathy (DR) (Gupta et al., 2003; Zeng et al., 2008).

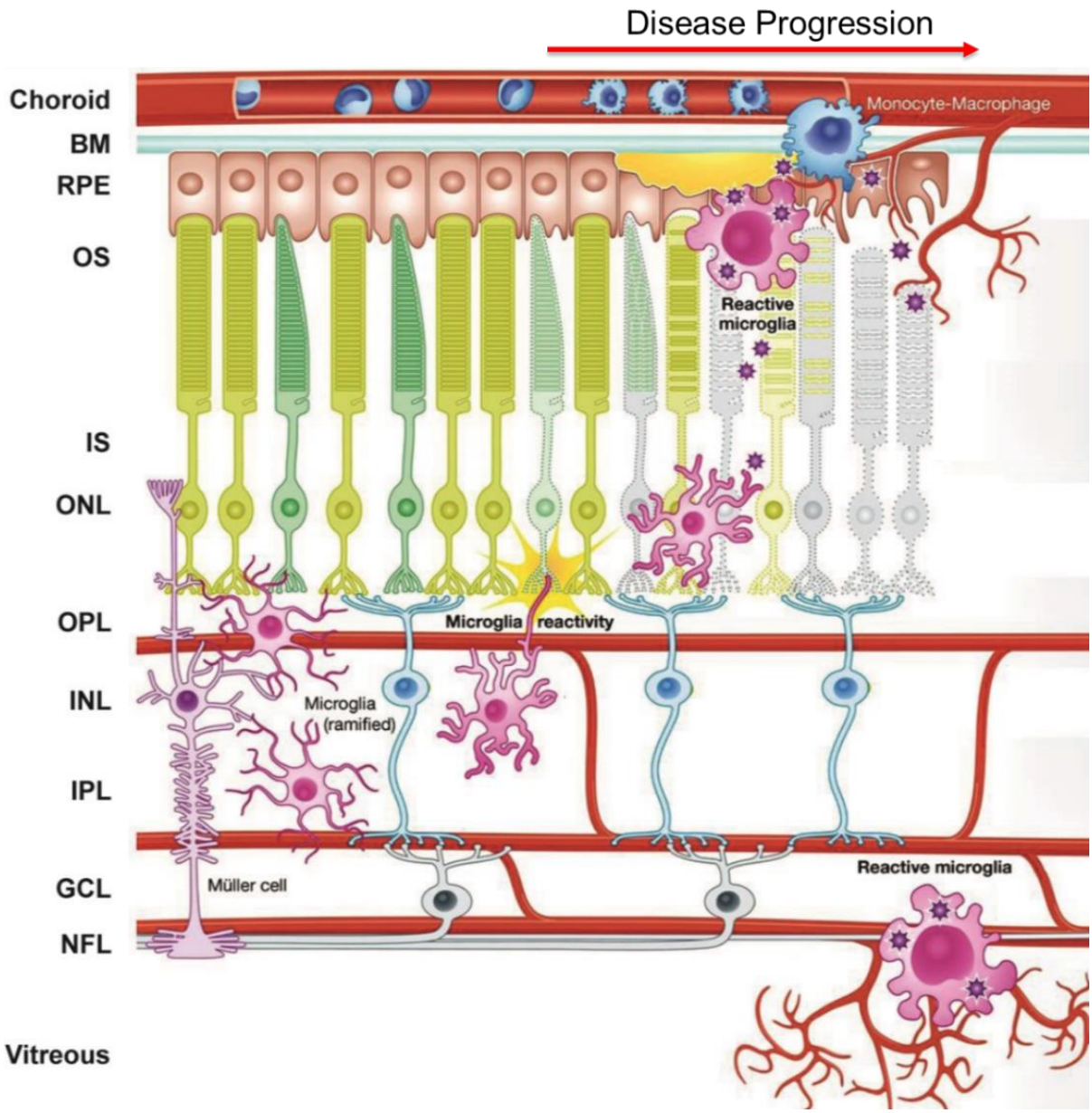

Figure 5 Localization of microglia and its activation in AMD.
In a healthy state, ramified microglia are localized in IPL or OPL and scan the environment with long processes. In a disease state, microglia migrate to lesion sites, change their morphology to amoeboid, phagocytose the dead cells, and maintain homeostasis. However, in a persistent disease state, microglia fail to maintain homeostasis and become highly active. Activated microglia upregulate the release of pro-inflammatory mediators and enhance the disease progression. Figure is modified from Akhtar-schäfer et al. (Akhtar-Schäfer et al., 2018).

1.3.5. Microglia modulation as targeted therapy

Microglia activation increases during retinal degeneration and microglia depletion studies highlighted the contribution of microglia in the maintenance of retinal structure

and integrity (Elmore et al., 2014). Microglia cells express CSF1R and an inhibitor of CSF1R (PLX5622) decreased the microglia accumulation and lesion size in a CNV animal model (Schwarzer et al., 2020). Microglia depletion did not alter the overall retinal thickness and structure. However, continuous microglia depletion in retina has been shown to enhance the neurodegeneration of photoreceptor synapses (Wang et al., 2016b). Furthermore, complete blockage of microglia would be undesirable because microglia have important homeostatic functions like phagocytosis of cell debri. Therefore, suppression of microglia activation with immunomodulatory compounds is opening a new avenue for the treatment of retinal neurodegenerative diseases including AMD (Rashid et al., 2019). To analyze the immunomodulatory compounds, in vivo models are required, which mimics the features of AMD.

Although the mouse has no macula, prolong light induced photo-oxidative damage causes degeneration of photoreceptor cells and mimics the certain features of dry AMD in the mouse model (Organisciak and Vaughan, 2010; Grimm and Remé, 2012). For example, acute white light exposed albino mice have an accumulation of activated microglia in SR space, photoreceptor cell death, and depletion of outer nuclear layer (ONL) in the retina. Furthermore, in this model, microglia mediated release of pro-inflammatory mediators (i-NOS, IL-1ß, CCL2, and IL-6) were upregulated. Moreover, the phagocytic capacity of microglia and neurodegeneration were also increased (Wenzel et al., 2005; Scholz et al., 2015b; Tisi et al., 2019). The laser coagulation model is used to study CNV in vivo. Laser beam induces CNV by breaking the BM and penetration of new choroidal capillaries (neoangiogenesis) into the retina. Laser lesions have also shown the accumulation of activated microglia and upregulation of cytokines and chemokines in the retinas of the mouse model (Lückoff et al., 2016; Wolf et al., 2020).

These in vivo models of AMD highlight that microglia play important role in retinal degeneration. Furthermore, microglia act as a potential therapeutic target to alleviate the retinal disease development and progression. Immunomodulatory compounds like minocycline reduced the microglia reactivity and prevented light-induced retinal degeneration in mice (Scholz et al., 2015b). Therefore, it is important to target microglia activation in a disease state to minimize the harmful effects and to enhance the protective effects of microglia. Although, inhibition of microglia activation led to prevent neurodegeneration in several studies mentioned above. To date, there is no cure for

AMD and there is an urgent need for new compounds targeting microglia activation for therapeutic treatment options of AMD.

1.4. Aryl hydrocarbon receptor (AhR)

Cells are responding in a constant state to the molecular changes exerted by external stimuli, diet, and host metabolism. Cells have a number of sensors that facilitate the biotransformation and elimination of these external signals (Larigot et al., 2018). The aryl hydrocarbon receptor (AhR) is one of the sensors that respond to external stimuli (Lamas et al., 2018). AhR is expressed in a variety of cells and highly conserved across the species, which highlights its fundamental role in a biological system (Busbee et al., 2013). Initially, it was identified for the xenobiotic metabolism (Frericks et al., 2007; Rothhammer and Quintana, 2019). In addition, AhR also performs several crucial functions to maintain cellular homeostasis and immunity (Hao and Whitelaw, 2013; Larigot et al., 2018).

1.4.1. AhR complex and its functional domains

The AhR is a ligand dependent transcriptional factor that localizes into cytoplasm with the association of heat shock protein 90 (HSP90), AhR-interacting protein (AIP; also known as XAP2), co-chaperone P23, and protein kinase SRC (Rothhammer and Quintana, 2019). AhR protein has three functional domains, basic helix-loop-helix (bHLH) which is responsible for the dimerization with AhR nuclear translocator (ARNT) and binding to DNA. The second functional domain has two Per-Arnt-Sim (PAS) domains, PAS A is responsible for the ARNT dimerization and PAS B is responsible for the ligand binding. Lastly, the third domain of AhR is known as C-terminal domain, having three further subdomains (acidic, glutamine-rich (Q-rich), proline, serine, and threonine (P/S/T) (Figure. 6) (Larigot et al., 2018).

AhR with associated proteins form a complex that interact with each other for proper functioning of this receptor (Tappenden et al., 2013). AhR is associated with two HSP90 proteins, one HSP90 binds to the PAS domain of AhR and second HSP90 binds to the basic helix-loop-helix and PAS domain (Fukunaga et al., 1995). AIP interacts with AhR and HSP90 and is responsible for the stabilization of the AhR-HSP90 interactions (Meyer and Perdew, 1999). AIP further participates in AhR folding

and regulates the AhR transport to the nucleus by inhibiting importin-β, which enhances the translocation. Moreover, AIP and P23 stabilize the AhR localization into the cytoplasm. P23 also inhibits the proteasome-mediated degradation (Kudo et al., 2018). The protein kinase SRC regulates AhR activation upon ligand binding (Enan and Matsumura, 1996). These interactions are responsible for the AhR stability and localization into cytoplasm. In addition, AhR complex has high affinity for the AhR agonists (Rothhammer and Quintana, 2019). Different domains for ligand, ARNT, DNA, and coactivator bindings are present within AhR. ARNT has similar domains and structure to AhR. However, ligand binding domain is absent in ARNT. Therefore, ARNT is responsible for AhR binding. Another protein, AhR repressor (AhRR) has functional domains, such as ARNT, DNA, and corepressor binding. AhRR is responsible for repressing the AhR activity (Figure. 6) (Larigot et al., 2018).

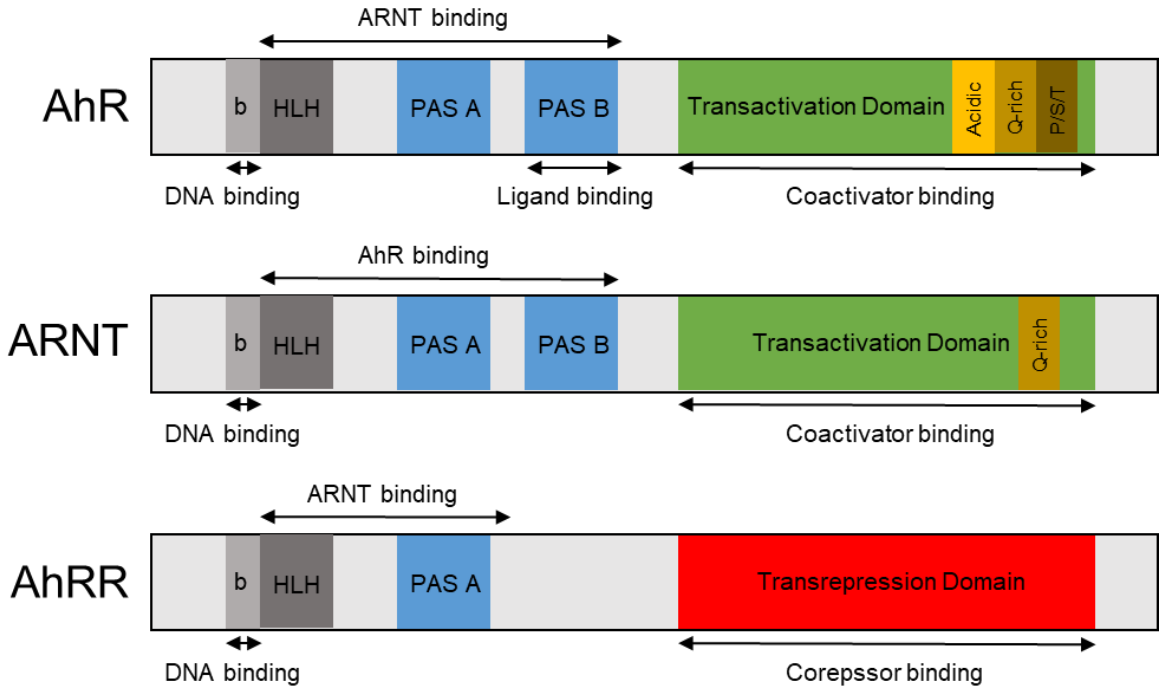

Figure 6 The functional domains of AhR, ARNT, and AhRR.
The AhR protein consists of a bHLH, two PAS domains (PAS A and B), and C-terminal domain. ARNT protein has a similar structure to AhR except ligand binding domain which is absent in ARNT. AhRR has bHLH, PAS A, and corepressor binding domains. Furthermore, AhRR binds to ARNT and responsible for AhR repression. Figure is adapted from Larigot et al. (Larigot et al., 2018).

1.4.2. AhR Signaling

In an active state, AhR with ligand translocate into the nucleus and bind to ARNT to form AhR-ARNT complex. This complex binds to AhR response elements known as dioxin or xenobiotic response elements (DRE or XRE) and transcribes different genes (cytochrome P450 superfamily genes (CYP1A1, CYP1B1), and NAD(P)H quinone oxidoreductase 1 (NQO1). These genes are responsible for xenobiotic metabolism (Lamas et al., 2018). AhRR binds to ARNT and forms AhRR-ARNT complex. This complex prevents the binding of ligand bound AhR to ARNT and regulates AhR activity (Figure. 7A) (Sakurai et al., 2017).

AhR has been shown to interact with different transcriptional factors and regulates the expression of those genes having no DRE or XRE (Figure. 7B). For example, AhR directly interacts with the retinoblastoma protein to inhibit cancer (Marlowe et al., 2008). In addition, AhR interacts with retinoic and estrogen receptor and modulates their activity. Moreover, AhR also regulates the target genes of P53, MYC, MAP kinases, ERK1, ERK2, HIF1 alpha, and NF-kB (Puga et al., 2002, 2009; Zhu et al., 2019). AhR interacts directly to NF-kb or indirectly through SOCS2 (Figure. 7B) (Rothhammer and Quintana, 2019). Other signaling pathways like Wnt/β-catenin also modulate AhR signaling (Esser and Rannug, 2015). Furthermore, AhR regulates the chromatin remodeling via histone acetylation and methylation (Schnekenburger et al., 2007; Winans et al., 2015). Collectively, AhR signaling is highly variable and versatile. The versatility of AhR signaling is associated with cell type, specific ligand, and activation of other signaling pathways which may crosstalk with AhR (Rothhammer and Quintana, 2019).

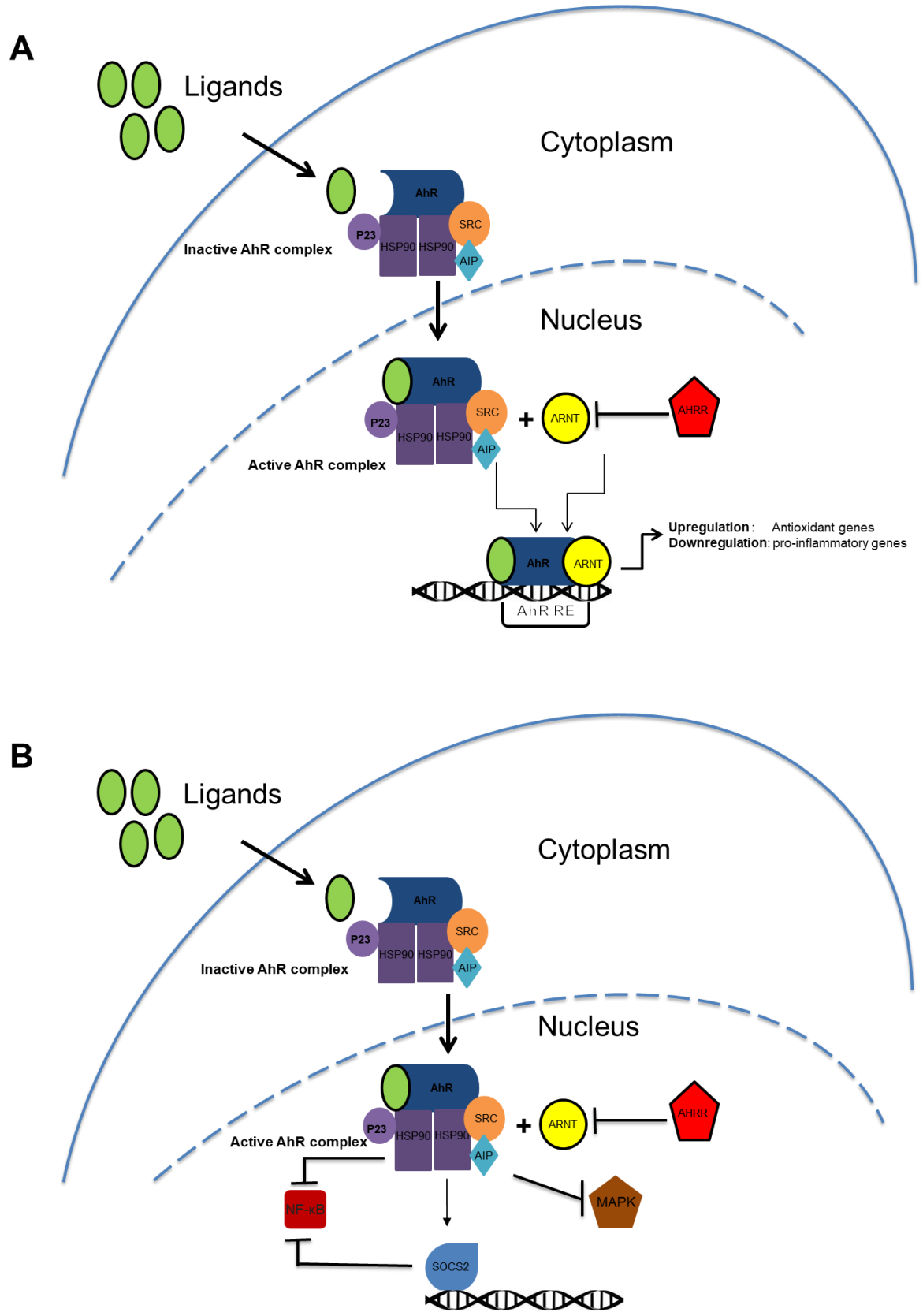

Figure 7 The AhR signaling pathway.

(A) Inactive AhR localizes into cytoplasm with the association of HSP90, AIP, co-chaperone P23, and protein kinase SRC. Upon ligand binding, AhR translocates into the nucleus and forms heterodimer with ARNT. AhR-ARNT complex binds to AhR

response elements, which is present in the promoter region of target genes. AhRR inhibits the dimerization of AhR complex with ARNT. AhR signaling pathway upregulates antioxidant genes and downregulates the pro-inflammatory genes (Busbee et al., 2013; Larigot et al., 2018). **(B)** AhR also interacts with other transcriptional regulators. AhR interacts directly with NF-kb or indirectly through SOCS2. In addition, ligand-mediated AhR activation reduces the MAP kinase signaling (Puga et al., 2009; Rothhammer and Quintana, 2019). Figures are adapted from Larigot et al. (Larigot et al., 2018).

1.4.3. AhR Ligands

Numerous AhR ligands have been discovered and their identification has increased the knowledge of AhR activity and its physiological functions (Lamas et al., 2018; Safe et al., 2018). AhR ligands are divided into two categories, such as exogenous and endogenous. Exogenous ligands are further classified as synthetic and natural ligands. For example, polycyclic aromatic hydrocarbon and synthetic flavonoid are synthetic ligands and induce AhR target genes (Busbee et al., 2013). Natural ligands of AhR are presented to biological systems through diet. Greater source of naturally occurring AhR ligands is in a diet having carotenoid, cantaxantine, astaxanthin, berberine, and flavonoids (Busbee et al., 2013).

Indole-3-carbinol (I3C) is a natural ligand (agonist) of AhR and present in green vegetables such as broccoli, cauliflowers, cabbage, kale, and Brussels sprouts. These vegetables contain glucobrassicin and when these vegetables are chopped, the enzyme myrosinase becomes active and converts the glucobrassicin into two unstable products that finally degrade into I3C (Figure. 8). I3C reacts with itself and with a variety of other chemicals in plants to form conjugates. Indole 3 cysteine, Indole 3-tryptophan, and indole-3-carboxaldehyde are the result of these reactions (Chamovitz et al., 2018). Furthermore, under acidic environmental conditions, I3C converts to form 3,3'-diindolylmethane (DIM) through condensation, hence having biological effects at cellular and molecular levels (Bjeldanes et al., 1991; Wang et al., 2016). In addition, I3C has anti-carcinogenic, anti-inflammatory, antioxidant, and anti-apoptotic properties (Choi et al., 2018; Lamas et al., 2018).

Endogenous ligands of AhR include molecules which are the result of different pathway metabolism, such as indirubin, indigo, formylindolo [3,2-b] carbazole (FICZ), tryptophan, metabolites of heme, arachidonic acid, and kynurenine pathway (Stejskalova et al., 2011; Larigot et al., 2018).

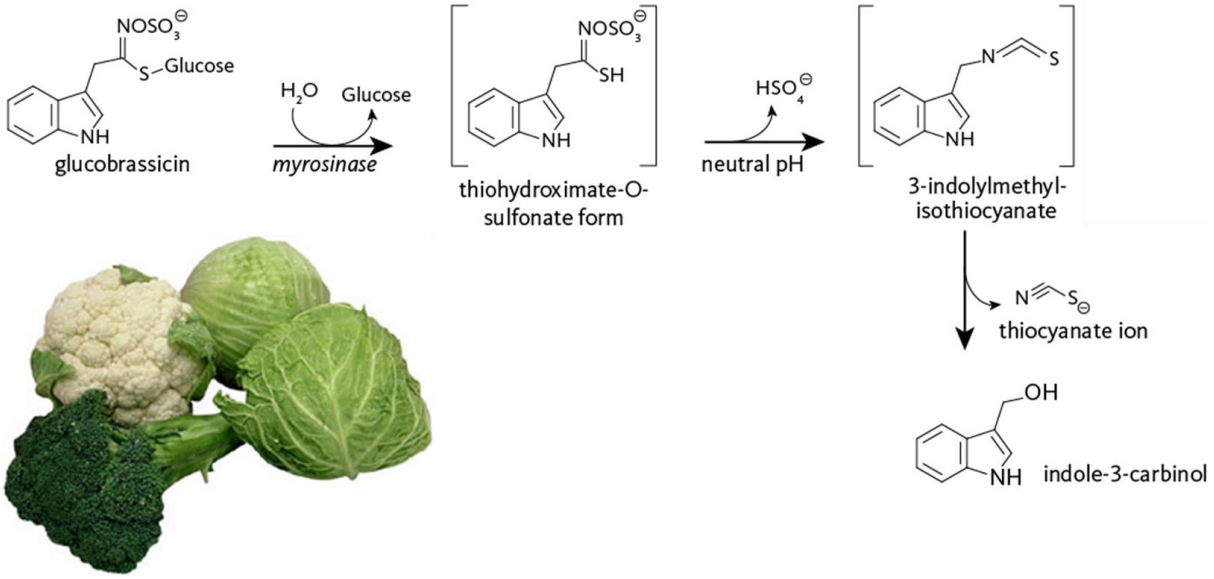

Figure 8 Breakdown of glucobrassin in vegetables and its conversion to I3C. Cruciferous vegetables (broccoli, cauliflower, and cabbage) contain glucobrassicin. Due to myrosinase activity, glucobrassicin is transformed into an unstable form (thiohydroximate–O-sulfonate). This product is further transformed into another unstable form (3-indolymethyl-isothiocyanate) upon sulfate ion release. This compound is converted into thiocyanate ion and I3C. Figures are modified from https://lpi.oregonstate.edu/mic/dietary-factors/phytochemicals/indole-3-carbinol and https://lancaster.unl.edu/hort/articles/2005/growcabbage.shtml.

1.4.4. AhR in the CNS

AhR is expressed by various immune cells including neurons, oligodendrocytes, glial precursor, astrocytes, and microglia (Juricek and Coumoul, 2018). AhR plays a significant role in immunity (Kerkvliet, 2009). Several genes which are responsible for the immune response, have a xenobiotic response element (XRE) sequence in their promoters. However, it is not clear whether AhR is directly involved in their regulation (Fujii-Kuriyama and Kawajiri, 2010).

AhR modulates the immune system in healthy and disease states (Gutiérrez-Vázquez and Quintana, 2018). Microglia coordinate with astrocytes at different levels to maintain cellular homeostasis through AhR (Figure. 9A). Recent study proposed that in a healthy CNS, AhR activation with agonists (Diet, gut flora and host metabolism) increased transforming growth factor alpha (TGF-α) and reduced nuclear factor k-light-chain-enhancer of activated B cells (NF-kB)-mediated vascular endothelial growth factor b (VEGFb) responses. Thus, in microglia and astrocytes, ligand-mediated AhR activation eventually reduced inflammation, neurotoxicity, and immune cells

recruitments (Figure. 9A). Whereas, in CNS inflammation, the absence of AhR agonists downregulated TGF-α and upregulated NF-kB-mediated VEGFb responses which ultimately enhanced inflammation, neurotoxicity, and immune cell recruitment (Figure. 9B) (Rothhammer and Quintana, 2019). In addition, toll like receptors (TLRs) activate different molecular signaling pathways and regulate inflammatory responses (Mulfaul et al., 2020). Previously, AhR has been shown to negatively regulate toll like receptor (Kimura et al., 2009). AhR deficient mice have been shown to increase inflammatory response and highlighted the physiological importance of this receptor (Juricek et al., 2017).

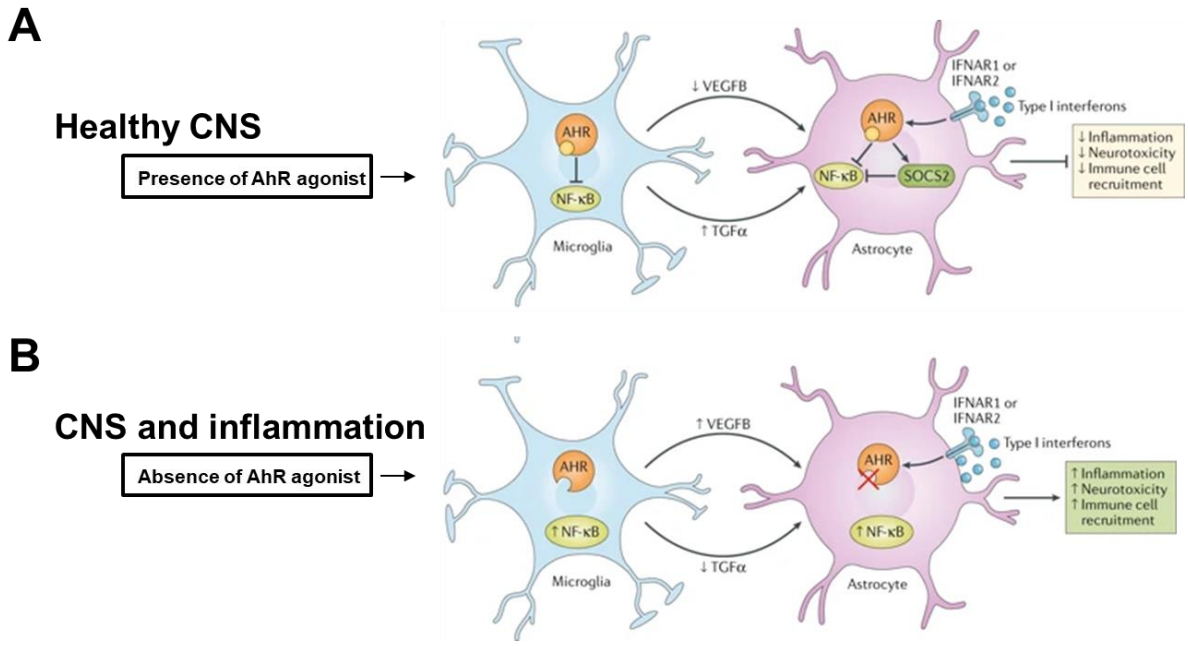

Figure 9 AhR in the CNS.
In a healthy CNS, AhR agonists cross the blood brain barrier and enhance the AhR signaling, resulting in NF-kB downregulation in microglia and astrocytes. AhR activation reduces inflammation, neurotoxicity, and immune cell recruitment and maintains CNS homeostasis. **(B)** In a diseased CNS, AhR agonists are not present, resulting in the upregulation of NF-kB in microglia and astrocytes. Absence of AhR activity enhances inflammation, neurotoxicity, and immune cell recruitment. Figures are modified from Rothhammer and Quintana. (Rothhammer and Quintana, 2019).

1.4.5. AhR as therapeutic target in CNS

AhR also plays an important role in the regulation of CNS pathogenesis (Wheeler et al., 2017). AhR knockout mice have been shown to develop an impaired immune system (Fernandez-Salguero et al., 1995; 1997). AhR-deficient mice exhibited

impaired neurogenesis in hippocampus and altered fear memory (Latchney et al., 2013). In addition, AhR deletion also enhanced the aberrant morphogenesis of granule cells in hippocampus with impaired hippocampus dependent memory (de la Parra et al., 2018). AhR activation with ligand has been shown to prevent microglia activation and LPS-induced inflammation in mouse brain (Kim et al., 2014). AhR signaling has been shown to regulate brain regeneration and restored neurogenesis in brain injury (Giaimo et al., 2018). Furthermore, AhR regulated the astrogliosis and neurogenesis in the brain of stroke-induced mice (Chen et al., 2019). AhR might be an important therapeutic target and AhR activation with ligands opens a new therapeutic option for various CNS related diseases (Wheeler et al., 2017; Rothhammer and Quintana, 2019). AhR activation with I3C and DIM prevented experimental autoimmune encephalomyelitis (EAE) and EAE-mediated infiltration of immune cells into the CNS (Rouse et al., 2013). Laquinimod has been reported to prevent EAE by activating AhR (Kaye et al., 2016). I3C reduced the clonidine-induced neurotoxicity through antioxidant mechanisms in rats (El-Naga et al., 2014). I3C reduced inflammatory responses and enhanced antioxidants in an experimental in vivo model of Parkinson's disease (Saini et al., 2020). Tryptophan mediated AhR activation reduced inflammatory responses in the CNS (Rothhammer et al., 2016).

1.4.6. AhR as therapeutic target in the eye

AhR plays a significant role in the physiological and pathological mechanisms involved in ocular compartment and AhR is a putative target to prevent different ocular diseases. For example, AhR knockout mice exhibited oculomotor deficiency (Chevallier et al., 2013). Thyroid eye disease (TED) is an inflammatory disease of the orbit, which is associated with dysregulated ocular tissue remodeling, myofibroblast aggregation, and immune cell activation. AhR ligands inhibited the myofibroblast activation and proliferation (Woeller et al., 2016). Recently, ligand-mediated AhR activation has been shown to decrease collagen accumulation and destructive tissue remodeling which occurs in the TED (Roztocil et al., 2020). Uveitis is another intraocular inflammatory disease and the leading cause of blindness. AhR knockout mice enhanced microglia recruitment and AhR activation reduced the inflammation and apoptosis in experimental autoimmune uveitis (Huang et al., 2018a). AhR knockout mice have been shown to enhance the carcinogen-induced retinal lesions (Tsai et al., 2020). Age-

related decline in AhR was found in the RPE cells, AhR knockout mice exhibited RPE dysregulation and dry-AMD like phenotype (Hu et al., 2013). In addition, fundus images of 3 to 12 months old AhR knockout mice showed yellow and white spots which were absent in wild type (WT) mice (Figure. 10A). In addition, the accumulation of SR microglia and RPE dysfunction were evident in AhR knockout mice (Figure. 10B) (Kim et al., 2014b). Retina-specific AhR knockout mice enhanced the retinal degeneration with a thinned retinal ONL. Moreover, retinal apoptosis was seen in these mice (Zhou et al., 2018). Absence of AhR has been shown to enlarge the CNV lesion size and increased inflammation with extracellular matrix dysregulation compared to wild-type mice of the same age (Choudhary et al., 2015).

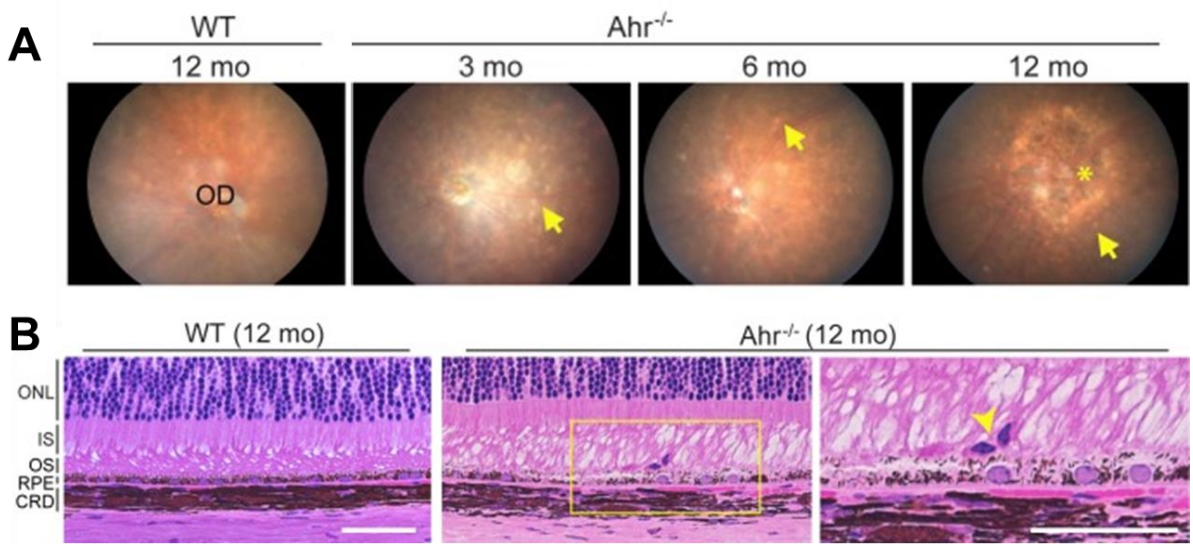

Figure 10 Fundus and histological examination of wild type (WT) and AhR knockout (AhR-/-) mice.
(A) Fundus images of 12 months old WT and 3, 6, and 12 months old AhR-/- mice. Fundi of AhR-/- show yellowish and white spots (arrows) with atrophic regions (asterisk). **(B)** Histological section of WT and AhR-/- of 12 months old mice. Outer segment (OS) of AhR-/- mice shows significantly high number of microglia compared to WT. Figures are taken from Kim et al. (Kim et al., 2014b).

Beneficial effects of AhR ligands have been seen in different animal models of AMD. A synthetic ligand of AhR, 2,2′-aminophenyl indole (2AI) has been reported to protect RPE cells to maintain the retinal homeostasis (Gutierrez et al., 2016), and induced AhR signaling has been shown to reduce the laser-induced CNV in aged mice (Takeuchi et al., 2009; Choudhary et al., 2018). These studies highlighted the importance of AhR signaling pathway and this receptor might be an important

therapeutic target for treatment of such diseases (Choudhary and Malek, 2020). Furthermore, AhR may act as major regulator and may control the AMD pathogenesis through the involvement in inflammation, oxidative stress, apoptosis, ECM dysregulation, lipid metabolism, immune response, angiogenesis, and neurodegeneration (Figure. 11) (Malek and Lad, 2014).

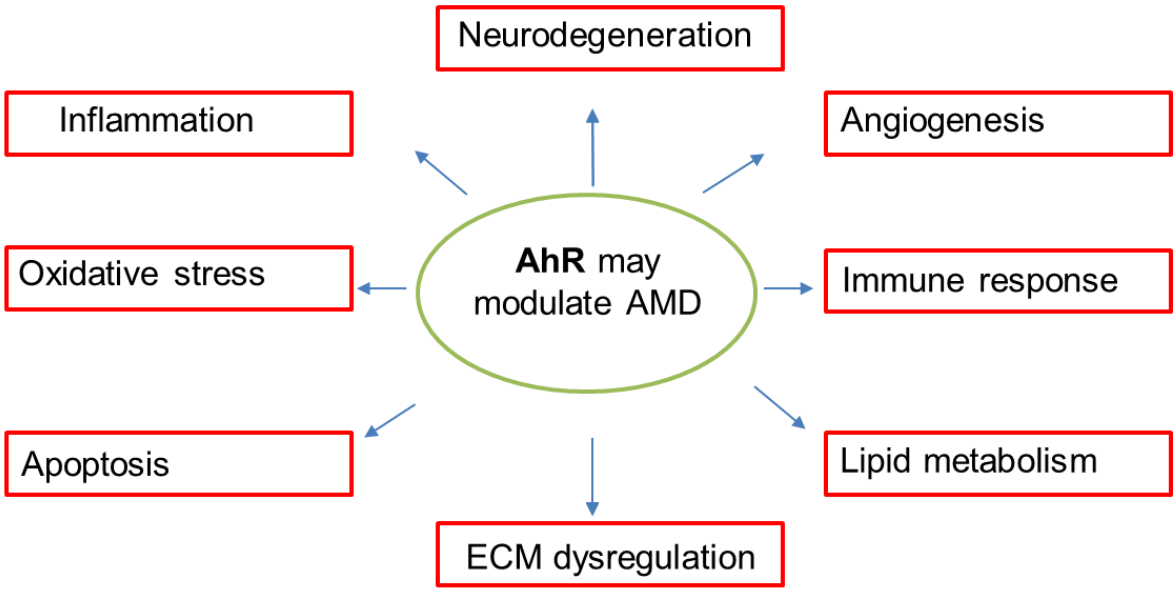

Figure 11 AhR may be important for AMD pathogenic signaling pathways.
AhR may regulate AMD pathogenesis through the involvement in inflammation, oxidative stress, apoptosis, ECM dysregulation, lipid metabolism, immune response, angiogenesis, and neurodegeneration. Figure is adapted from Malek and Lad. (Malek and Lad, 2014).

1.4.7. Microglia modulation through AhR signaling

Microglia cells play a crucial role in the healthy and diseased retina and microglia modulation is an important avenue for AMD treatments (Rashid et al., 2019). Furthermore, AhR is expressed by microglia and AhR has been shown to regulate microglia homeostasis (Lee et al., 2017; Rothhammer & Quintana, 2019). A number of AhR natural ligands are present in food, which are less toxic and easily consumable, such as flavonoid, resveratrol, carotenoids, and indoles (Busbee et al., 2013). In addition, luteolin, quercetin, resveratrol, and curcumin are indirect activators of AhR and have been shown to regulate the AhR activity (Jin et al., 2018; Mohammadi-Bardbori et al., 2012; Zhang et al., 2003). Luteolin, a plant-derived flavone reduced

lipopolysaccharides (LPS)-induced pro-inflammatory and apoptotic gene expression in BV-2 microglia cells (Jang et al., 2008). Luteolin has been shown to reduce microglia-mediated neurotoxicity to photoreceptor cells (Dirscherl et al., 2010). Another flavone quercetin has been shown to reduce LPS-induced pro-inflammatory markers and nitric oxide release. Furthermore, quercetin induced the expression of anti-oxidant genes in microglia cells (Sun et al., 2015). Quercetin has been shown to reduce the LPS-induced microglia activation in the brain (Khan et al., 2018). Resveratrol, a naturally occurring non-flavonoid polyphenol found in red grape seed (red wine)-induced the dynamic changes at transcriptome level and inhibited the inflammatory phenotype in BV-2 and primary microglia cells (Lu et al., 2010; Wiedemann et al., 2018). Curcumin is a lipophilic polyphenol found in the rhizome of the curcuma longa and interacts with AhR. Curcumin potently reduced LPS-induced pro-inflammatory transcripts and microglia-mediated neurotoxicity to photoreceptor cells (Karlstetter et al., 2011).

1.5. Aims of the study

Microglia are important immune cells in the CNS including the retina. Microglia regulate inflammatory responses to reduce neurodegeneration and provide necessary defense against damage and maintain the retinal homeostasis. However, chronic inflammatory responses result in the permanent activation of microglia, which is a major hallmark of retinal degenerative diseases including AMD. Microglia modulation might act as targeted therapy to slow down these diseases. However, new pharmacological targeting to inhibit the microglia activation is highly required for future treatments of retinal degeneration. AhR is also responsible for reducing the external stress through xenobiotic metabolism and AhR activation is important for regulating the immune response. AhR knockout mice have been shown to accumulate activated microglia in SR space and mimicked dry AMD-like phenotype.

Hence, the present study dealt with the understanding of AhR in link with microglia modulation. We aimed on elucidating that the AhR natural agonist I3C may regulate microglia activation to prevent inflammatory responses. For this, potential immunomodulatory and neuroprotective effects of I3C in microglia cell lines, primary microglia, retinal explants cultures, and retinas of light-damage BALB/cJ mice were analyzed.

2 Materials and Methods

2.1. Materials

2.1.1. Cell lines

Table 1 List of cell lines used in this study

Cell line	Origin
BV-2 murine microglia cells	Primary microglia cells were isolated from 1-week old C57BL/6 mice infected with a recombinant retrovirus (V-raf/v-myc) (Blasi et al., 1990).
SV-40 human microglia cells	Applied Biological Materials Inc., Richmond, BC, Canada.
ARPE-19 retinal pigment epithelial cells	RPE is derived from normal eye of a male donor 19-years old (Dunn et al., 1996).
661 W photoreceptor cells	Prof. Muayyad Al-Ubaidi, University of Okalahoma health sciences center, Oklahoma, USA.

2.1.2. Reagents used in cell culture

Table 2 Cell culture reagents used in this study

Cell culture reagents	Manufacturer, Cat. No.
Roswell Park memorial Instituite (RPMI) 1640	Gibco,#21875034
Dulbecco's Modified Eagle Medium (DMEM)	Sigma-Aldrich, #D6429
DMEM F-12	Gibco,#11554546
Dulbecco's Phosphate-Buffered Saline (DPBS)	Gibco, #14190-094
Fetal Calf Serum (FCS)	Gibco, #10270-106
Pennicilin/Streptomycin	Gibco, #15140-122
Trypsin/EDTA	Sigma-Aldrich, #T3924
ß-Mercaptoethanol	Sigma-Aldrich, #M-7154

2.1.3. Cell lines with medium composition

Table 3 Medium for the cells were prepared as indicated

Cells	medium Formula
BV-2	RPMI 4640
	5 % FCS
	1 % Penicillin/Streptomycin
	1% L-Glutamine
	195 nM ß Marceptoethanol
SV-40	DMEM high glucose
	10 % FCS
	1 % Penicillin/Streptomycin
ARPE-19	DMEM/F-12
	10 % FCS
	1 % Penicillin/Streptomycin
661 W photoreceptor	DMEM
	5 % FCS
	1 % Penicillin/Streptomycin

2.1.4. Mice

Table 4 Mouse strain, eye drops, and systemic anesthesia

Mice	Origin and husbandry
BALB/cJ	Animals (male and female) used for this work were housed in an air-conditioned environment at 20-24 °C on a 12 hours light-dark schedule. Mice had full access to food and water ad libitum.
Eye drops	**Manufacturer**
Hylo-Vision Gel sine eye drops	OmniVision
Phenylephrin 2.5 % / Tropicamid 0.5 %	Pharmacy University Hospital Cologne

Anesthetic solution - Formula	Manufacturer
8.5 ml of 0.9 % isotonic NaCl	Fresenius Kabi
1 ml Ketaminehydrochloride (Ketaset)	Zoetis
0.5 ml Xylazinhydrochloride (Rompun)	Bayer HealthCare
0.1 ml /10 g bodyweight used	

2.1.5. Buffers and solutions

Table 5 Buffers and solutions were prepared as indicated

Buffer/Solution	Formula	Manufacturer, Cat. No.
1x PBS, pH 7.4	137 mM Sodium chloride	
	2.7 mM Potassium chloride	Amresco, #E404
	10 mM Disodium phosphate	1 tablet/100 ml dH2O
	1.8 mM Monopotassium phosphate	
1x TBE	1 M Tris, pH 7.5	Roth, #4855.3
	1 M Boric acid	Sigma-Aldrich,#B6768
	20 mM EDTA	Merck, #108421
1x TBS-T	150 mM NaCl	see above
	200 mM Tris	see above
	0.1 % v/v Tween-20	see above
6x Loading dye	60 % v/v Glycerine	Roth, #3783.1
	20 mM EDTA	see above
	0.25 % w/v Bromphenol blue	Sigma-Aldrich,#B-6131
Antibody solution 1	5 % w/v Bovine serum albumin	Roth, #3854.2
	in 1x TBS-T	see above
Antibody solution 2	1x TBS-T	see above
Blotto	1 % w/v Milk powder	Roth, #T145.3
	0.01 % v/v Tween-20 in 1x PBS	Merck, #822184

PBST-X	3 ml Triton X-100	Sigma-Aldrich, #T8787
	in 1L PBS	see above
Membrane blocking buffer	5 % w/v Milk powder in TBS-T	see above
RIPA buffer	50 mM Tris-HCl pH 7.4	see above
	150 mM NaCl	see above
	1 % v/v NP-40	Calbiochem, #492016
	0.5 % w/v Sodium deoxycholate	Sigma-Aldrich, #D6750
	0.1 % w/v Sodium dodecyl sulfate (SDS)	Serva, #20765.03
	2 mM Phenylmethanesulfonyl fluoride (PMSF)	Applichem, #A0999
	cOmplete™ mini protease inhibitor	Roche, #11836153001
Running buffer	192 mM Glycine	AppliChem, #1067
	250 mM Tris	see above
	0.1 % w/v SDS	see above
Tranfer buffer	192 mM Glycine	see above
	250 mM Tris	see above
	20 % v/v Methanol	Chemosolution, #1437.2511
Stripping buffer	192 mM Glycine, pH 2.2	see above
	0.0001 % w/v SDS	see above
	0.01 % v/v Tween-20	see above
PERM/Block buffer	2.5ml Normal Donkey Serum	LINARIS, #ADI-NDKS-10
	0.1 g Bovine serum albumin	see above
	0.15 ml Triton X-100	Sigma-Aldrich, #T8787

2.1.6. Kits

Table 6 Kits used in this study as indicated

Kits systems	Manufacturer, Cat. No.
CellTiter 96® Cell Proliferation Assay	Promega, #G4000
Caspase-Glo® 3/7 Assay	Promega, #G8090
Griess Reagent System	Promega, #G2930
LightCycler® 480 Probes Master	Roche Applied Science, #04707494001
Mouse CCL2/JE/MCP-1Duoset® ELISA	R&D SYSTEMS, # 740955
NucleoSpin® RNA Isolation Kit	Macherey-Nagel, #740955
Pierce™ BCA Protein Assay Kit	ThermoFisher Scientific, #23225
Pierce™ ECL Western Blotting Substrate	ThermoFisher Scientific, #32109
RevertAid RT Kit	ThermoFisher Scientific, #K1691
RNeasy Micro kit	Qiagen, #74004
Takyon™ No Rox Probe 2X MasterMix dTTP	Eurogentec, #-NPMT-B0701
SignalFire™ Elite ECL Reagent	Cell Signaling Technology, #12757

2.1.7. Enzymes and buffers

Table 7 Enzymes and buffers used as indicated

Enzymes and buffers	Manufacturer, Cat. No.
RevertAid H Minus Reverse Transcriptase	ThermoFisher Scientific, Kit#K1622
5x Reaction buffer	ThermoFisher Scientific, Kit#K1622
Proteinase K	Merck Chemicals GmbH, 20-298

2.1.8. Primers and probes

Table 8 Mouse and human primers with probes for qRT-PCR used in this study

Target gene	Forward primer	Reverse primer	Probe #
m i-NOS	5'-ctttgccacggacgagac-3'	5'-tcattgtactctgagggctga-3'	13
m IL-1ß	5′-tcttctttgggtattgcttgg-3′,	5′- tgtaatgaaagacggcacacc-3′	38
m CCL2	5′-catccacgtgttggctca-3	5′-gatcatcttgctggtgaatgagt-3′	62
m IL-6	5′-gatggatgctaccaaactggat-3	5′-ccaggtagctatggtactccaga-3′	6
m NQO1	5′- agcgttcggtattacgatcc-3′	5′- agcgttcggtattacgatcc-3′	50
m HMOX1	5′-agggtcaggtgtccagagaa-3′	5′-cttccagggccgtgtagata-3′	9
m CAT1	5′-ccttcaagttggttaatgcaga -3′	5′-caagtttttgatgccctggt-3′	34
m ATP5B	5′-ggcacaatgcaggaaagg-3′	5'-tcagcaggcacatagatagcc-3'	77
h IL-1ß	5′-tacctgtcctgcgtgttgaa-3′	5′-tctttgggtaatttttgggatct-3′	78
h NLRP3	5′-atccactcctcttcaatgctg-3′	5′-aaagagatgagccgaagtgg-3′	72
h IL-6	5′-gatgagtacaaaagtcctgatcca-3′	5′-ctgcagccactggttctgt-3′	40
h CCL2	5′-agtctctgccgcccttct-3′	5′-gtgactggggcattgattg-3′	40
h IL-8	5′-agacagcagagcacacaagc-3′	5′-cacagtgagatggttccttcc-3′	72
h IL-18	5′-aacaaactatttgtcgcaggaat-3′	5′-tgccacaaagttgatgcaat-3′	46
h NQO1	5′-tcccttgcagagagtacatgg-3′	5′-atgtatgacaaaggacccttcc-3′	21
h HMOX1	5′-ggcagagggtgatagaagagg-3′	5′-agctcctgcaactcctcaaa-3′	15
h CAT1	5′-tcatcagggatcccatattgtt-3′	5′-ccttcagatgtgtctgaggattt-3′	76
h GAPDH	5′-agccacatcgctcagacac-3′	5′-gcccaatacgaccaaatcc-3′	60

2.1.9. Small interfering RNA (siRNA)

Table 9 AhR and negative control siRNAs used in this study

siRNA	Target sequence	Manufacturer, Cat. No.
Mm_AhR_2	agggattaacttctagatgaa	Qiagen, 100205744
Mm_AhR_5	tggcattaagataaagataaa	Qiagen, 102672257
Mm_AhR_6	atggtgcattgtataaacata	Qiagen, 102692501
Mm_AhR_7	atgatttataatgtccttaaa	Qiagen, 1027155139
Negative Control		Qiagen, 1022076

2.1.10. Western blot gels

Table 10 Western blot gels were prepared as indicated

Gels	Formula	Manufacturer, Cat. No.
Running gel	10% v/v Acrylamide	Roth, #A124.1
	0.4 M Tris pH 8.8	see above
	0.1 % w/v SDS	see above
	0.1 % w/v Ammonium persulfate (APS)	Sigma-Aldrich, #A3678
	0.01 % v/v TEMED	Roth, #2367.1
Stacking gel	5 % v/v Acrylamide	see above
	0.125 M Tris pH 6.8	see above
	0.1 % w/v SDS	see above
	0.1 % w/v APS	see above
	0.005 % v/v TEMED	see above

Table 11 List of all antibodies used in this study

Antibodies	Dilution	Manufacturer, Cat. No.
Anti-I-NOS	1:2000	BioSciences, #610329
Anti-IL-1ß	1:200	Santa Cruz Biotechnology, #B122
Anti-IBA 1	1:500	Wako, #01-1074
Anti-p-NFkB p65	1:500	Santa Cruz Biotechnology, #136548
Anti-COX2	1:500	Abcam, #15191
Anti-HMOX1	1:1000	Abcam, #137749
Anti-NQO1	1:500	Santa Cruz Biotechnology, #32793
Anti-p44/42 MAPK	1:1000	Cell Signalling Technology, #4695
Anti-Phospho-p44/42 MAPK	1:2000	Cell Signalling Technology, #4370
Anti-ß-Actin	1:200	Santa Cruz Biotechnology, #47778
Alexa Fluor® 488 (goat anti-rabbit)	1:1000	LifeTechnologies, #A11008
Goat anti-mouse IgG-HRP	1:4000	Agilent Dako, #P0447
Goat anti-rabbit IgG-HRP	1:4000	Agilent Dako, #P0448
DAPI	0.1 µg/ml	Invitrogen, #D1306
Phalloidin-TRITC	1:500	Sigma-Aldrich, #P1951

2.1.11. Compounds and reagents

Table 12 Compounds and reagents used in this study

Compounds and reagents	Manufacturer, Cat. No.
Indole-3-carbinol	Sigma-Aldrich, #I7256-5G
LPS from E. coli :B4	Sigma-Aldrich, #L4391
Phorbol-12-myristate-13-acetate (PMA)	Sigma-Aldrich, #1585
Zymosan A from Saccharomyces cerevisiae	Sigma-Aldrich, #Z4250

β-mercaptoethanol	Sigma-Aldrich, #M-7154
Collagen I, bovine	Gibco, #A10644
Dimethylsufoxid (DMSO)	Serva, #20385.01
Ethanol 70%	Applichem, #A2192
Ethanol	Applichem, #A3678
Fluorescence Mounting Medium	Dako, #S302380-2
Goat Serum	Abcam, #AB7481
HistoFix 4%	Roth, #P087.4
Isopropanol	Merck, #100995
Laemmli sample buffer	Bio-Rad, #161-0747
Lipofectamine™ 3000 Transfection Reagent	ThermoFisher Scientific, L3000015
Methanol	Chemosolution, #1437.2511
PageRuler™ Prestained Protein Ladder	ThermoFisher Scientific, #26616
Polystyrene microparticles	Sigma-Aldrich, #72986
RNase away	Molecular Biopro., #70003
Tissue Tek OCT-Compound	Sakura, #4583
Trypan blue	Biochrom AG, #L6323
VECTASHIELD® HardSet™	Vector Laboratories, #H-1400

2.1.12. General consumables and devices

Table 13 General consumables and devices used as indicated

Consumables	**Manufacturer, Cat. No.**
Amicon® Ultra-15 filter units 30k	Merck, #UFC903008
Biosphere R filter tips 2.5 µL	Sarstedt, #70.1130.212
Biosphere R filter tips 200 µL	Sarstedt, #70.760.211
Biosphere R filter tips 1000 µL	Sarstedt, #70.762.211

Black 96-well microtiter plates	ThermoFischer Scientific #611F96BK
Cell scraper	Sarstedt, #83.1830
Cover glasses 18x18mm	Th.Geyer, #7695023
FrameStar® 384-well plates with seal	4titude, #4ti-0382
Gloves	Dermagrip, #100176
Microtome Blades C35 TYPE	Feather, #207500003
Nitrocellulose membrane 0.45 µm	Bio-Rad, #1620115
Nunc® TripleFlasks	Sigma-Aldrich, #F8542
PCR stripes	Kisker Biotech, #G003-SF
Superfrost Plus™ Microscope Slides	ThermoFischer-Scientific, #J1800AMNZ
Tissue-Tek® Cryomold® Molds	VWR, #R 4557
T75 culture flask	Sarstedt, #83.3911.002
White 96-well microtiter plates	Costar, #3912
1-mL syringe	BD, #309628
20G needle	BD, #301300
30 µl Impact 384 tips	Thermo Scientific, #7431
1.5 ml micro tube	Sarstedt, #72.690
1.5 ml micro tube black	Roth, #AA80.1
2 ml micro tube	Sarstedt, #72.689
15 ml reaction tube	Sarstedt, #62.554.502
50 ml reaction tube	Sarstedt, #62.554.254
6-well cell culture plates	Sarstedt, #83.3920
12-well cell culture plates	Sarstedt, #83.3921

96-well microtiter plates	Sarstedt, #83.3924

Devices	**Manufacturer**
Adventurer Pro balance	Ohaus®
ApoTome.2	Zeiss
AxioCam ICc 1 camera	Zeiss
AxioCam MRm camera	Zeiss
Centrifuge 5415 R	Eppendorf
Centrifuge Mini Star	VWR International
Cryostat CM3050	Leica
Explorer R Ex 124 balance	Ohaus®
Galaxy 170S CO2 incubator	New Brunswick Scientific
Imager. M2 microscope	Zeiss
Infinite®F200 Pro plate reader	Tecan
Light damage device	custom-built
LightCycler® 480 Instrument II	Roche Applied Science
Matrix™ Multichannel Pipette	ThermoFisher Scientific
Mini-Protean® Tetra System	Bio-Rad
MiniTrans-Blot® Cell Module	Bio-Rad
MSC-Advantage hood	Thermo Scientific
MultiImageII	Alpha Innotech
NanoDrop 2000 Spectrophotometer	Thermo Scientific
Neubauer counting chamber	OptikLabor
Orbital incubator S1500	Stuart®
PCR workstation	VWR International
peQSTAR 2x cycler	peQlab

See-saw rocker SSL4	Stuart®
Spectralis™ HRA+OCT	Heidelberg Engineering
Thermomixer compact	Eppendorf
Ultrasonic Liquid Processor	Vibra-Cell™
TW20 watherbath	Julabo
VisiLight® binocular	VWR International
Vortex-genie®	Scientific IndustriesTM

2.1.13. Software

Table 14 Software programs used in this study

Software	**Manufacturer**
AlphaView FluorChem FC2	Cell Biosciences
CSl Adobe Creative Suite	Adobe Systems
GraphPad Prism version 7	GraphPad Software, Inc.
ImageJ 1.50i	National Institutes of Health
LightCycler® 480 software 1.5.1	Roche Applied Science
Mendely	Elsevier
Nanodrop2000/2000c	ThermoFisher Scientific
Office Suite 2010	Microsoft Corporation
Spectralis HRA+OCT Software	Heidelberg Engineering
Tecan i-control 1.9	PerkinElmer
Zen 2012	Zeiss

2.2. Methods

2.2.1. Cell culture

Murine BV-2 and 661 W photoreceptor cells (Table 1) were seeded in T75 flasks and confluent cells were rinsed with PBS and gently scraped off in a fresh medium (Table 3). In addition, human SV-40 and retinal pigment epithelium (ARPE-19) cells were also used (Table 1). SV-40 cells were seeded in collagen-coated T75 flasks. For this, 5 ml collagen (7 µg/cm²) was added in T75 flasks and incubated for 2 hours at room temperature followed by aspiration of collagen. These flasks were stored at 4 °C for further use for 2 weeks. Confluent SV-40 cells were incubated with trypsin (5 ml) for 5 minutes for detaching adherent cells from plates. Trypsin reaction was stopped by adding fresh medium. The cell suspension was transferred to a 50 ml falcon tube followed by centrifugation (800 x g) for 10 minutes to separate the cells from medium containing trypsin. ARPE-19 cells were seeded in T75 flasks and were detached by trypsin treatments similar to SV-40 cells. All cells were split by 1:3 to 1:5 ratio (every second day) in confluence-dependent manner. The appropriate volume of cells was added to 10 ml of warm medium. Mediums were warmed at 37 °C in a water bath before using them. All cell lines were cultured and maintained at 37 °C in a humidified atmosphere of 5% CO_2.

2.2.1.1. Primary microglia extraction

C57BL/6J pups were used for the extraction of primary microglia cells. Heads were cut off, followed by removal of the skin and skull to obtain the whole brain. The entire brains were washed in ice-cold Hanks BSS. Vessels and meninges were also removed from the brains under the microscope. The brains were cut into small pieces with small scissors and transferred to tubes filled with trypsin-EDTA for enzymatic dissociation. This enzyme reaction was performed at 37 °C for 15 minutes. Next, an equal amount of ice-cold FCS with DNase (0.5 mg/ml) was added to the brains. The brains were mechanically dissociated with a 1000-µl pipette tip. This suspension was filtered through a cell strainer followed by centrifugation (500 x g) for 10 minutes at 23 °C. After the removal of supernatants, the pellet was re-suspended in a medium (DMEM containing 10% FCS and 1% penicillin/streptomycin). The cells were seeded in poly D

lysine-coated T75 flasks with the density of three brains per flask. This culture was maintained at 37 °C in a humidified atmosphere with 5 % CO_2. In the next two days, cells were washed with PBS and refreshed with the medium. After 10 to 14 days of cultivation, flasks were shaken at 250 rpm for 1 hour at 37 °C to harvest microglia cells from the adherent astrocytes. The supernatants were transferred to 50 ml falcon and centrifuged (800 x g) for 10 minutes to get the pellet of microglia cells. Cells were counted and seeded in 6-well plates for further experiments.

2.2.1.2. Retinal explants of BALB/cJ mice

10-14 weeks old, BALB/cJ mice were sacrificed by cervical dislocation and the whole eyes were removed with curved forceps. The eyes were placed in a petri dish with PBS and retinas were isolated. These retinas were incubated with a medium (DMEM F-12 with 1% PBS).

2.2.1.3. Cell culture treatments

BV-2, primary microglia, and retinal explants of BALB/cJ mice were seeded in culture plates treated with 50 µM I3C for 4 hours and followed by 4 hours treatment with 50 ng/ml LPS. SV-40 cells were cultured and treated with 50 µM I3C for 4 hours followed by 100 nM PMA and 50 µg/ml Zymosan (Zym) for 4 hours. I3C was diluted in DMSO that served as solvent control.

2.2.2. RNA extraction and quantification

Total RNA was extracted from the cells using the NucleoSpin® RNA Mini Kit, according to the manufacturer's instructions. Total RNA from retinas of BALB/cJ mice was extracted using the Qiagen RNeasy Micro Kit according to the manufacturer's instructions as well. Retinas were homogenized with sonication. Cells were washed with PBS and RA1 lysis buffer was used for cell lysis. This buffer inactivates RNASE activity and provides the appropriate binding conditions to RNA in silica membrane. DNA, which also binds to the silica membrane, was degraded with DNase. Excessive salts and metabolites were removed with desalting and washing buffers. Finally, RNase free water was added to elute the RNA. RNA concentration was quantified with

a NanoDrop 2000 spectrophotometer. 260/280 ratio of 2.0 is considered as pure RNA and used for reverse transcription.

2.2.2.1. Reverse transcription

First stand complementary DNA (cDNA) synthesis was performed using the Thermo RevertAid RT Kit. 0.1 ng to 5.0 µg of RNA can be transcribed with this kit. RiboLock RNase inhibitor protects the template RNA from degradation. cDNA was stored at -20 °C for further use.

2.2.2.2. Quantitative real time PCR (qRT-PCR)

qRT-PCR analysis was performed with the Takyon™ qPCR Kit and the Roche Probe library using the LightCycler® 480 II machine. Roche probe consists of the fluorescent reporter and quencher. Once the reaction starts, the probe binds to the target sequence and leaves the fluorophore unquenched. The intensity of fluorophore increases with the upregulation of the target gene. qRT-PCR was performed in 10 µl final volume by combining the reaction components (Table 15). The reaction mixture was incubated at 95 °C to activate polymerase activity followed by 40 cycles of amplification (Table 16).

Table 15 Reaction components used in qRT-PCR

Reaction components	
Template DNA	25-50 ng
Forward primer	1 µM
Reverse primer	1 µM
Roche probe	125 nM
LightCycler® 480 Probes Master	5 µL
dH_2O	Up to 10 µL

Table 16 qRT-PCR cycling conditions

PCR step	Temperature	Time	
Initial denaturation	95 °C	5 minutes	
Denaturation	95 °C	15 seconds	40 cycles
Annealing	60 °C	1 minute	
End			

2.2.3. Protein extraction and quantification

Cells were incubated with RIPA buffer supplemented with protease inhibitor cocktail for 30 minutes on ice to extract the cell lysates. Samples were centrifuged at maximum speed for 15 minutes at 4 °C. Supernatants were transferred to ice-cold tubes. Mouse retinas were homogenized in PBS using sonication. Insoluble debris was removed by centrifugation for 30 minutes at maximum speed and supernatants were taken. Protein quantification was determined using the PierceTM Bicinchoninic Acid (BCA) Protein Assay Kit. Proteins can reduce the Cu+2 to Cu+1 in biuret reaction resulting in purple color due to the bicinchoninic acid. Infinite® F200 Pro plate reader (Tecan) at wavelength of 562nm, spectrophotometrically determines the change in color that indicates the protein quantity. The BSA reference curve was used to calculate the protein concentration.

2.2.3.1. ELISA and Western blot

The concentration of CCL2 in total retinal lysates was measured using ELISA according to the manufacturer's instructions (Mouse CCL2/JE/MCP-1 DuoSet ELISA). In Western blot, for denaturation, Laemmli buffer was added to protein samples (cell or tissue lysate) and incubated for 95 °C for 10 minutes. Equal amounts of protein (~20 µg) and pre-stained protein ladder were separated by sodium dodecyl sulfate–polyacrylamide gel electrophoresis (SDS-PAGE) on 10 % gels at 100 volts (V) for 120 minutes. Subsequently, proteins were transferred onto 0.45 µm nitrocellulose membranes at 4 °C at 100 V for 100 minutes. The membranes were incubated in blocking solution for 1 hour, to prevent unspecific binding. After washing steps, membranes were incubated with primary antibodies (Table 11) for overnight at 4 °C. The next day, the membranes were washed with TBS-T for 5 minutes for three times followed by incubation with secondary antibodies for 1 hour at room temperature (Table

11). The blots were visualized with SignalFire™ Elite ECL reagent and MultiImage II system (Alpha Innotech, Santa Clara, CA, USA). The band intensities were quantified using Image J software (NIH).

2.2.4. Nitric oxide (NO) assay

Nitric oxide concentrations were determined using the Griess reagent system (Promega). 50-µl cell culture supernatants of BV-2 microglia cells were incubated with 50-µl sulfanilamide in 96 well microtiter plate for 20 minutes at room temperature and protected from light. Moreover, 50 µl of NED solution (N-1-napthylethylenediamine dihydrochloride under acidic conditions) was added. After 10 minutes of incubation at room temperature, absorbance was measured at 540 nm on an Infinite®F200 Pro plate reader (Tecan). Nitrite concentrations were calculated by comparison with the absorbance to nitrite standard reference curve as described (Scholz et al., 2015b).

2.2.5. Caspase 3/7 assay

To determine microglia neurotoxicity, a culture system of 661 W photoreceptor cells with the microglia-conditioned medium was established. 661 W photoreceptor cells were incubated for 48 hours either in their own medium or with culture supernatants from treated BV-2 cells. The 661 W photoreceptor cells morphology was assessed by phase-contrast microscopy. Caspase-Glo® 3/7 assay kit was used to determine the caspase 3/7 activities as described (Scholz et al., 2015b).

2.2.6. Phagocytosis assay

BV-2 microglia cells were pre-treated with 50 µM I3C for 2 hours and followed by 50 ng/ml LPS for 2 hours. After treatments, 2-µl latex bead solution (Polystyrene microparticles) was added to the wells for 4 hours. Five micrographs per well were taken using an AxioVert.A1 inverted microscope. The phagocytic activity was determined by calculating the number of cells, which phagocytosed 10 or more latex beads.

2.2.7. Scratch wound healing assay

BV-2 microglia cells were seeded in six-well plates as 80-90% confluent monolayers and were scratched with a sterile 200-µl pipette tip. Thereafter, the cells were treated with 50 µM I3C and 50 ng/ml LPS. Migration of cells into the open scar was documented with microphotographs taken after 8 hours of scratching using an AxioVert.A1 inverted microscope.

2.2.8. Morphological analysis

BV-2 microglia cells were seeded on coverslips in six-well plates. Cells were treated as described in section 2.2.1.3. Thereafter, the cells were fixed with 4% HistoFix and washed with PBS. Next, cells were permeabilized with 0.1% Triton X-100 followed by F-actin was labeled using 0.1 µg/ml Phalloidin-TRITC in the dark. The nuclei were stained using 4′,6-diamidino-2-phenylindole (DAPI), and coverslips were mounted onto slides using the Dako fluorescent mounting medium. Photos were taken with a Zeiss Imager M.2 equipped with Apotome.2.

2.2.9. siRNA-mediated AhR gene silencing

BV-2 microglia cells were seeded in 12-well plates for overnight. Next day, 30 minutes before the transfection, cells were washed with DPBS and the medium was changed with Opti-MEM I reduced serum media. The cells were transfected with siRNAs (AhR and the negative control siRNAs). All transfections were performed with lipofectamine 3000 for 6 hours followed by medium refreshment and cells were further incubated for 48 hours. During this incubation time, cells were treated with 50 µM I3C and 50 ng/ml LPS.

2.2.10. Murine Model of dry AMD

2.2.10.1. Light-induced retinal damage

All in vivo experiments were performed with 8-10 week old BALB/cJ mice of both sexes. The animals were kept in an air-conditioned environment with 12-h light and dark cycle and had full access to water and food ad libitum. All experimental

procedures followed ARVO Statement for the Use of Animals in Ophthalmic and Vision Research. The animal protocols were approved by government office of animal welfare in North Rhine-Westphalia, Germany (reference number 81-02.04.2019.A092). Mice were divided into three groups, such as untreated, vehicle plus light, and I3C plus light. The mice received intraperitoneal injections of I3C at a dose of 15 mg/kg body weight, dissolved in DMSO or DMSO alone as vehicle control, starting 1 day before the light damage and then once daily for the remaining 3 days. Before light exposure, BALB/cJ mice were dark-adapted for 16 hours. After dark adaptation, Pupil dilation was induced by topical application with 2.5% phenylephrine and 0.5% tropicamide under dim red light before the mice were exposed to bright white light (15,000 lux) for 1 hour. After light exposure, the animals were kept in dark-reared conditions overnight and then maintained under normal light conditions (12-hours light and dark cycle) for the remaining experimental period.

2.2.10.2. Retina preparation

BALB/cJ mice were sacrificed by cervical dislocation and the eyes were enucleated with curved forceps by putting pressure around eyes. Eye bulbs were removed by disconnecting the optic nerve from the tissue behind it. Eyes were washed in PBS and placed in a petri dish filled with PBS. With a micro scissor, the cornea was cut and lens was removed. Next, the retina was detached by cutting the choroid/sclera attached to the retina. Finally, the optic nerve was also cut to free the retina from the RPE. These retinas were further used in experiments.

2.2.10.3. Preparation of retinal flat mounts and immunohistochemistry

Enucleated eyes were fixed with 4% paraformaldehyde for 2 hours at room temperature. Retinal flat mounts were prepared and incubated overnight with PERM/Block buffer for permeabilization and to block non-specific antigen binding. Subsequently, retinal flat mounts were incubated with primary antibody (rabbit anti-IBA 1) for overnight at 4 °C (Table 11). After washing steps, the retinal flat mounts were incubated with secondary antibody (goat anti-rabbit) for 1 hour at room temperature (Table 11). After washing steps, retinal flat mounts were mounted on a microscopic slide and embedded with fluorescence mounting medium (VECTASHIELD®

HardSet™ Antifade Mounting Medium H-1400). Images were taken with a Zeiss Imager M.2 equipped with Apotome.2.

2.2.10.4. Preparation of retinal cryosections and immunohistochemistry

For immunohistochemical analyses of cryosections, enucleated eyes were fixed with 4% paraformaldehyde for 2 hours at room temperature. Whole eyes were incubated with 30% sucrose overnight. Next, the eyes were embedded in TissueTek optimal cutting temperature (OCT) compound and shock frozen on dry ice. 10 µm sections of eyes were obtained with a cryostat. Sections were mounted on microscopic slides and stored at -20 °C. Sections were thawed at room temperature and rehydrated with PBS for 10 minutes. Sections were blocked with BLOTTO (1% milk powder and 0.3% Triton X-100 in PBS) for 1 hour followed by incubation with primary antibody (rabbit anti-IBA 1) (Table 11) at 4 °C for overnight. Next day, after washing steps, sections were incubated with secondary antibody (goat anti-rabbit) for 1 hour at room temperature (Table 11). Sections were kept in the dark because secondary antibody was fluorescently labelled. After washing steps, the sections were mounted with Flouromount and counterstained with Dapi at room temperature. Images were taken with a Zeiss Imager M.2 equipped with Apotome.2.

2.2.10.5. Spectral domain-optical coherence tomography (SD-OCT)

For SD-OCT, mice were anesthetized by intraperitoneal injection of ketamine hydrochloride and xylazine hydrochloride, diluted in sodium chloride solution (Table 4). Before SD-OCT, the pupil dilation was induced by topical application of 2.5% phenylephrine and 0.5% tropicamide. SD-OCT was performed on both eyes with a Spectralis™ HRA/OCT device to quantify the retinal thickness using the Heidelberg Eye Explorer Software with circular ring scans (circle diameter 3 and 6 mm), centered around the optic nerve head.

2.2.11. Statistical analysis

Data were analyzed using GraphPad Prism version 7. All data were analyzed using analysis of variance (one-way ANOVA) and Dunnett's multiple comparison test. $p < 0.05$ was considered as statistically significant.

3 Results

3.1. I3C inhibited pro-inflammatory and enhanced the anti-oxidant mRNA expression levels in BV-2 cells

Firstly, to examine the effects of AhR ligand I3C on the pro-inflammatory gene expression, BV-2 microglia cells were pre-treated with 50 µM I3C for 4 hours and then stimulated with 50 ng/ml LPS for additional 4 hours. LPS binds to toll-like receptor 4 (TLR-4) and enhances pro-inflammatory responses in BV-2 microglia (Scholz et al., 2015b; Fiebich et al., 2018). LPS stimulation induced mRNA expression levels for inducible-nitric oxide synthase *(i-NOS)* (Figure. 12A), interleukin-1ß (*IL-1ß)* (Figure. 12B), NLR family pyrin domain containing 3 *(NLRP3)* (Figure. 12C), interleukin-6 (*IL-6)* (Figure. 12D), and chemokine (C-C motif) ligand 2 *(CCL2)* (Figure. 12E) and treatment with I3C significantly reduced the expression of these pro-inflammatory genes (Figure. 12A-E). Since the AhR ligands are known to have anti-oxidant properties (Busbee et al., 2013; Dietrich, 2016). mRNA expression levels of NADH quinone oxidoreductase 1 (*NQO1)* (Figure. 12F), heme oxygenase 1 (*HMOX1)* (Figure. 12G), and catalase 1 (*CAT1)* (Figure. 12H) were also measured by qRT-PCR. Treatments with I3C and LPS significantly enhanced these mRNA levels (Figure. 12F-H). Taken together, I3C inhibited LPS-induced pro-inflammatory and enhanced the anti-oxidant gene expression in BV-2 microglia cells.

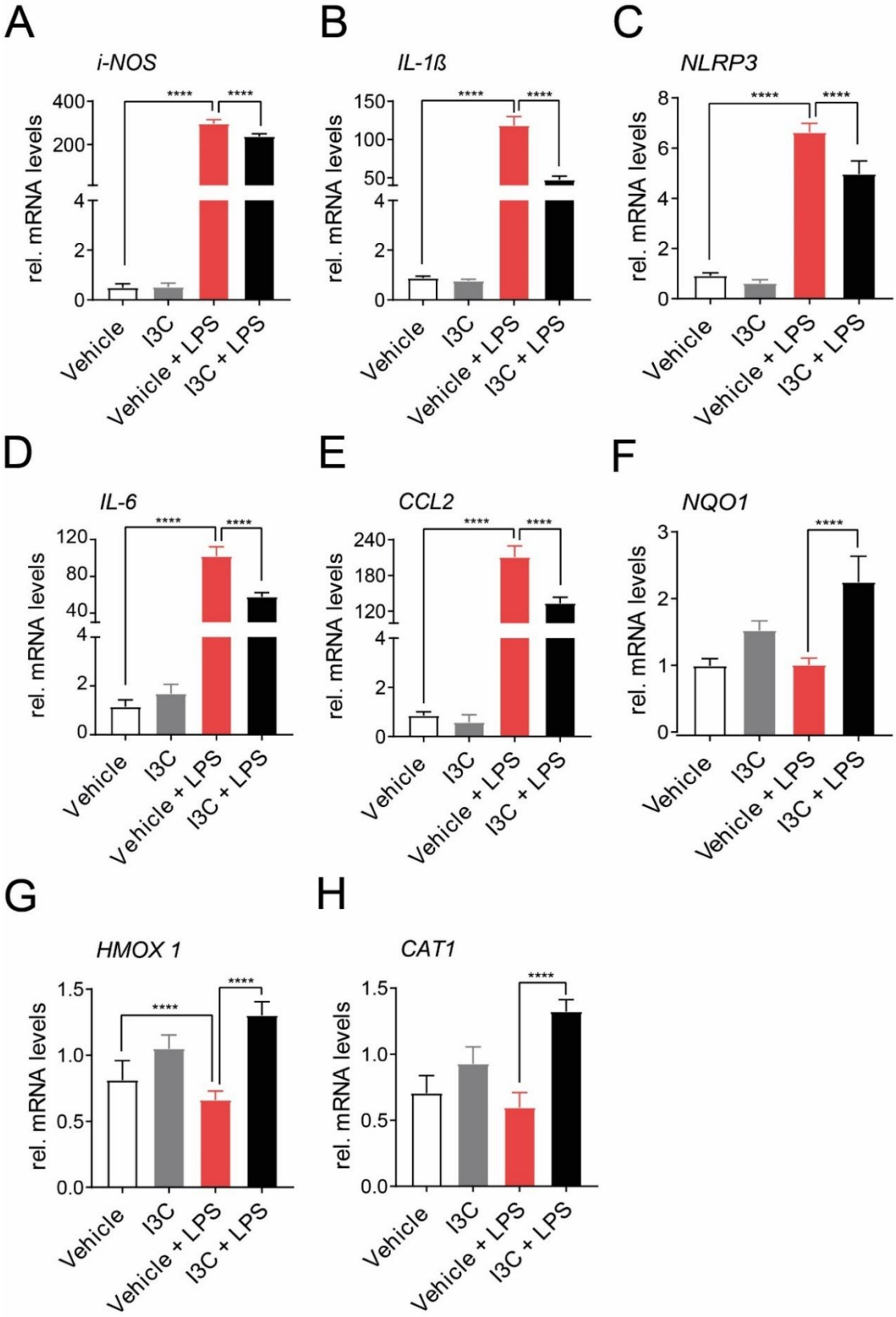

Figure 12 Effects of I3C on pro-inflammatory and anti-oxidant mRNA expression levels in BV-2 cells.

(A-H) BV-2 microglia cells were treated with 50 µM I3C or DMSO as a vehicle for 4 hours followed by 50 ng/ml LPS for 4 hours. After 8 hours, mRNA expression levels of *i-NOS* (A), IL-*1ß* (B), *NLRP3* (C), *IL-6* (D), *CCL2* (E), *NQO1* (F), *HMOX1* (G) and *CAT1*

(H) were analyzed by real-time PCR. Data show mean ± SEM out of three independent experiments (n = 3/group, measured in triplicates) with * p = 0.0127 and ****p < 0.0001.

3.1.1. I3C regulated the pro-inflammatory and anti-oxidant protein levels in BV-2 cells

To further analyze the effects of I3C at protein levels, western blots were performed. Western blot results revealed that the LPS-induced pro-inflammatory i-NOS, IL-1ß, cyclooxygenase 2 (COX2), and phosphorylated-extracellular signal-regulated kinase 1/2 (P-ERK1/2) protein levels compared to vehicle (Figure. 13A-C). I3C significantly reduced these levels (Figure. 13A-C). Whereas, I3C increased HMOX1 protein level. However, NQO1 was unchanged (Figure.13A, D). Taken together, treatment with I3C reduced LPS-mediated i-NOS, IL-1ß, COX2, P-ERK1/2, and enhanced HMOX1 protein levels in BV-2 microglia cells.

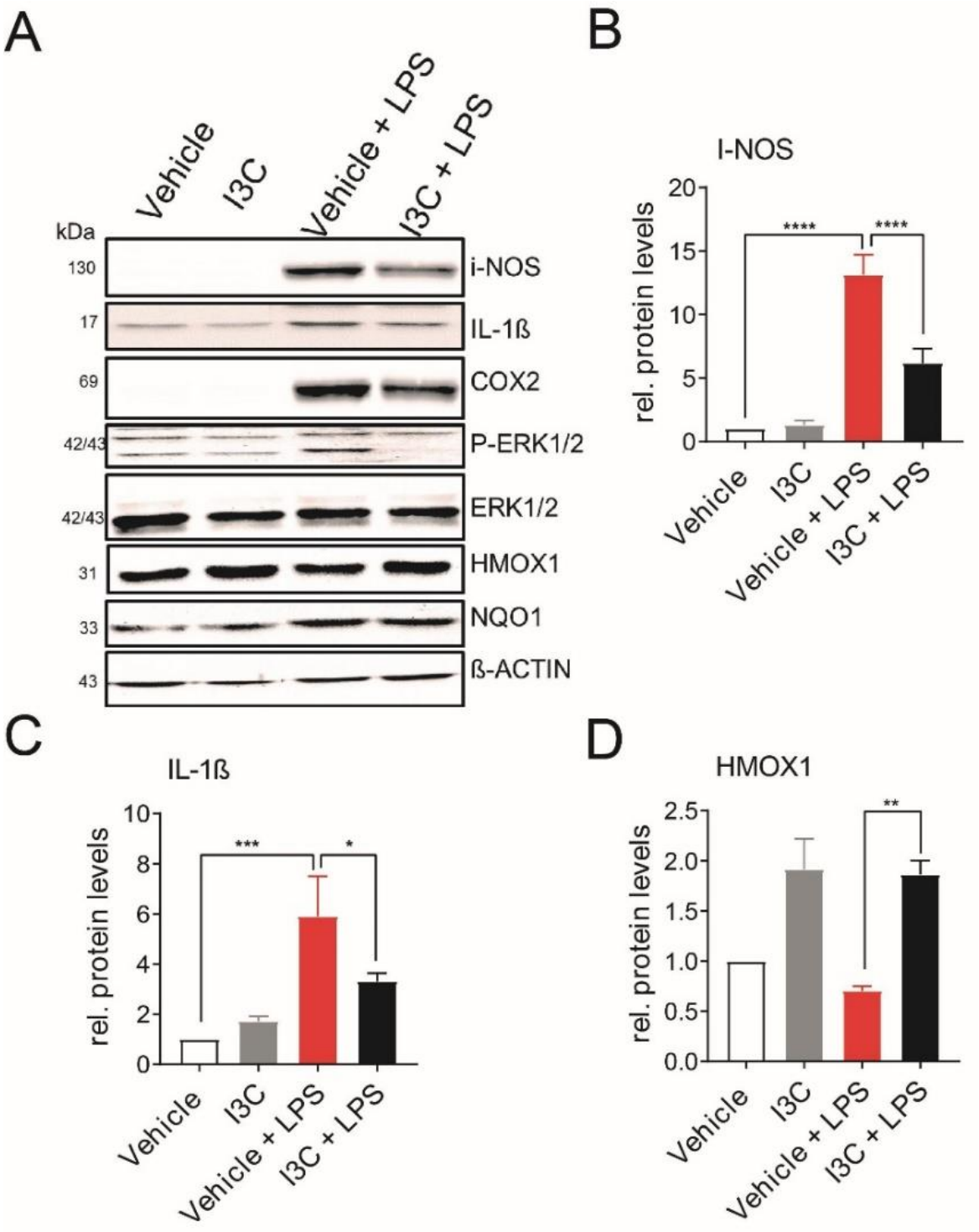

Figure 13 Effects of I3C on pro-inflammatory and anti-oxidant protein levels in BV-2 cells.

(A-D) BV-2 microglia cells were treated with 50 µM I3C or DMSO as a vehicle for 4 hours followed by 50 ng/ml LPS for 4 hours. (A) Western blot results show i-NOS, IL-1ß, COX2, P-ERK1/2, ERK1/2, HMOX1, NQO1, and ß-Actin protein levels. Mean relative protein levels of i-NOS (B), IL-1ß (C), and HMOX1 (D) are shown. Data show mean ± SEM out of three independent experiments (n = 3/group, measured in triplicates) with * p = 0.0127, **P = 0.0016 and ****p < 0.0001.

3.1.2. I3C reduced LPS-induced nitric oxide secretion and neurotoxicity

Next, the influence of I3C on the functional parameters of BV-2 microglia, such as nitric oxide (NO) secretion and microglia-mediated neurotoxicity to photoreceptor cells were analyzed. LPS induced NO secretion and I3C significantly reduced this induction in BV-2 microglia cells (Figure. 14A). To analyze the neurotoxicity, supernatants of treated BV-2 cells were incubated with 661 W photoreceptor cells for 48 hours. Supernatants of LPS-treated microglia induced the caspase 3/7 activity in 661 W photoreceptor cells and I3C significantly reduced this activity (Figure. 14B). Taken together, I3C reduced the NO secretion in BV-2 cells and microglia-mediated neurotoxicity to 661 W like photoreceptor cells.

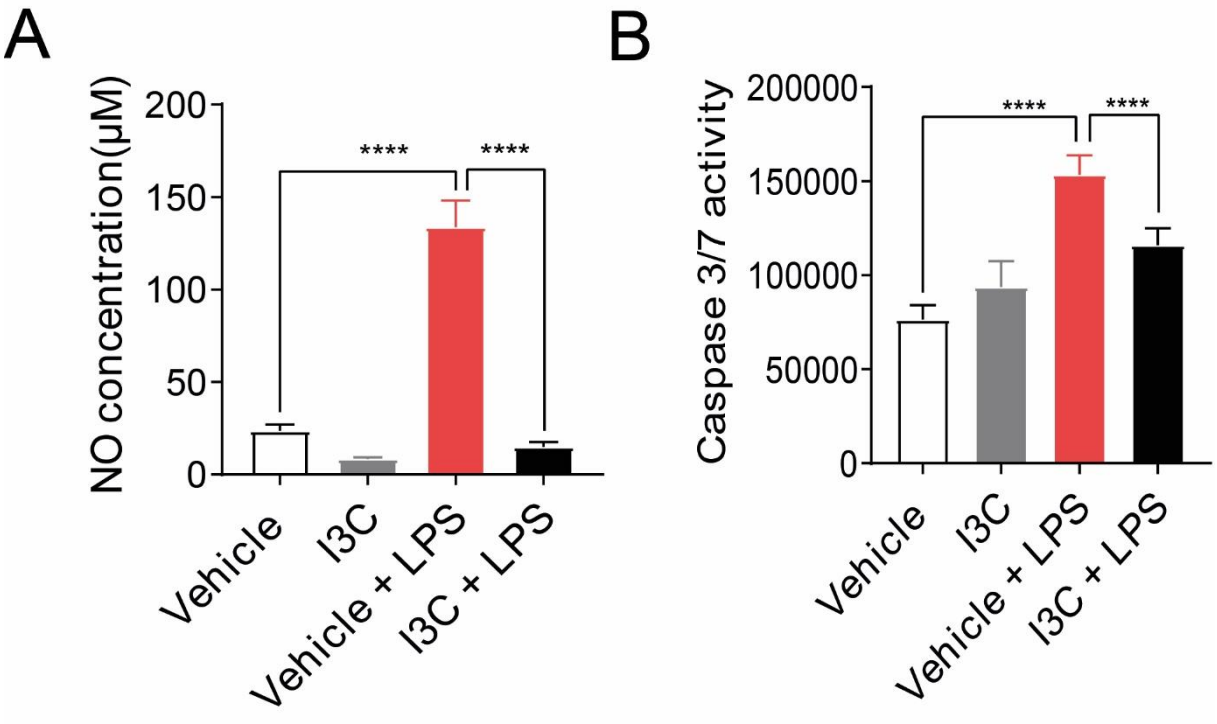

Figure 14 Effects of I3C on LPS-induced nitric oxide (NO) and caspase 3/7 activity. BV-2 microglia cells were treated with 50 µM I3C or DMSO as a vehicle for 4 hours followed by 50 ng/ml LPS for 4 hours. **(A)** After 24 hours, cell culture supernatant was taken for measuring the concentration of NO by Griess assay. **(B)** To determine the neurotoxicity, supernatants of BV-2 microglia cells were added to 661 W photoreceptor cells. After 48 hours, caspase 3/7 activity was measured to analyze the apoptotic cell death. Data show mean ± SEM out of three independent experiments (n = 3/group, measured in triplicates) with ****$p < 0.0001$.

3.1.3. I3C reduced the LPS-induced phagocytosis of BV-2 microglia cells

To analyze the effects of I3C on phagocytosis, BV-2 microglia cells were treated with I3C and LPS for 4 hours and then latex polystyrene beads (10 µm in size) were added for an additional 4 hours. LPS enhanced the phagocytosis of beads in BV-2 microglia cells and I3C significantly reduced this phagocytic capacity (Figure. 15A-B).

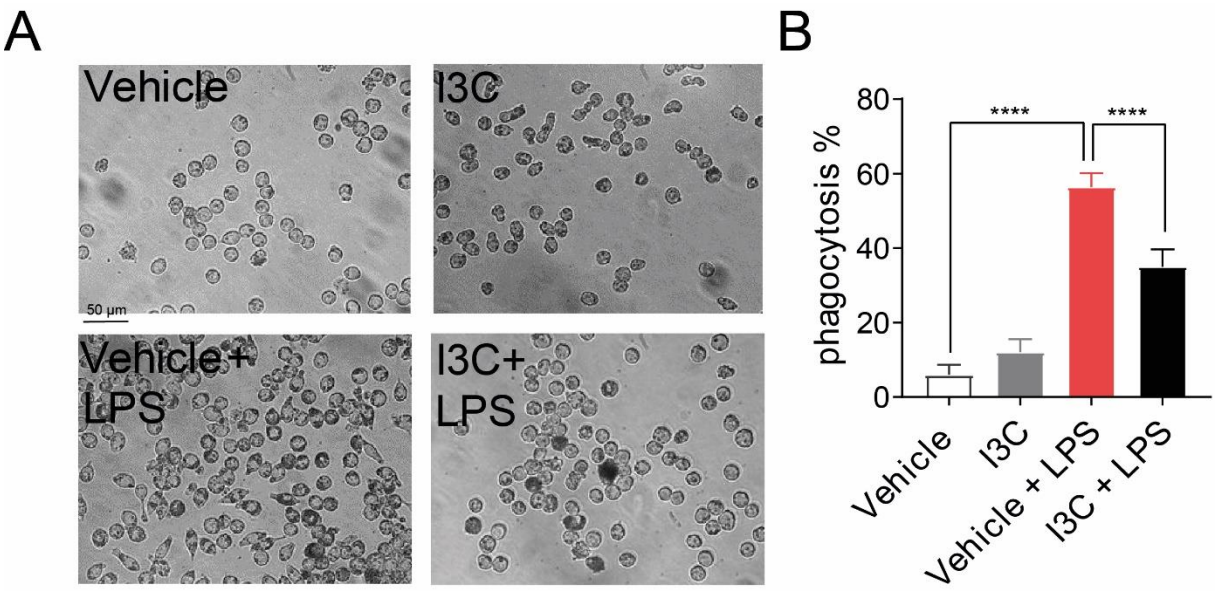

Figure 15 Effects of I3C on LPS-induced phagocytosis of BV-2 microglia cells.
BV-2 microglia cells were treated with 50 µM I3C and 50 ng/ml LPS for 4 hours followed by incubation with polystyrene beads for 4 hours. **(A)** Representative images of microglia incubated with polystyrene beads after treatments. (**B)** Relative phagocytosis of BV-2 microglia cells was calculated by counting cells having more than 10 latex beads and scale bar is 50 µm. Data show mean ± SEM out of three independent experiments (n = 3/group, measured in triplicates) with ****$p < 0.0001$.

3.1.4. I3C reduced the LPS-induced migration of BV-2 microglia cells

Next, to analyze the effects of I3C on microglia cells migration, wound-healing scratch assays were used. Treatment with LPS induced the migration of BV-2 microglia cells into the scratched area and I3C effectively blocked this migration (Figure. 16).

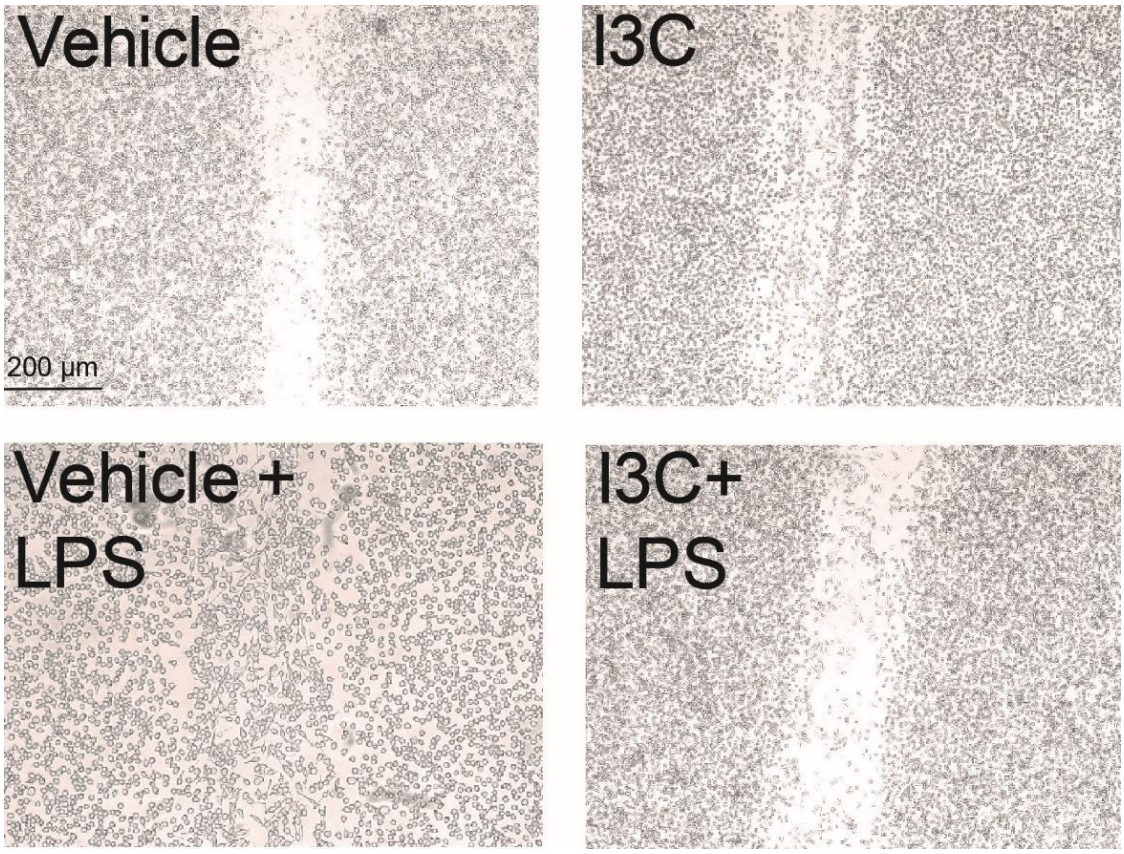

Figure 16 Effects of I3C on LPS-induced migration of BV-2 microglia cells.
BV-2 microglia cells were treated with 50 µM I3C or DMSO as a vehicle for 4 hours followed by 50 ng/ml LPS after scratch with a sterile pipette tip. Representative images of microglia migration towards scratch area are taken with a microscope after 8 hours and scale bar is 200 µm (n = 3/group, measured in triplicates).

3.1.5. I3C induced the protective phenotype in BV-2 microglia cells

The morphology is a hallmark of microglia activation. BV-2 microglia cells were treated with I3C and LPS. Subsequently, F-actin cytoskeleton was stained with Phallodin-TRITC to analyze the morphology of cells. LPS induced the amoeboid phenotype and I3C clearly transformed this amoeboid phenotype into ramified with most of cells containing long filopodia (Figure. 17).

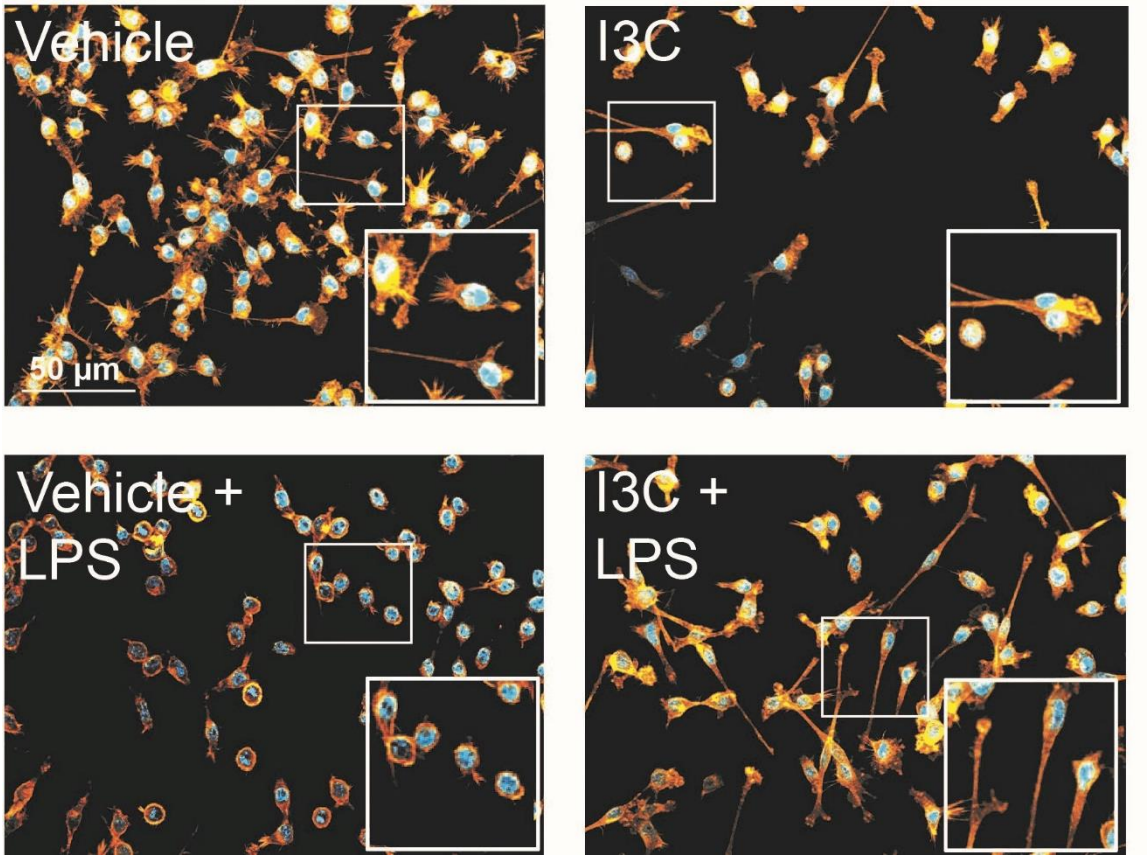

Figure 17 Effects of I3C on morphology of BV-2 microglia cells.
BV-2 microglia cells were treated with 50 µM I3C or DMSO as a vehicle followed by 50 ng/ml LPS. Representative fluorescence images of the BV-2 microglia morphology stained with phalloidin and DAPI (blue) and higher magnification inserts show the differences in microglia ramifications. Scale bar is 50 µm (n = 3/group, measured in triplicates).

3.1.6. AhR pathway is involved in the anti-inflammatory effects of I3C in BV-2 microglia cells

To further investigate the AhR signaling pathway in regulation of pro-inflammatory gene levels, siRNA-mediated knockdown of *AhR* was executed in BV-2 microglia cells. The cells were treated with *AhR* siRNA or negative control siRNA. siRNA-mediated knockdown of *AhR* reduced the *AhR* mRNA (Figure. 18A). Treatment with *AhR* siRNA transfected cells with I3C plus LPS increased *i-NOS* (Figure. 18B), *IL-1ß* (Figure.18C), and *NLRP3* compared to negative control (Figure.18D). However, *IL-6* mRNA expression levels were not changed in the presence of *AhR* siRNA (Figure. 18E). Taken together, siRNA-mediated knockdown of *AhR* partially prevented the anti-inflammatory response of I3C on LPS-activated BV-2 microglia cells.

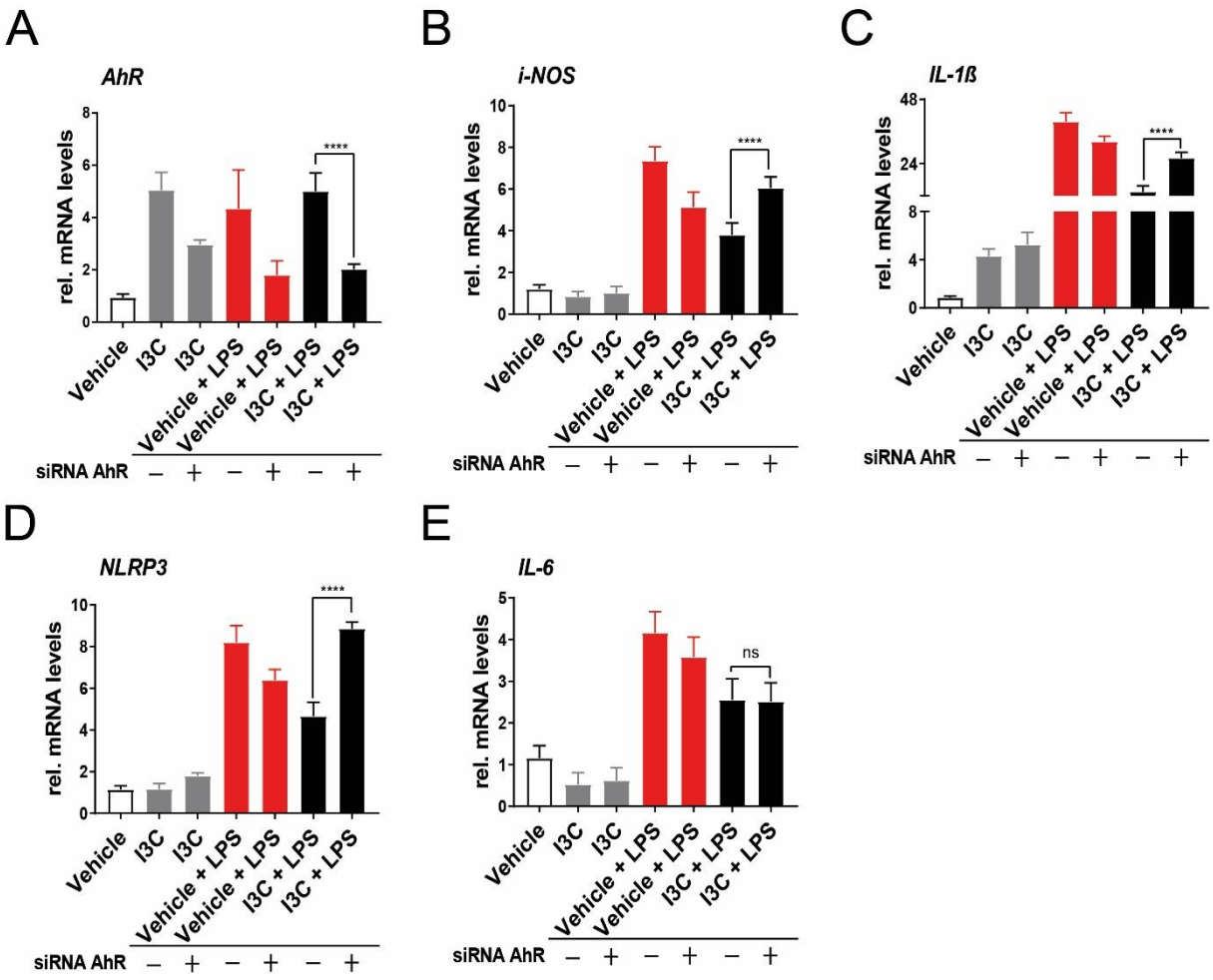

Figure 18 Effects of *AhR* knockdown on pro-inflammatory gene levels in BV-2 microglia cells.

Cells were transfected with siRNAs (AhR or negative control) for 6 hours followed by treatment with I3C and LPS. **(A-E)** mRNA expression levels of *AhR* (A), *i-NOS* (B), *IL-1ß* (C), *NLRP3* (D), and *IL-6* (E) were analyzed by real-time PCR. Data show mean ± SEM out of three independent experiments (n = 3/group, measured in triplicates) with ****$p < 0.0001$.

3.2. I3C regulated pro-inflammatory and anti-oxidant mRNA expression levels in SV-40 cells

Next, effects of I3C on a selected set of pro-inflammatory and anti-oxidant markers in immortalized human microglia cells (SV-40) were examined. For this, SV-40 cells were pre-treated with 50 µM I3C for 4 hours followed by 100 nM phorbol 12-myristate 13-acetate (PMA) and 50 µg/ml Zymosan (Zym). PMA is a protein kinase C activator, which enhances the translocation of NF-kB into the nucleus. Zym is a glucan and binds to dectin-1 receptor. PMA and Zym enhance microglia activation and both are strong

pro-inflammatory stimuli for SV-40 cells (Madeira et al., 2018). Treatments with PMA plus Zym enhanced the *IL-1ß* (Figure. 19A), *NLRP3* (Figure. 19B), *IL-6* (Figure. 19C), *CCL2* (Figure. 19D), interleukin-8 (*IL-8)* (Figure. 19E), and interleukin-18 (*IL-18)* (Figure. 19F) mRNA levels compared to vehicle. I3C significantly reduced PMA plus Zym-induced *IL-1ß*, *NLRP3*, and *IL-6* mRNA levels (Figure. 19A-C). However, I3C did not reduce PMA and Zym-induced *CCL2*, *IL-8*, and *IL-18* mRNA levels (Figure. 19D-F). Furthermore, I3C induced *NQO1* (Figure. 18G), *HMOX1* (Figure. 18H), and *CAT1* mRNA levels (Figure. 18I) in SV-40 cells.

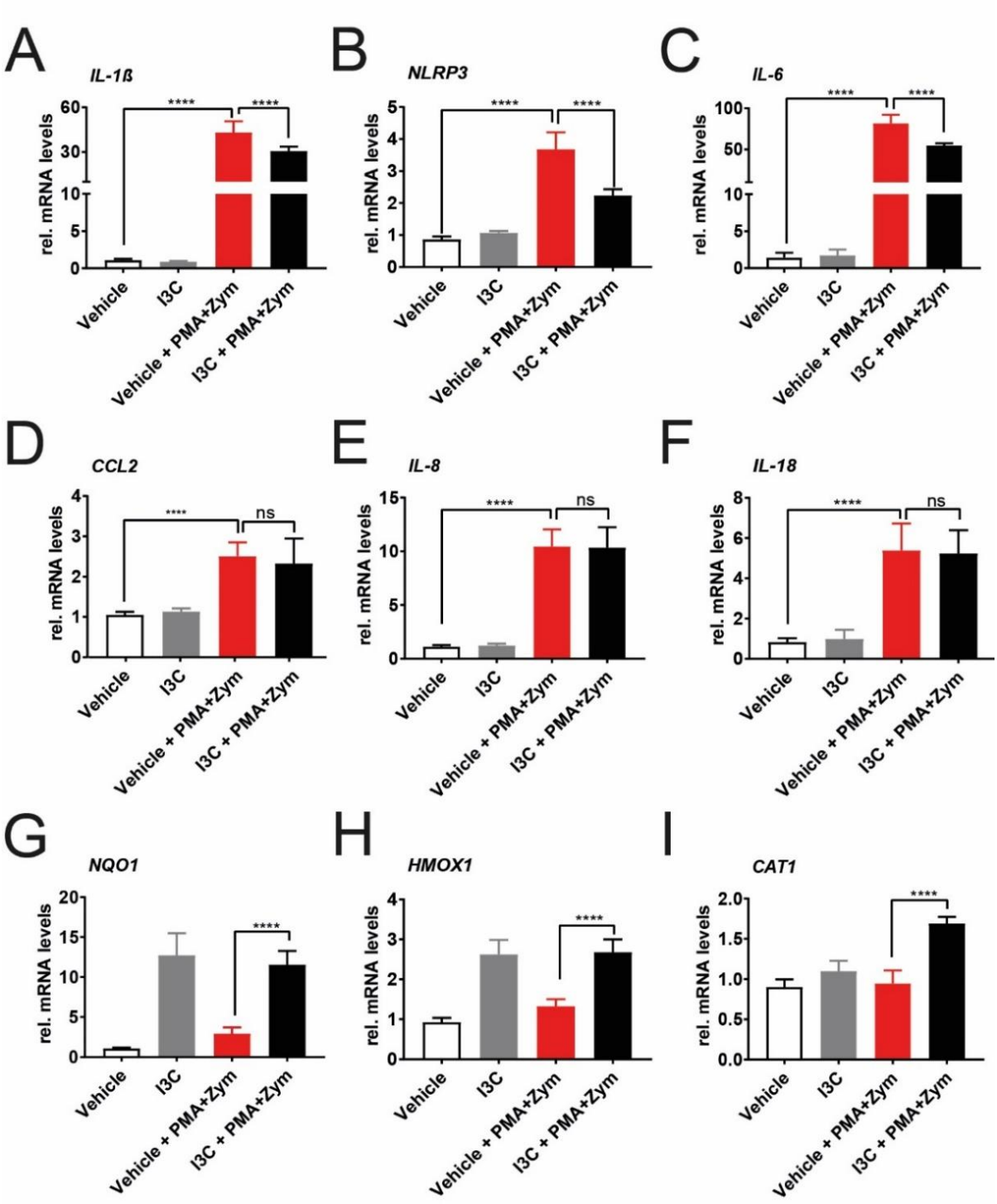

Figure 19 Effects of I3C on pro-inflammatory and anti-oxidant mRNA expression levels in SV-40 cells.

(A-H) SV-40 microglia cells were treated with 50 µM I3C for 4 hours followed by 100 nM PMA and 50 mg/ml Zym for 4 hours. After 8 hours, mRNA expression levels of *IL-1ß* (A), *NLRP3* (B), *IL-6* (C), *CCL2* (D), *IL-8* (E), *IL-18* (F), *NQO1* (G), *HMOX1* (H), and *CAT1* (I) were analyzed by real-time PCR. Data show mean ± SEM out of three independent experiments (n = 3/group, measured in triplicates) with ****$p < 0.0001$.

3.3. I3C did not regulate BV-2 microglia-mediated neurotoxic effects in ARPE-19 cells

Microglia mediated inflammatory responses enhance degeneration of RPE, which is a hallmark of AMD (Rashid et al., 2018). Previously, supernatants of activated microglia have been shown to enhance the pro-inflammatory markers in ARPE-19 cells (Nebel et al., 2017; Rashid et al., 2020). In the present study, BV-2 microglia cells were treated with I3C for 4 hours followed by LPS for another 4 hours. Supernatants of these cells were incubated with ARPE-19 cells to analyze the microglia-mediated pro-inflammatory effects. In ARPE-19 cells, supernatants of LPS-treated BV-2 microglia cells enhanced *IL-1ß* (Figure. 20A) and *CCL2* (Figure. 20C) mRNA expression levels compared to vehicle. However, supernatants of I3C-treated BV-2 cells did not reduce the LPS-induced *IL-1ß* (Figure. 20A) and *CCL2* (Figure. 20C) mRNA expression levels. Furthermore, *IL-6* (Figure. 20B) and *IL-8* (Figure. 20D) mRNA levels were not changed.

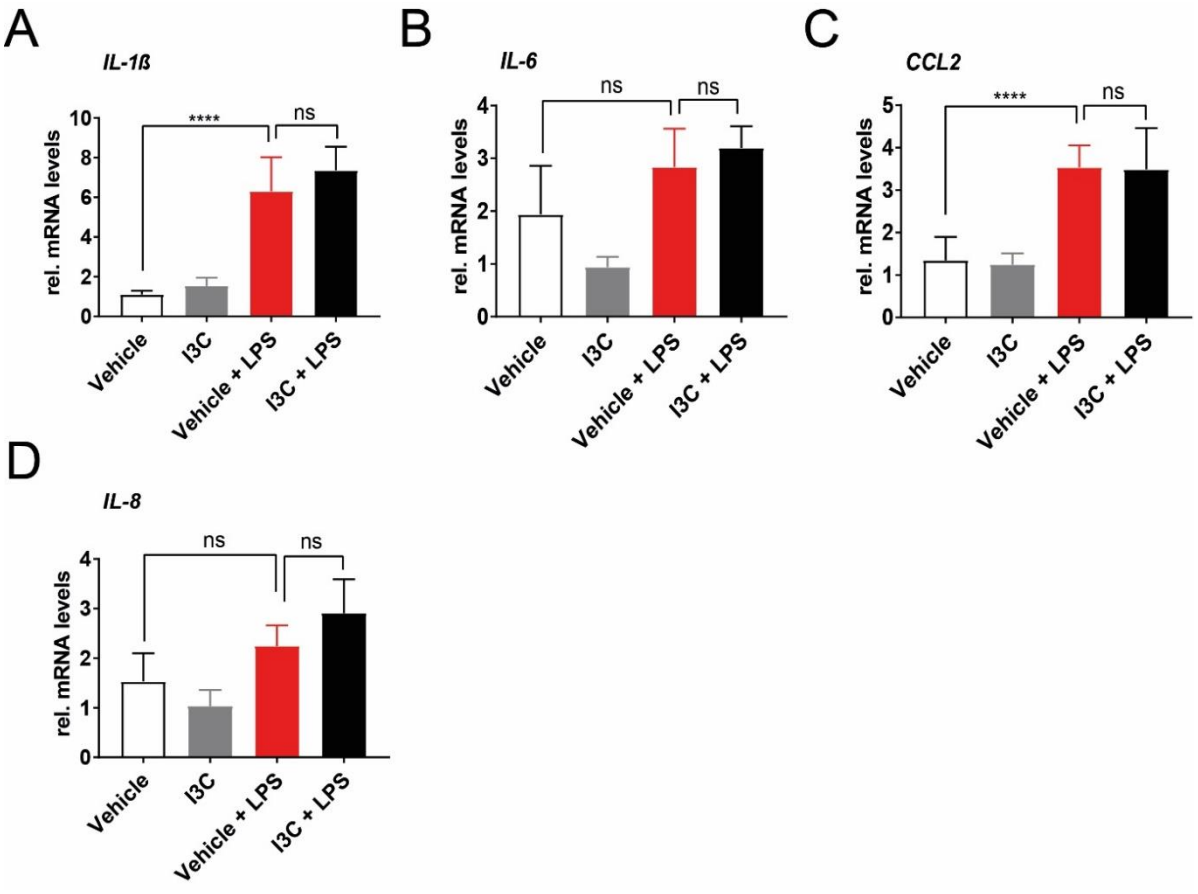

Figure 20 Effects of BV-2 microglia conditioned medium in ARPE-19 cells.
(A-D) BV-2 microglia cells were treated with 50 µM I3C for 4 hours followed by 50 ng/ml LPS for 4 hours. Supernatants of BV-2 microglia were transferred to ARPE-19 cell for 48 hours. mRNA expression of *IL-1ß* (A), *IL-6* (B), *CCL2* (C), and *IL-8* (D) were

analyzed by real-time PCR. Data show mean ± SEM out of two independent experiments (n = 3/group, measured in triplicates) with ****p < 0.0001.

3.3.1. I3C regulated the SV-40 microglia-mediated neurotoxic effects in ARPE-19 cells

Next, supernatants of SV-40 microglia cells were incubated with ARPE-19 cells. In ARPE-19 cells, supernatants of PMA plus Zym-treated SV-40 cells enhanced the pro-inflammatory *IL-1ß* (Figure. 21A), *IL-6* (Figure. 21B), *CCL2* (Figure. 21C), *IL-8* (Figure. 21D), and *IL-18* (Figure. 21E) mRNA expression levels. However, I3C did not reduce *IL-1ß* (Figure. 21A) and *IL-6* (Figure. 21B) mRNA levels. Furthermore, supernatants of I3C-treated SV-40 cells significantly reduced the PMA plus Zym-induced *CCL2* (Figure. 21C), *IL-8* (Figure. 21D), and *IL-18* (Figure. 21E) mRNA expression levels in ARPE-19 cells. In addition, I3C also enhanced the *NQO1* mRNA expression level (Figure. 21F).

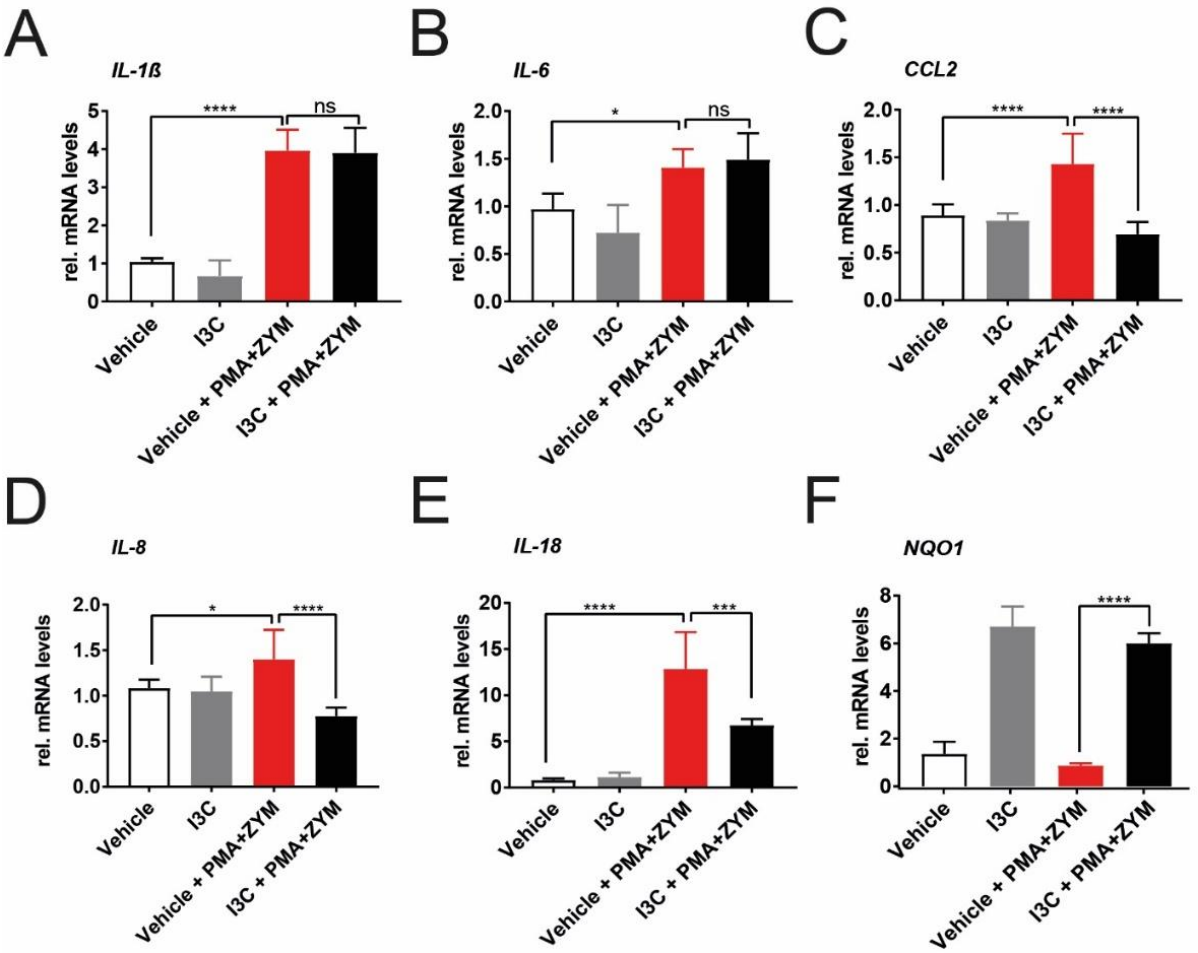

Figure 21 Effects of SV-40 microglia conditioned medium in ARPE-19 cells.
(A-F) SV-40 cells were treated with 50 µM I3C or DMSO as a vehicle for 4 hours followed by 100 nM PMA and 50 mg/ml Zym for another 4 hours. After 8 hours, supernatants of SV-40 microglia cells were transferred to ARPE-19 cell. mRNA expression of *IL-1ß* (A), *IL-6* (B), *CCL2* (C) and *IL-8* (D), *IL-18* (E), and *NQO1* (F) were analyzed by real-time PCR. Data show mean ± SEM out of three independent experiments (n = 3/group, measured in triplicates) with ****p < 0.0001.

3.4. I3C regulated the pro-inflammatory and anti-oxidant mRNA expression in primary microglia cells

To further evaluate the effects of I3C in murine primary microglia, cells were treated with I3C for 4 hours followed by LPS for another 4 hours. qRT-PCR results showed that LPS induced *i-NOS* (Figure. 22A), *IL-1ß* (Figure. 22B), *NLRP3* (Figure. 22C), and *CCL2* (Figure. 22D) mRNA levels and I3C did not reduce LPS-induced *i-NOS* (Figure. 22A) and *IL-1ß* (Figure. 22B) mRNA levels. However, I3C significantly reduced LPS-induced *NLRP3* (Figure. 22C) and *CCL2* (Figure. 22D) mRNA levels. In addition, I3C upregulated *NQO1* mRNA expression level in primary microglia cells (Figure. 22E).

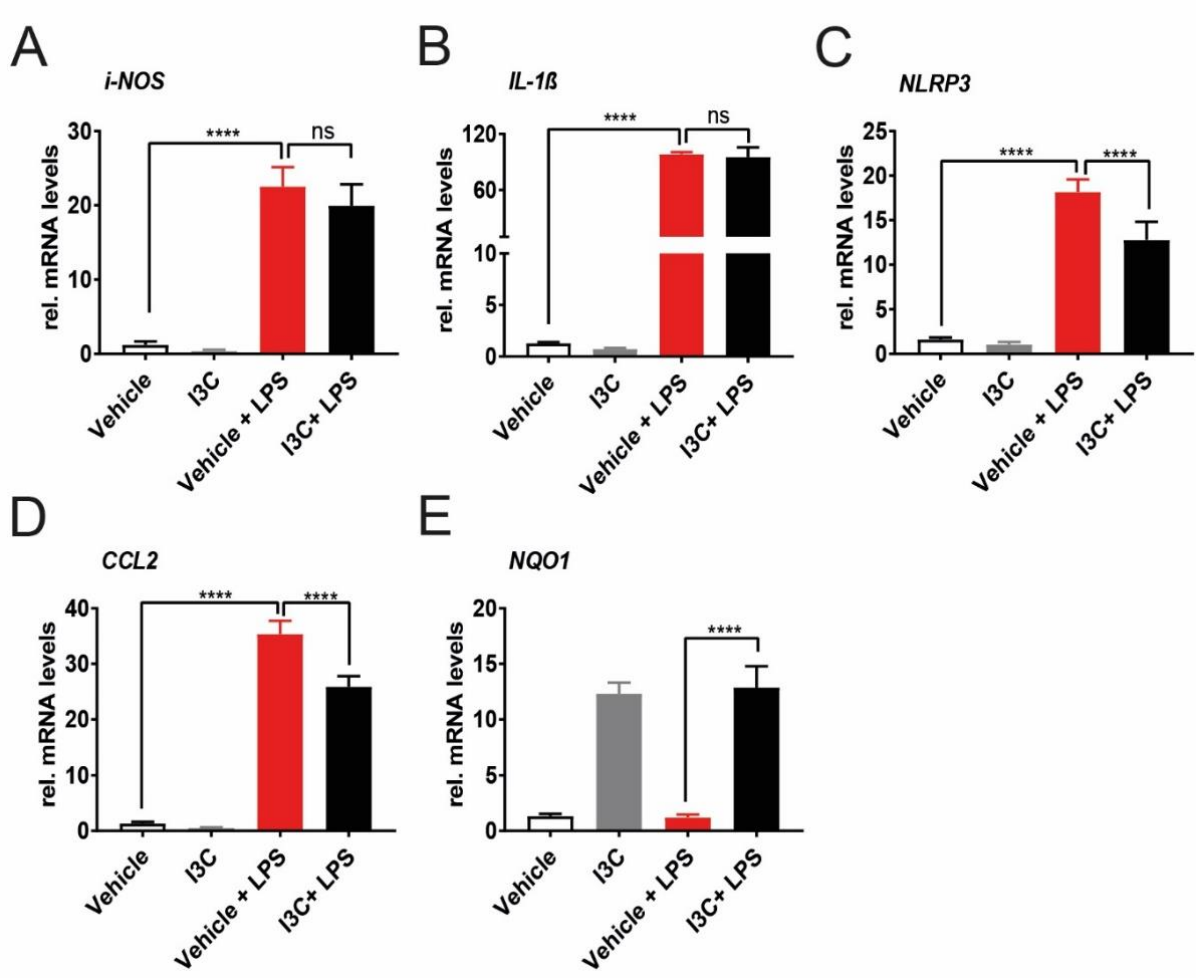

Figure 22 Effects of I3C on primary microglia cells.
(A-E) primary microglia cells were treated with 50 µM I3C for 4 hours followed by 50 ng/ml LPS for 4 hours. After 8 hours, mRNA expression of *i-NOS* (A), *IL-1ß* (B), *NLRP3* (C), *CCL2* (D), and *NQO1* (E) were analyzed by real-time PCR. Data show mean ± SEM out of two independent experiments (n = 3/group, measured in triplicates) with ****p < 0.0001.

3.5. I3C reduced the pro-inflammatory and enhanced the anti-oxidant mRNA expression levels in retinal explants of BALB/cJ mice

To examine the effects of I3C on a selected set of pro-inflammatory and anti-oxidant markers in retinal explants of BALB/cJ mice (10-14 weeks old), retinas were treated with I3C for 4 hours followed by LPS for another 4 hours. LPS-treatment induced *i-NOS* (Figure. 23A), *IL-1ß* (Figure. 23B), *NLRP3* (Figure. 23C), and *CCL2* (Figure. 23D) mRNA expression levels in retinal explants. I3C significantly reduced these levels (Figure. 23A-D). Furthermore, I3C significantly induced *NQO1* mRNA level (Figure. 23E). However, I3C did not change *HMOX1* mRNA level (Figure. 23F).

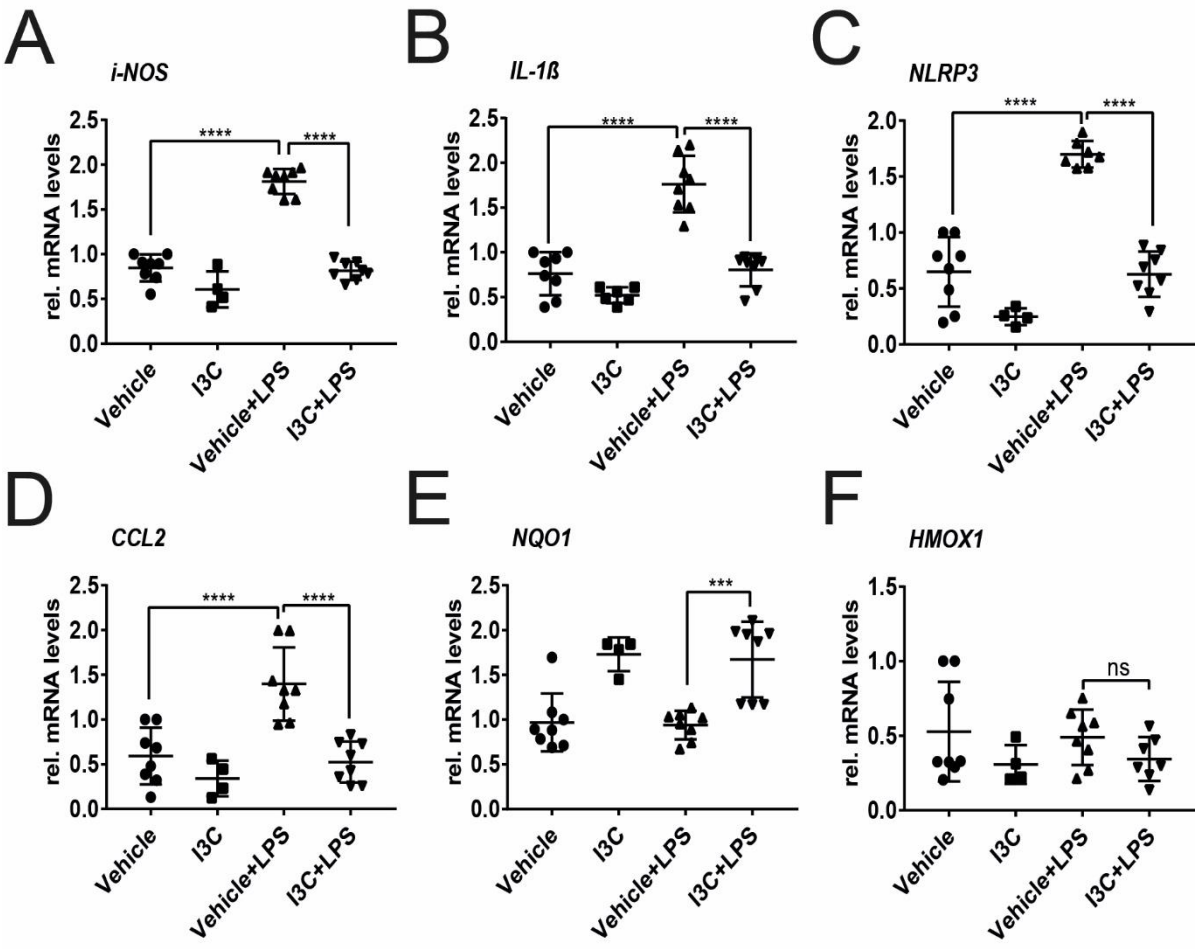

Figure 23 Effects of I3C on retinal explants.
(A-F) Retinas were isolated from eyes and treated with 50 µM I3C for 4 hours followed by 50 ng/ml LPS for additional 4 hours. After 8 hours, mRNA expression of *i-NOS* (A), *IL-1ß* (B), *NLRP3* (C), *CCL2* (D) *NQO1* (E), and *HMOX1* (F) were analyzed by real-time PCR. Data show mean ± SEM out of two independent experiments (vehicle=8 retinas, I3C = 4 retinas, vehicle + LPS= 8 retinas and I3C + LPS= 8 retinas) with ****$p < 0.0001$.

3.6. Acute white light-induced retinal degeneration model and mode of I3C administration in BALB/cJ mice

In this study, BALB/cJ mice were subjected to an established light damage paradigm of retinal degeneration and this model mimics the certain features of AMD with damaged retina (Scholz et al., 2015b) and the effects of I3C in retinas were analyzed. For this, light-sensitive BALB/cJ mice were dark-adapted for 16 hours before the mice were exposed to white light with an intensity of 15,000 lux for 1 hour. Pupil dilation was induced before the light exposure. Mice received intraperitoneal injections of 15 mg/kg I3C or DMSO as vehicle, the day before the light exposure, and then once daily for the

remaining 3 days (Figure. 24). 4 days after the light damage, retinas were isolated for further analyses.

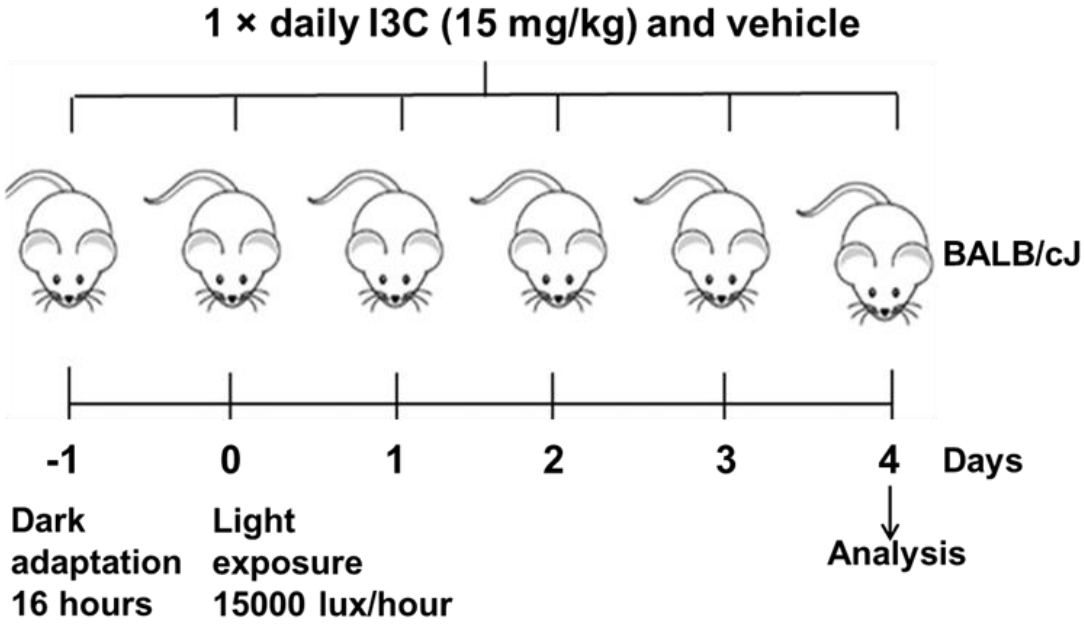

Figure 24 Schematic overview of mice experimental design.
8-10 week-old BALB/cJ mice of both sexes were used. Mice were dark-adapted for 16 hours before the mice were exposed to white light with intensity 15.000 lux for 1 hour. Before the light exposure, mice pupils were dilated. Mice received intraperitoneal injections of 15 mg/kg I3C and vehicle (DMSO), 1 day before the light exposure and once daily for the remaining 3 days.

3.6.1. I3C reduced the light induced pro-inflammatory mRNA expression levels in the retina of BALB/cJ mice

Four days after light exposure, retinal mRNA expression levels of *i-NOS* (Figure. 25A), *IL-1ß* (Figure. 25B), *NLRP3* (Figure. 25C), *IL-6* (Figure. 25D), *CCL2* (Figure. 25E), and *NQO1* (Figure. 25F) were determined via real-time PCR. Vehicle treated and light-exposed mice showed upregulation of all these genes in retinas (Figure. 25A-F). Interestingly, I3C treatments significantly reduced *i-NOS*, *IL-1ß*, *IL-6*, and *CCL2* mRNAs (Figure. 25A-E). However, *NQO1* mRNA was not changed (Figure. 25F).

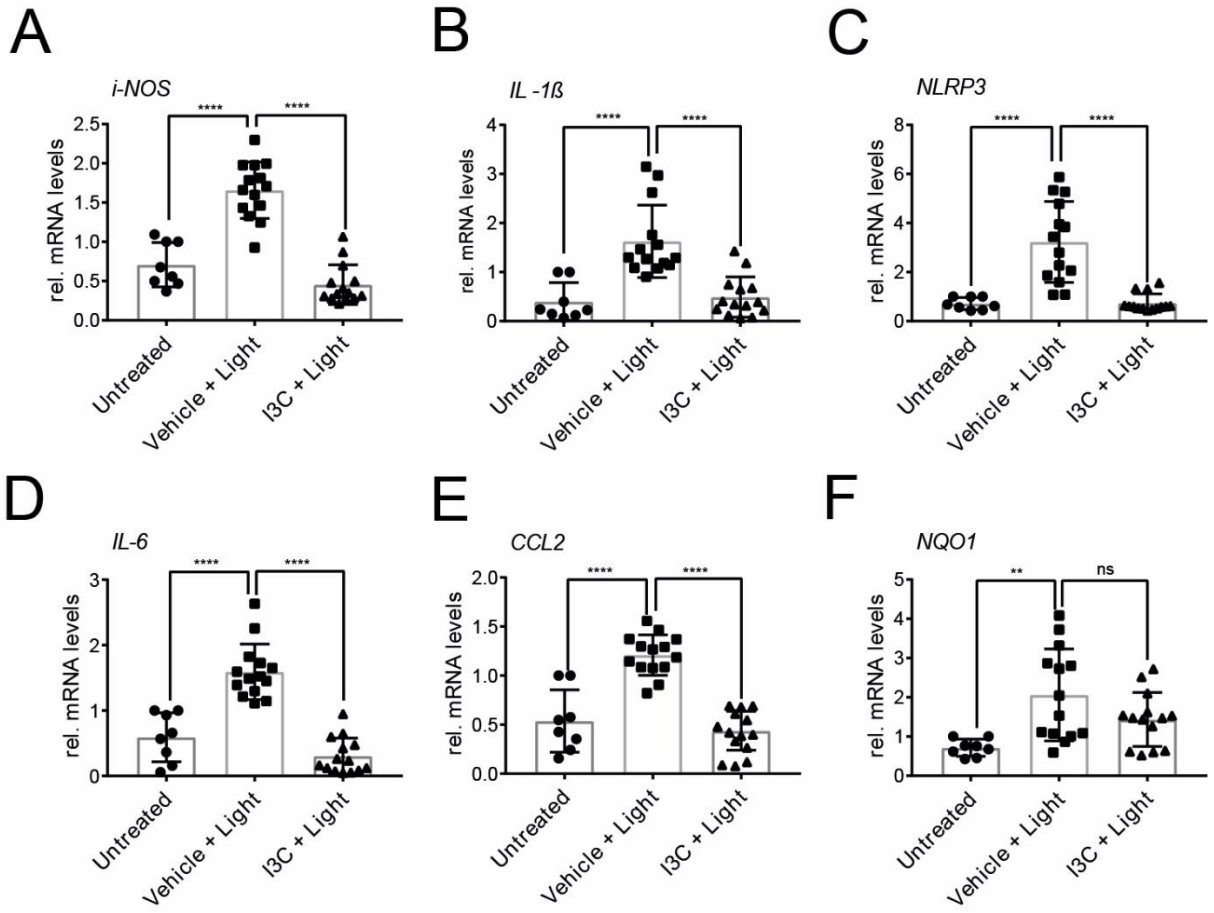

Figure 25 Effects of I3C on mRNA expression level elicited by light in BALB/cJ mice. Four days after the light exposure, **(A-F)** mRNA expression levels of *i-NOS* (A), *IL-1ß* (B), *NLRP3* (C), *IL-6* (D), *CCL2* (E), and *NQO1* (F) were analyzed by real-time PCR. Data show mean ± SEM out of three independent experiments for mRNA expression levels (untreated n = 8 retinas, vehicle + light n = 14 retinas, light + I3C treatment n = 14 retinas each dot is showing one retina) with ** p 0, 0015, and ****p < 0.0001.

3.6.2. I3C regulated pro-inflammatory and anti-oxidant proteins in retinas of BALB/cJ mice

To further verify the effects of I3C on retinal protein levels, ELISA and Western blots were performed. Vehicle treated and light-exposed mice induced CCL2 protein in retinas. However, I3C treatments significantly reduced CCL2 protein level (Figure. 26A). Western blot results revealed that vehicle treated and light-exposed mice upregulated i-NOS, IL-1ß, and p-NFkB p65 protein levels and I3C treatments significantly reduced these levels (Figure. 26B-D). Furthermore, NQO1 and HMOX1 protein levels were upregulated in light exposed and I3C treated BALB/cJ mice (Figure. 26B, E). Taken together, I3C significantly reduced the light-induced pro-inflammatory

protein levels and enhanced the light-reduced anti-oxidant protein levels in retinas of BALB/cJ mice.

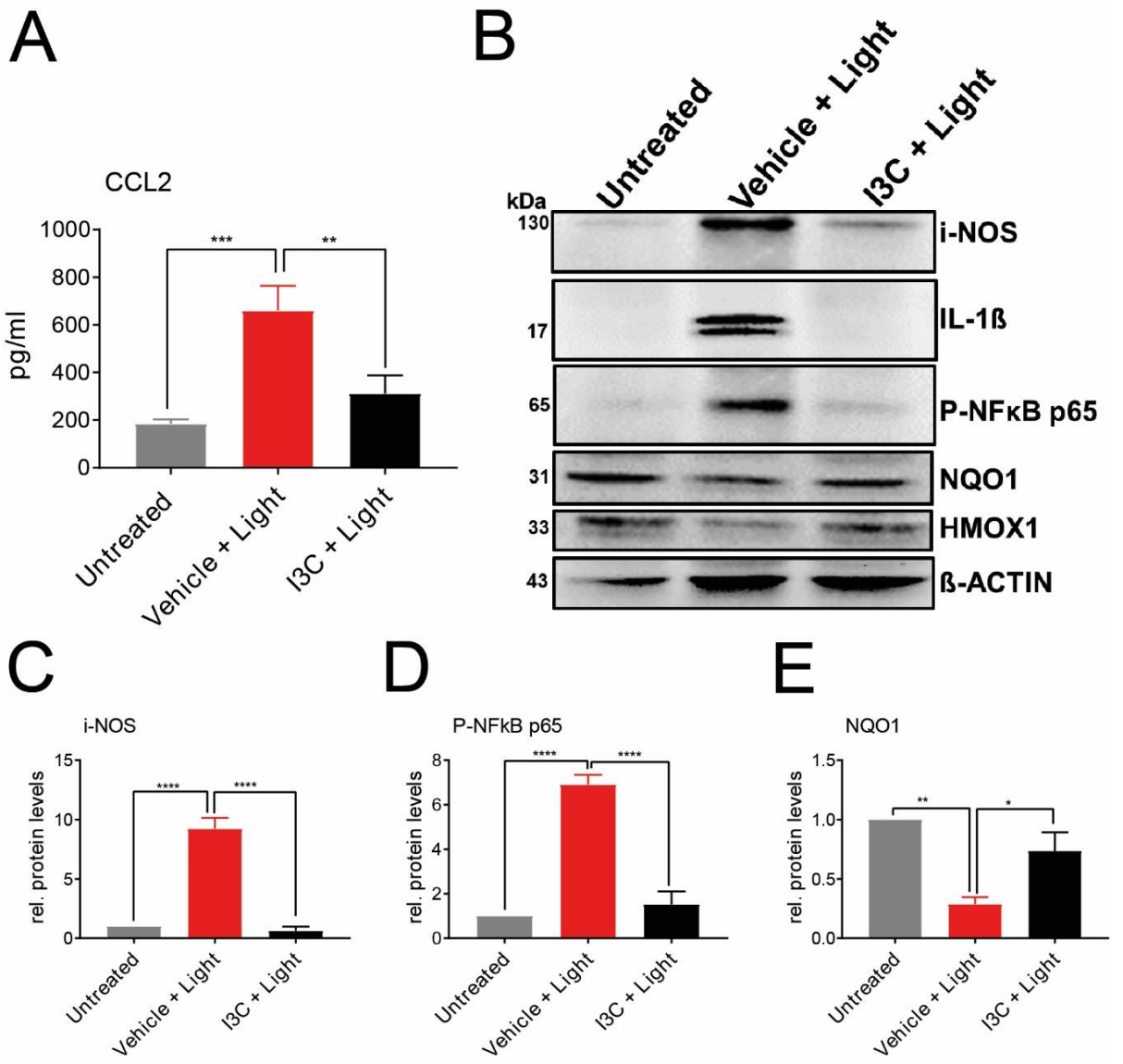

Figure 26 Effects of I3C on the pro-inflammatory and anti-oxidant protein levels in light-exposed mice.

Four days after the light exposure, retina lysates were extracted to perform ELISA of CCL2 **(A)** and Western blot **(B)** showing i-NOS, IL- 1ß, p-NFKB65, NQO1, and HMOX1 protein levels. Beta-actin is loading control. Relative protein levels i-NOS **(C)**, p-NFkBp65 **(D)**, and NQO1 **(E)** are shown. Data show mean ± SEM out of three independent experiments for ELISA and Western blots are performed (one retina per group) with * p 0.0168, ** p 0, 0015, and ****p < 0.0001.

3.6.3. I3C reduced the light–induced microglia reactivity in BALB/cJ mice

To analyze the effects of I3C on retinal microglia in BALB/cJ mice, retinal flat mounts were stained with ionized calcium binding adaptor molecule 1 (IBA 1) antibody, used as a marker for microglia. Retinas of untreated mice showed no microglia in SR space (Figure. 27A, D). Retinas of vehicle treated and light-exposed mice showed abundant amoeboid-shaped microglia in SR space (Figure. 27B, D). However, I3C prevented light-induced accumulation of amoeboid shaped microglia in SR space (Figure. 27C, D). Quantification results also showed that I3C reduced the light-induced amoeboid shaped microglia number in SR space in retinas (Figure. 27D). In addition, outer plexiform layer (OPL) of untreated mice showed the ramified microglia with long filopodia (Figure. 27E). In contrast, vehicle treated and light-exposed mice had more amoeboid and a less ramified morphology (Figure. 27F). Again, these signs of microglia reactivity were diminished by I3C treatments (Figure. 27G). Taken together, light induced the amoeboid shaped microglia in SR space and OPL of the retina in BALB/cJ mice. However, I3C transformed the light-induced amoeboid shaped microglia to ramified state.

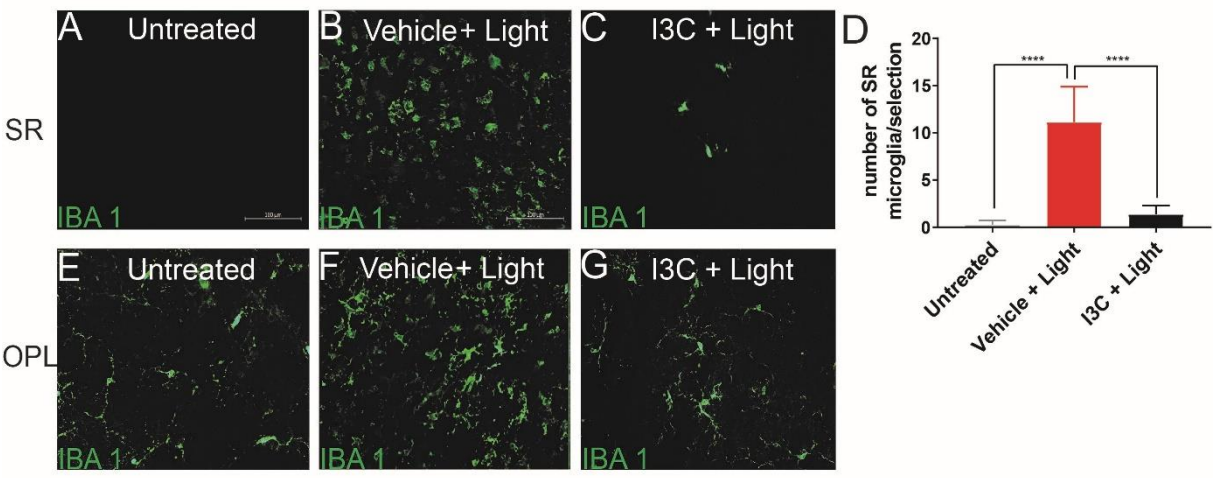

Figure 27 Effects of I3C in retinal microglia reactivity elicited by light in BALB/cJ mice. **(A-G)** Representative photomicrographs of IBA 1 stained microglia (green) of retinal flat mounts. Microglia in the SR space and outer plexiform layer (OPL) of untreated (A, E), vehicle + light (B, F), and I3C + light (C, G) treated mice. (D) Total IBA 1 positive cells were counted in the SR. Data show mean ± SEM with ****$p < 0.0001$ and (Untreated n=20 retinas, vehicle + light= 20 retinas and I3C + light n= 20 retinas). Scale bar is 100µm.

3.6.4. I3C reduced the light induced amoeboid microglia in the ONL of retinas in BALB/cJ mice

Next, to localize the IBA 1 positive microglia cells in different retinal layers, cryosections were stained with IBA 1 antibody. Untreated BALB/cJ mice showed the ramified microglia in inner and outer plexiform layers (IPL, OPL) (Figure. 28A). In vehicle treated and light-exposed BALB/cJ mice showed abundant amoeboid microglia in the outer nuclear layer (ONL) (Figure. 28B). Remarkably, I3C inhibited this light-induced amoeboid shaped-microglia accumulation in the ONL (Figure. 28C). Furthermore, Dapi staining of cryosections of vehicle treated and light-exposed mice showed significant cell loss in the ONL which was prevented with I3C (Figure. 28B-D).

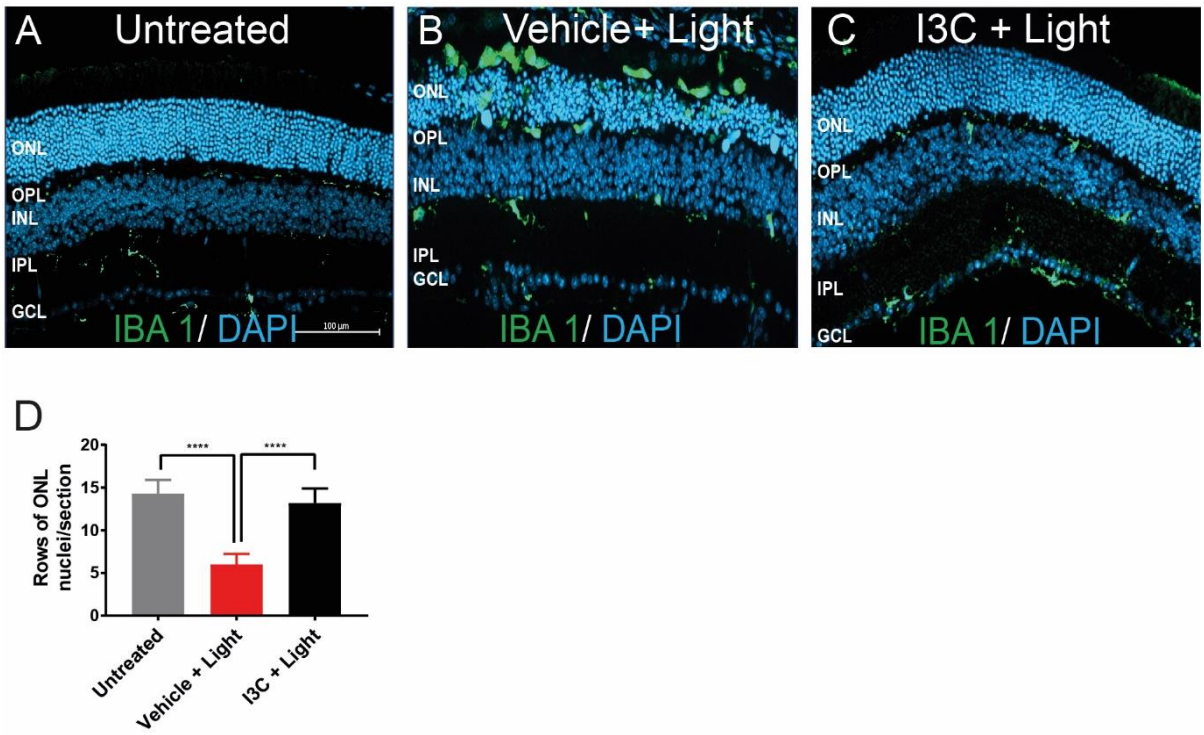

Figure 28 I3C reduced the microglia accumulation in the ONL elicited by light in BALB/cJ mice.
(A-C) Representative photomicrographs show retinal sections of control (A), vehicle + light (B), and I3C + light (C) treated mice stained with IBA 1 (green) and DAPI (blue). **(D)** For quantification of ONL thickness, rows of photoreceptor nuclei were counted. (Untreated n = 10 retinas, Vehicle + light n = 10 retinas, I3C + light n= 10 retinas). Data show mean ± SEM with ****p < 0.0001. ONL outer nuclear layer, OPL outer plexiform layer, INL inner nuclear layer, IPL inner plexiform layer, GCL ganglion cell layer.

3.6.5. I3C prevented the light-induced retinal thinning of the retina

Finally, after four days of acute light exposure, effects of I3C on retinal degeneration were analyzed. Mice were anesthetized and pupils were dilated for in vivo imaging with spectral domain-optical coherence tomography (SD-OCT). SD-OCT results showed strong retinal depletion and nearly complete loss of the ONL in vehicle treated and light-exposed mice compared to untreated mice (Figure. 29A, B). Treatment with I3C completely prevented this retinal depletion (Figure. 29C), which was further confirmed by repeated analyses of central retinal thickness within 3 and 6 mm ring scan areas (Figure. 29D, E). Taken together, light induced the retinal depletion and I3C completely prevented this retinal degeneration in BALB/cJ mice.

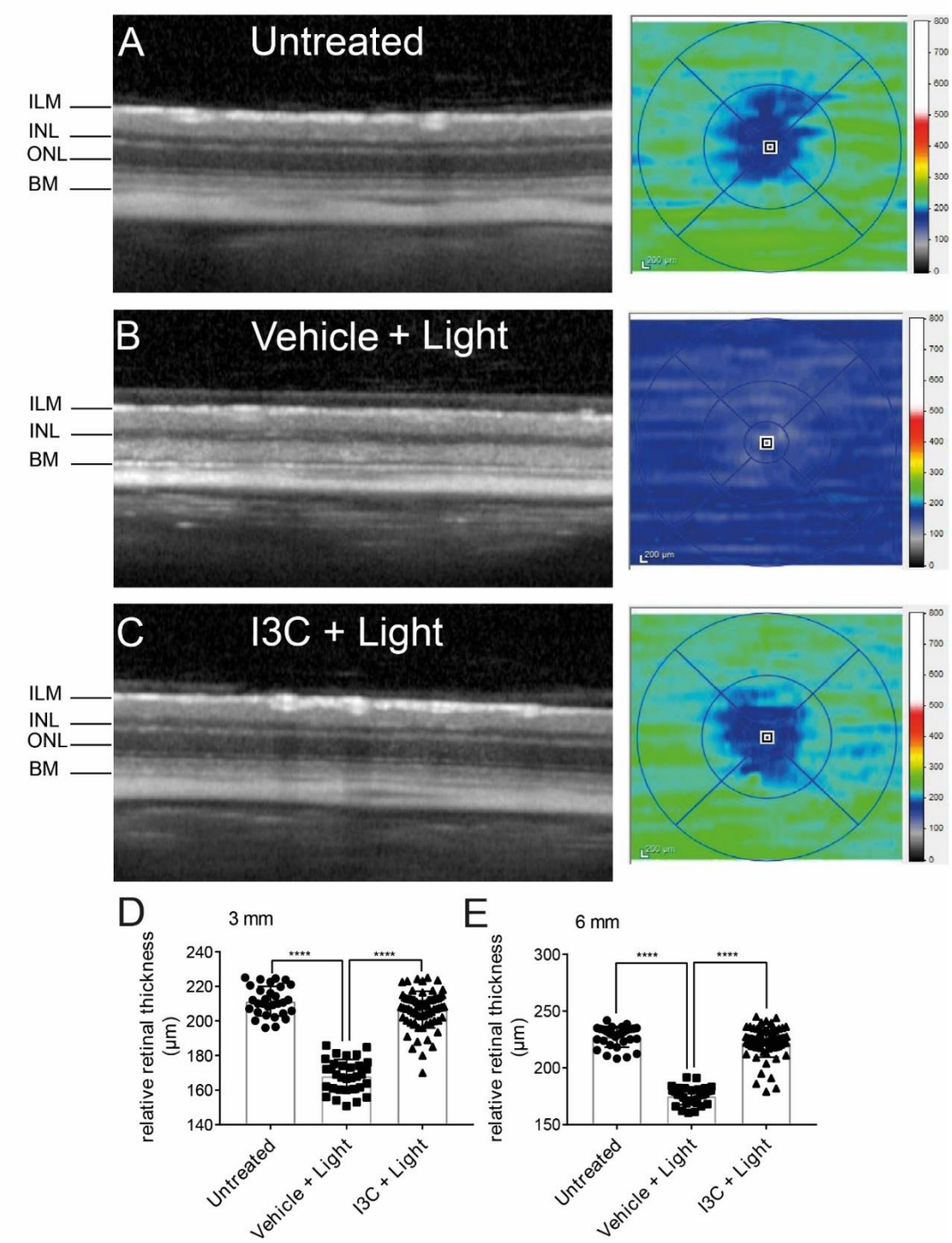

Figure 29 Effects of I3C on retinal thickness in light-damaged BALB/cJ mice.
(A-C) Four days after light damage, SD-OCT was performed to analyze the changes in retinal thickness displaying heat maps of (A) untreated, (B) vehicle + light, and (C) I3C + light treated mice. **(D-E)** Relative retinal thickness (µm) in 3 and 6 mm areas were calculated using SD-OCT software, where one data point represents the average thickness of the central retina. Data show mean ± SEM (untreated n = 30 eyes, vehicle + light n = 32 eyes, light + I3C treatment n = 70 eyes). ****$p < 0.0001$.

4 Discussion

Hence, microglia play a significant role in physiological and pathophysiological state of the retina and microglia reactivity is a major hallmark of neurodegenerative diseases including AMD (Rashid et al., 2018). This present study analyzed the effects of I3C on the modulation of microglia reactivity in vitro and in vivo using light damage mouse model of dry AMD.

Microglia are the immune cells of the CNS including retina (McCarthy et al., 2013). They perform multiple tasks including immune surveillance and removal of cell debris to maintain retinal homeostasis. However, in retinal degeneration, microglia become active. Uncontrolled microglia activation often upregulates the inflammatory markers. In this state, microglia phagocytose the healthy photoreceptors, which lead to neurodegeneration (Karlstetter et al., 2015). Therefore, pharmacological inhibition of dysregulated microglia-mediated inflammatory responses that enhances the neuroprotective functions may be an emerging option for the treatment of retinal degeneration. Aryl hydrocarbon receptor is a ligand dependent transcriptional factor widely expressed in different cell types including microglia (Shinde and McGaha, 2018). Although, AhR was initially identified as the regulator of environmental pollutants and receptor for the dioxins, recent studies have shown that AhR also regulates cellular homeostasis and immunity (Stockinger et al., 2014; Esser, 2016). Dysregulation in the uptake or production of AhR may contribute to the inflammatory phenotype in immune-related diseases (Rothhammer et al., 2016). AhR agonists have been shown to exhibit immunomodulatory properties and reduce the inflammation (Busbee et al., 2013). AhR ligand, I3C is highly abundant in green vegetables. Emerging evidence has indicated that I3C exhibits anti-proliferative, anti-metastatic, anti-inflammatory and immunomodulatory properties (Weng et al., 2008; Aronchik et al., 2014). Therefore, this present study postulates that I3C may exhibit similar immunomodulatory properties on microglia, inhibiting microglia activation and associated retinal degeneration.

4.1. Immunomodulatory effects of I3C in microglia cells

Firstly, the effects of I3C were analyzed in immortalized murine BV-2 microglia cell line. This cell line was generated by infecting primary microglia cells with a retrovirus containing a raf/myc oncogene (Blasi et al., 1990). BV-2 microglia cells share 90% similarities with primary microglia cells and represent a good alternative for primary

microglia cells (Stansley et al., 2012). Liposaccharides (LPS), a component of cell wall of gram-negative bacteria, was used as inflammatory stimulus in BV-2 microglia. In vitro data showed that LPS induced the well-established pro-inflammatory mediators, *i-NOS*, *IL-1ß*, *NLRP3*, *IL-6*, and *CCL2* (Karlstetter et al., 2014; Scholz et al., 2015b; Wiedemann et al., 2018). I3C significantly reduced these transcripts. AhR ligands also mediate anti-oxidant effects (Dietrich, 2016). In the present study, I3C significantly induced mRNA expression levels of *NQO1* and *HMOX1* in BV-2 microglia cells. NQO1 and HMOX1 are cytoprotective mediators that prevent brain inflammation (Velagapudi et al., 2018). LPS upregulates several signaling molecules including NF-kB, mitogen-activated protein kinases (MAPKs), and TLR-4 in microglia (Lim et al., 2018). In an another study, LPS has been shown to induce the NO, IL-1ß, and p-ERK1/2 protein levels in BV-2 cell (Choi et al., 2009). The present study showed that I3C significantly reduced the pro-inflammatory i-NOS, IL-1ß, phosphorylated-ERK1/2, and induced the HMOX1 protein levels. These results are in line with a previous report, I3C blocked LPS-induced IL-1β, IL-6, and NO in RAW264.7 macrophage cells (Jiang et al., 2013). AhR has been shown to regulate the transcription of the COX2 (Vogel et al., 2007). AhR ligand, 2,3,7,8-tetrachlorodibenzo-p-dioxin (TCDD) induced transcription activity of COX2 and enhanced the inflammation (Degner et al., 2009). However, in the present study, I3C significantly reduced the LPS-induced COX2 protein level, suggesting that I3C has different mechanism of actions compared to TCDD. In the present study, I3C potently inhibits pro-inflammatory mediators at both mRNA and protein levels on the one hand, and increases anti-oxidant mRNA and protein levels on the other hand, in BV-2 microglia cells.

Another important phenomenon is photoreceptor cell death, which is a prominent hallmark of retinal diseases including AMD (Dunaief et al., 2002). Microglia activation enhances photoreceptor cell death and an inhibition of microglia activation improves photoreceptor survival (Rashid et al., 2019). In the present study, BV-2 microglia cells were treated with a combination of I3C and LPS, 661 W photoreceptor cells were then incubated in culture supernatants from BV-2 cells to assess microglia neurotoxicity. In the present study, I3C reduced the LPS-induced caspase 3/7 activity in 661 W photoreceptor cells, contrary to reported induced apoptosis in several cancers (Aggarwal and Ichikawa, 2005; Chang et al., 2011; Chen et al., 2013). Furthermore, despite the limitation that 661 W photoreceptor cells are cone-specific (Tan et al.,

2004). These cells have been reported as a reliable in vitro model to study molecular signaling in photoreceptor apoptosis (Sayyad et al., 2017; Wheway et al., 2019).

Microglia phagocytosis is a complex process, tailored from specific outcomes from the phagocytic target and relies on the shape of target (Paul et al., 2013). Moreover, microglia phagocytosis is dependent on several cell surface receptors and downstream signaling pathways (Fu et al., 2014). In a healthy state, microglia phagocytose dead cells for the maintenance of the retina homeostasis. In a disease state, activated microglia phagocytose the healthy neurons and aggravate retinal neurodegeneration (Rashid et al., 2019). Inhibition of such phagocytosis is effective in slowing down the disease process (Zhao et al., 2015). BV-2 microglia cells were stimulated with LPS, which enhanced the phagocytosed latex beads number, consistent with a previous finding (Scholz et al., 2015b). These findings suggest that LPS may induce molecular signaling pathways to activate phagocytosis of latex beads in BV-2 cells. In the present study, I3C significantly reduced this phagocytic capacity. However, phagocytosis assay with latex beads has clear limitation because it does not accurately recapitulate in vivo phagocytosis with complex molecular signaling mechanisms involved in vivo phagocytosis, which are different from in vitro phagocytosis assay (Napoli and Neumann, 2009; Galloway et al., 2019; Puigdellívol et al., 2020). Nevertheless, phagocytosis of latex beads and apoptotic photoreceptor debri have a good concurrence (Karlstetter et al., 2014).

Dynamic migration is a hallmark of activated microglia, which invokes neurodegeneration (Bachiller et al., 2018; Hickman et al., 2018). Microglia activation enhances the release of different chemoattractants, which affect the cellular movement. For example, CCL2 is a potent inducer of microglia migration (Bose et al., 2016). The present study has shown that I3C reduced the LPS-induced *CCL2* mRNA level. Phosphorylated-ERK1/2 (p-ERK1/2) has been shown to enhance the migration of microglia (Romero-Sandoval et al., 2009). Western blot results revealed that I3C reduced the LPS-induced p-ERK1/2 protein level. However, I3C alone did not change the p-ERK1/2 protein level compared to vehicle in BV-2 microglia cells. In the migration assay, I3C reduced the LPS-induced migration of BV-2 microglia cells. However, I3C alone did not reduce the migration of BV-2 microglia cells effectively. These results from two different experiments interrelate p-ERK1/2 with the migration of BV-2 microglia cells. A previous study has also shown that LPS-induced migration of BV-2

microglia cells is associated with upregulation MAPKs (Nam et al., 2018). However, further experiments are required to fully understand the molecular mechanisms involved in I3C-mediated inhibition of microglia migration in the presence of LPS.

Morphology is another important functional feature of microglia, which is associated with microglia activation (Fernández-Arjona et al., 2017). In an activated state, microglia transform their morphology from ramified to amoeboid (Tao et al., 2018). LPS transformed ramified BV-2 microglia cells to amoeboid shaped as expected and I3C inhibited this transformation. Previously, AhR activation modulated the cellular plasticity in macrophages and epithelial cells (Diry et al., 2006; Cui et al., 2020).

The specificity of I3C towards its receptor was analyzed with siRNA-mediated knockdown of AhR in microglia cells. Knockdown of *AhR* prevented the I3C mediated effects on *i-NOS*, *IL-1ß* and *NLRP3* mRNAs. Our results are in line with previous findings that AhR deletion in microglia enhanced the pro-inflammatory transcripts (Rothhammer et al., 2018). Furthermore, AhR activation downregulated *NLRP3* and *IL-1ß* mRNA levels in peritoneal macrophages and siRNA-mediated knockdown of *AhR* reversed this effect (Huai et al., 2014). Another study showed that loss of AhR reduced the anti-inflammatory marker in macrophages (Zhu et al., 2018). However, the present study showed that AhR knockdown did not alter *IL-6* mRNA compared to negative control in BV-2 microglia cells. This suggests that AhR is not directly involved in LPS-induced *IL-6* gene regulation.

Effects of I3C were also analyzed in human immortalized microglia SV-40 cells. These cells were stimulated with PMA and zymosan (Zym), known to induce the microglia activation and mimic the pathogenic infection (Smith et al., 1998; Harrigan et al., 2008; Madeira et al., 2018). In the present study, I3C reduced the PMA plus Zym-induced *IL-1ß*, *NLRP3* and *IL-6*. I3C also induced *NQO1*, *HMOX1*, and *CAT1* mRNAs.

4.1.2. Effects of SV-40 conditioned medium on ARPE-19 cells

It has been shown that activated microglia crosstalk with RPE membrane and regulate the pro-inflammatory responses (Nebel et al., 2017; Rashid et al., 2020). Incubation of ARPE-19 cells with supernatants of LPS-treated BV-2 cells showed the upregulation *IL-1ß* and *CCL2* mRNA expression levels. However, supernatants of I3C treated BV-2 microglia cells did not affect pro-inflammatory genes in ARPE-19 cells. Interestingly,

supernatants of SV-40 microglia cells regulated the pro-inflammatory and anti-oxidant mRNA expression levels in ARPE-19 cells. This may be due to species-specific effects because SV-40 and ARPE-19 are human cell lines, whereas BV-2 is murine. Supernatants of I3C treated SV-40 cells significantly inhibited PMA plus Zym-induced *CCL2* and *IL-8* mRNAs in ARPE-19 cells. However, mRNA levels of *IL-1ß* and *IL-6* were not changed. These results also suggest that I3C-mediated inhibition of pro-inflammatory markers in SV-40 cells is not sufficient to fully prevent the microglia-mediated effects on ARPE-19 cells.

4.2. Effects of I3C on LPS-treated primary microglia and retinal explants

In the present study, primary microglia treated with LPS upregulated *i-NOS*, *IL-1ß*, *NLRP3* and *CCL2* mRNA levels similar to BV-2 cells. I3C reduced LPS-induced *NLRP3* and *CCL2* mRNAs. These results are in line with this finding that primary microglia cells treated with AhR agonist reduced the pro-inflammatory markers (Rothhammer et al., 2018). However, I3C did not reduce LPS-induced *i-NOS* and *IL-1ß* mRNA levels in primary microglia. BV-2 and primary microglia cells have similar functions, but not to the same extent (Henn et al., 2009).

Mouse retinal explants were also used to analyze the effects of I3C. Retinal explants act as a rapid tool to identify and analyze the neuroprotective drugs for retinal degeneration before further investigation in animal models (Pattamatta et al., 2016). LPS has been shown to induce the pro-inflammatory cytokines in retinal explants (Ferrer-Martín et al., 2015). In the present study, I3C reduced the LPS-induced *i-NOS*, *IL-1ß*, *NLRP3*, and *CCL2* and induced *NQO1* mRNA expression levels in retinal explants. These experiments highlighted the direct effect of I3C on pro-inflammatory and anti-oxidant markers at mRNA levels in retinal explants.

4.3. Light-induced retinal degeneration model

AMD is a multifactorial and heterogeneous disease associated with macula (Cascella et al., 2014). The macula is not present in rodents, which is a challenge to develop AMD related mouse model (Fletcher et al., 2014). Furthermore, the reduced cone density and absence of RPE deposit (drusen) reflect the limitations of the rodent AMD model. To date, there is no single model, which mimics all the features of AMD in

progressive age-related manner (Fletcher et al., 2014). However, numerous mouse models for the AMD struggle to have similarities with human retinal degeneration to investigate the disease development and progression. The accurate AMD model can help to develop the new drug for the disease (Pennesi et al., 2012). In the present study, BALB/cJ mice were used to investigate the effect of I3C in an established model of light-induced retinal degeneration. Light is a pathogenic stimulus and used for the investigation of retinal degeneration (Grimm and Remé, 2012). Although, light activates different molecular signaling pathways for photoreceptor damage compared to inherited degeneration model (Grimm et al., 2004). However, light-induced photoreceptor damage provides advantages over genetically induced degeneration (Wenzel et al., 2005). For example, light damage is an easy and reproducible method, which stimulates synchronized damage to photoreceptor cells and these affected cells have almost the same stage of damage and shift to the next stage of damage at the same time. This process provides an opportunity to investigate the cellular and molecular mechanisms. However, in genetically induced degeneration, photoreceptor cells have different stages of damage. Furthermore, light-induced damage to photoreceptor cells is dependent on the intensity and duration of light exposure, which enables to control this process. Moreover, light-induced rapid retinal degeneration compared to other retinal degeneration models (Wenzel et al., 2005). In the present study, BALB/cJ mice were challenged with established standards of acute white light (15000 lux/hour) which activates microglia and causes photoreceptor cell death (Scholz et al., 2015b). These mice are extensively used in retinal degeneration studies because of their susceptibility to light-induced damage (Bell et al., 2015). This susceptibility depends on the mutation in the RPE65 in BALB/c. RPE65 is the retinol isomerase, which transform the all-trans-retinol to the 11-cis configuration in RPE that is essential for the normal visual cycle (Danciger et al., 2000). The single base substitution of leucine to methionine at codon 450 (L450M) causes mutation in RPE65 protein, which causes the alteration in levels of retinol isomerase. Therefore, BALB/c mice are more susceptible to light damage as compared to C57BL/6J mice. BALB/c mice have abundant RPE65; extensive bleaching caused the accumulation of toxins and retinoid metabolites, which increase the retinal degeneration (Bell et al., 2015). Furthermore, light induces the pro-inflammatory cytokines in the retinas of BALB/c mice (Bian et al., 2016). Prolong exposure of light also induce the degeneration of the retina (Contín et al., 2016).

4.3.1. Effects of I3C on light-induced retinal degeneration

Age-related decline in AhR expression and its activity has been previously shown (Hu et al., 2013; Brinkmann et al., 2020). AhR knockout mice have reduced visual functions and AMD like phenotype (Kim et al., 2014b). These reports highlight the importance of AhR in ocular compartment. In the present study, light induced the mRNA expression levels of *i-NOS*, *IL-1ß*, *NLRP3*, *IL-6*, and *CCL2*. However, I3C-treated animals significantly inhibited these inductions. I3C has been shown to prevent ischemic reperfusion-induced inflammation (Ampofo et al., 2017). I3C also improved neurobehavioral symptoms in a cerebral ischemic stroke model (Paliwal et al., 2018). AhR agonists have been shown to reduce pro-inflammatory gene expression in the experimental autoimmune uveitis (Huang et al., 2018a). Furthermore, AhR knockout mice upregulated the pro-inflammatory marker, IL-1ß, IL-6, and CCL2 in the optic nerves (Juricek et al., 2017).

In the present study, I3C prevented light-induced CCL2 protein in the retina. It has been shown that light exposure induced the CCL2 levels in the retina and CCL2 knockdown prevented the light-mediated retinal degeneration (Rutar et al., 2011, 2012). In addition, AMD patients showed a significant upregulation of CCL2 levels in serum compared to a healthy population (Anand et al., 2012). In the present study, I3C prevented light-induced IL-1ß and p-NFkB-p65 protein levels in the retina. Likewise, it has been shown that AhR activation limits IL-1ß and NFkB in peritoneal macrophages (Huai et al., 2014). Furthermore, AhR knockout upregulated the NFkB-p65 in experimental autoimmune encephalomyelitis mouse model (Rothhammer et al., 2018).

The retina is one of the highest oxygen consuming tissue (Mulfaul et al., 2020). External stimuli like light, smoking, and radiation can induce the ROS level and cellular stimuli like inflammation, photosensitizers, phagocytosis, and inflammation can upregulate the ROS. These ROS levels cause oxidative damage in the retina. However, anti-oxidant machinery decreases these ROS levels to establish homeostasis (Bellezza, 2018; Domènech and Marfany, 2020). Nevertheless, with age, oxidative damage increases and anti-oxidant machinery fails to create the homeostasis that lead to the development and progression of AMD (Jarrett and Boulton, 2012). In the present study, I3C upregulated NQO1 and HMOX1 protein levels in the retina of light-treated animals. These results are consistent with previous findings, a synthetic

AhR ligand (2AI) increased the anti-oxidant battery of genes in the retina (Gutierrez et al., 2016) and I3C has been shown to reduce inflammation through anti-oxidant mechanism in clonidine-induced animal model (El-Naga et al., 2014). Indeed, AhR is essential for normal immune physiology as AhR-deficient mice display a highly inflammatory phenotype with high levels of oxidative stress in the retina (Kim et al., 2014b).

Previously, AhR knockout mice studies showed that AhR maintains the RPE and photoreceptor cells homeostasis. Furthermore, AhR ligand 2AI reduced the light-induced damage through RPE homeostasis (Gutierrez et al., 2016). However, in the present study, the effects of I3C have been shown on light-induced microglia reactivity in the retina. Acute white light exposure caused accumulation of amoeboid shaped microglia in SR space, which is consistent with previous findings (Scholz et al., 2015a; Jiang et al., 2019). Acute white light has been previously shown to reduce the AhR gene expression in retinas of BALB/c mice, suggesting to boost the AhR pathway may enhance the neuroprotection (Gutierrez et al., 2016). In the present study, I3C reduced light-induced accumulation of amoeboid shaped microglia in SR of retinas of BALB/cJ mice and induced the ramified phenotype in microglia. This present study clearly show that I3C can potently block the microglia reactivity and preserves retinal thickness and layer integrity.

In the present study, I3C showed previously unrevealed effects on microglia activation in a retinal light damage model. I3C is a known anti-inflammatory agent (Aggarwal and Ichikawa, 2005; Chang et al., 2011). For example, I3C also reduced inflammatory markers and enhanced the anti-oxidant levels in experimental in vivo model of Parkinson's disease (Saini et al., 2020). In the present study, intraperitoneal injections of I3C to light-exposed BALB/cJ mice protected their retinas from degeneration. Systemically administered I3C has been shown to rapidly absorb and distribute in the blood, liver, kidney, lung, heart, and brain (Anderton et al., 2004). AhR is expressed by various retinal cells including RPE, photoreceptors, retinal ganglion cells, and microglia (Gutierrez et al., 2016; Juricek and Coumoul, 2018; Rothhammer and Quintana, 2019). Previous studies also highlighted the significant role of AhR in retinal degeneration without emphasizing on microglia (Hu et al., 2013; Kim et al., 2014b; Gutierrez et al., 2016). In the present study suggests that AhR activation with I3C in light-damaged retina may have beneficial effects on microglia homeostasis.

5 Conclusions and future perspectives

Briefly, the findings from this present study show that AhR ligand I3C that is present in the green vegetables, regulates the microglia homeostasis.

Interestingly, I3C markedly reduced the LPS-induced pro-inflammatory mRNA expression and protein levels in BV-2 microglia cells. I3C reduced the LPS-induced NO secretion and caspase 3/7 activity. Furthermore, I3C reduced the LPS-induced phagocytosis and migration and induced the protective phenotype in BV-2 microglia cells. Notably, the therapeutic action of I3C revolves around AhR because knockdown of AhR partially reversed the effects of I3C. I3C significantly downregulated the pro-inflammatory mRNA expression levels in SV-40, ARPE-19 with conditioned medium, primary microglia cells, and retinal explants. Furthermore, I3C also attenuated light induced pro-inflammatory mRNA expression and protein levels and induced the anti-oxidant proteins in the retina. I3C also significantly reduced microglia reactivity and preserved the retina from light-induced degeneration.

Taken together, this study provides useful information about I3C that regulates the microglia homeostasis. I3C could represent a potential therapeutic candidate in the treatment of retinal degeneration.

6 References

Abdelsalam A, Del Priore L, Zarbin MA (1999) Drusen in age-related macular degeneration: Pathogenesis, natural course, and laser photocoagulation-induced regression. Surv Ophthalmol 44:1–29.

Aggarwal BB, Ichikawa H (2005) Molecular targets and anticancer potential of indole-3-carbinol and its derivatives. Cell Cycle 4:1201–1215.

Ajami B, Bennett JL, Krieger C, Tetzlaff W, Rossi FMV V (2007) Local self-renewal can sustain CNS microglia maintenance and function throughout adult life. Nat Neurosci 10:1538–1543.

Akhtar-Schäfer I, Wang L, Krohne TU, Xu H, Langmann T (2018) Modulation of three key innate immune pathways for the most common retinal degenerative diseases. EMBO Mol Med 10.e8259.

Alexander P, Thomson HAJ, Luff AJ, Lotery AJ (2015) Retinal pigment epithelium transplantation: Concepts, challenges, and future prospects. Eye 29:992–1002.

Ambati J, Atkinson JP, Gelfand BD (2013) Immunology of age-related macular degeneration. Nat Rev Immunol 13:438–451.

Ambati J, Fowler BJ (2012) Mechanisms of age-related macular degeneration. Neuron 75:26–39.

Ampofo E, Lachnitt N, Rudzitis-Auth J, Schmitt BM, Menger MD, Laschke MW (2017) Indole-3-carbinol is a potent inhibitor of ischemia–reperfusion–induced inflammation. J Surg Res 215:34–46.

Anand A, Sharma NK, Gupta A, Prabhakar S, Sharma SK, Singh R, Gupta PK (2012) Single Nucleotide Polymorphisms in MCP-1 and Its Receptor Are Associated with the Risk of Age Related Macular Degeneration. PLoS One 7:e49905.

Anderton MJ, Manson MM, Verschoyle RD, Gescher A, Lamb JH, Farmer PB, Steward WP, Williams ML (2004) Pharmacokinetics and tissue disposition of indole-3-carbinol and its acid condensation products after oral administration to mice. Clin Cancer Res 10:5233–5241.

Aronchik I, Kundu A, Quirit JG, Firestone GL (2014) The antiproliferative response of indole-3-carbinol in human melanoma cells is triggered by an interaction with NEDD4-1 and disruption of wild-type PTEN degradation. Mol Cancer Res

12:1621–1634.

Bachiller S, Jiménez-Ferrer I, Paulus A, Yang Y, Swanberg M, Deierborg T, Boza-Serrano A (2018) Microglia in neurological diseases: A road map to brain-disease dependent-inflammatory response. Front Cell Neurosci 12:488.

Bell BA, Kaul C, Bonilha VL, Rayborn ME, Shadrach K, Hollyfield JG (2015) The BALB/c mouse: Effect of standard vivarium lighting on retinal pathology during aging. Exp Eye Res 135:192–205.

Bellezza I (2018) Oxidative stress in age-related macular degeneration: NRF2 as therapeutic target. Front Pharmacol 9.

Benmamar-Badel A, Owens T, Wlodarczyk A (2020) Protective Microglial Subset in Development, Aging, and Disease: Lessons From Transcriptomic Studies. Front Immunol 11:430.

Bhutto I, Lutty G (2012) Understanding age-related macular degeneration (AMD): Relationships between the photoreceptor/retinal pigment epithelium/Bruch's membrane/choriocapillaris complex. Mol Aspects Med 33:295–317.

Bian M, Du X, Cui J, Wang P, Wang W, Zhu W, Zhang T, Chen Y (2016) Celastrol protects mouse retinas from bright light-induced degeneration through inhibition of oxidative stress and inflammation. J Neuroinflammation 13:50.

Bjeldanes LF, Kim JY, Grose KR, Bartholomew JC, Bradfield CA (1991) Aromatic hydrocarbon responsiveness-receptor agonists generated from indole-3-carbinol in vitro and in vivo: Comparisons with 2,3,7,8-tetrachlorodibenzo-p-dioxin. Proc Natl Acad Sci USA 88:9543–9547.

Blasi E, Barluzzi R, Bocchini V, Mazzolla R, Bistoni F (1990) Immortalization of murine microglial cells by a v-raf / v-myc carrying retrovirus. J Neuroimmunol 27:229–237.

Bodeutsch N, Thanos S (2000) Migration of phagocytotic cells and development of the murine intraretinal microglial network: An in vivo study using fluorescent dyes. Glia 32:91–101.

Bose S, Kim S, Oh Y, Moniruzzaman M, Lee G, Cho J (2016) Effect of CCL2 on BV2 microglial cell migration: Involvement of probable signaling pathways. Cytokine 81:39–49.

Bowes Rickman C, Farsiu S, Toth CA, Klingeborn M (2013) Dry age-related macular

degeneration: Mechanisms, therapeutic targets, and imaging. Investig Ophthalmol Vis Sci 54:14 ORSF68–ORSF80.

Brinkmann V, Ale-Agha N, Haendeler J, Ventura N (2020) The Aryl Hydrocarbon Receptor (AhR) in the Aging Process: Another Puzzling Role for This Highly Conserved Transcription Factor. Front Physiol 10.

Brzezinski JA, Reh TA (2015) Photoreceptor cell fate specification in vertebrates. Dev 142:3263–3273.

Busbee PB, Rouse M, Nagarkatti M, Nagarkatti PS (2013) Use of natural AhR ligands as potential therapeutic modalities against inflammatory disorders. Nutr Rev 71:353–369.

Carneiro Â, Andrade JP (2017) Nutritional and Lifestyle Interventions for Age-Related Macular Degeneration: A Review. Oxid Med Cell Longev 2017:6469138.

Casano AM, Peri F (2015) Microglia: Multitasking specialists of the brain. Dev Cell 32:469–477.

Cascella R, Ragazzo M, Strafella C, Missiroli F, Borgiani P, Angelucci F, Marsella LT, Cusumano A, Novelli G, Ricci F, Giardina E (2014) Age-Related Macular Degeneration: Insights into Inflammatory Genes. J Ophthalmol 2014: 582842.

Chamovitz DA, Katz E, Nisani S (2018) Indole-3-carbinol: A plant hormone combatting cancer. F1000Research 7:689.

Chang H-P, Wang M-L, Hsu C-Y, Liu M-E, Chan M-H, Chen Y-H (2011) Suppression of inflammation-associated factors by indole-3-carbinol in mice fed high-fat diets and in isolated, co-cultured macrophages and adipocytes. Int J Obes 35:1530–1538.

Chen M, Xu H (2015) Parainflammation, chronic inflammation, and age-related macular degeneration. J Leukoc Biol 98:713–725.

Chen SJ, Cheng CY, Peng KL, Li AF, Hsu WM, Liu JH, Chou P (2008) Prevalence and associated risk factors of age-related macular degeneration in an elderly Chinese population in Taiwan: The Shihpai Eye Study. Investig Ophthalmol Vis Sci 49:3126–3133.

Chen WC, Chang LH, Huang SS, Huang YJ, Chih CL, Kuo HC, Lee YH, Lee IH (2019) Aryl hydrocarbon receptor modulates stroke-induced astrogliosis and

neurogenesis in the adult mouse brain. J Neuroinflammation 16:187.

Chen Z, Tao Z-Z, Chen S-M, Chen C, Li F, Xiao B-K (2013) Indole-3-Carbinol Inhibits Nasopharyngeal Carcinoma Growth through Cell Cycle Arrest In Vivo and In Vitro. PLoS One 8:e82288.

Chevallier A, Mialot A, Petit JM, Fernandez-Salguero P, Barouki R, Coumoul X, Beraneck M (2013) Oculomotor Deficits in Aryl Hydrocarbon Receptor Null Mouse. PLoS One 8:e53520.

Chiu CJ, Taylor A (2011) Dietary hyperglycemia, glycemic index and metabolic retinal diseases. Prog Retin Eye Res 30:18–53.

Choi Y, Abdelmegeed MA, Song BJ (2018) Preventive effects of indole-3-carbinol against alcohol-induced liver injury in mice via antioxidant, anti-inflammatory, and anti-apoptotic mechanisms: Role of gut-liver-adipose tissue axis. J Nutr Biochem 55:12–25.

Choi Y, Lee MK, Lim SY, Sung SH, Kim YC (2009) Inhibition of inducible NO synthase, cyclooxygenase-2 and interleukin-1β by torilin is mediated by mitogen-activated protein kinases in microglial BV2 cells. Br J Pharmacol 156:933–940.

Choudhary M, Kazmin D, Hu P, Thomas RS, McDonnell DP, Malek G (2015) Aryl hydrocarbon receptor knock-out exacerbates choroidal neovascularization via multiple pathogenic pathways. J Pathol 235:101–112.

Choudhary M, Malek G (2020) The Aryl Hydrocarbon Receptor: A Mediator and Potential Therapeutic Target for Ocular and Non-Ocular Neurodegenerative Diseases. Int J Mol Sci 21:6777.

Choudhary M, Safe S, Malek G (2018) Suppression of aberrant choroidal neovascularization through activation of the aryl hydrocarbon receptor. Biochim Biophys Acta - Mol Basis Dis 1864:1583–1595.

Contín MA, Benedetto MM, Quinteros-Quintana ML, Guido ME (2016) Light pollution: The possible consequences of excessive illumination on retina. Eye 30:255–263.

Copland DA, Calder CJ, Raveney BJE, Nicholson LB, Phillips J, Cherwinski H, Jenmalm M, Sedgwick JD, Dick AD (2007) Monoclonal antibody-mediated CD200 receptor signaling suppresses macrophage activation and tissue damage in experimental autoimmune uveoretinitis. Am J Pathol 171:580–588.

Cui Z, Feng Y, Li D, Li T, Gao P, Xu T (2020) Activation of aryl hydrocarbon receptor (AhR) in mesenchymal stem cells modulates macrophage polarization in asthma. J Immunotoxicol 17:21–30.

Danciger M, Matthes MT, Yasamura D, Akhmedov NB, Rickabaugh T, Gentleman S, Redmond TM, La Vail MM, Farber DB (2000) A QTL on distal Chromosome 3 that influences the severity of light-induced damage to mouse photoreceptors. Mamm Genome 11:422–427.

de la Parra J, Cuartero MI, Pérez-Ruiz A, García-Culebras A, Martín R, Sánchez-Prieto J, García-Segura JM, Lizasoain I, Moro MA (2018) AhR deletion promotes aberrant morphogenesis and synaptic activity of adult-generated granule neurons and impairs hippocampus-dependent memory. eNeuro 5:4.

Degner SC, Papoutsis AJ, Selmin O, Romagnolo DF (2009) Targeting of Aryl Hydrocarbon Receptor-Mediated Activation of Cyclooxygenase-2 Expression by the Indole-3-Carbinol Metabolite 3,3#-Diindolylmethane in Breast Cancer Cells 1,2. J Nutr Biochem Mol Genet Mech J Nutr 139:26–32.

Dietrich C (2016) Antioxidant Functions of the Aryl Hydrocarbon Receptor. Stem Cells Int 2016.

Dirscherl K, Karlstetter M, Ebert S, Kraus D, Hlawatsch J, Walczak Y, Moehle C, Fuchshofer R, Langmann T (2010) Luteolin triggers global changes in the microglial transcriptome leading to a unique anti-inflammatory and neuroprotective phenotype. J Neuroinflammation 7:3.

Diry M, Tomkiewicz C, Koehle C, Coumoul X, Bock KW, Barouki R, Transy C (2006) Activation of the dioxin/aryl hydrocarbon receptor (AhR) modulates cell plasticity through a JNK-dependent mechanism. Oncogene 25:5570–5574.

Domènech EB, Marfany G (2020) The relevance of oxidative stress in the pathogenesis and therapy of retinal dystrophies. Antioxidants 9:4.

Dong A, Xie B, Shen J, Yoshida T, Yokoi K, Hackett SF, Campochiaro PA (2009) Oxidative stress promotes ocular neovascularization. J Cell Physiol 219:544–552.

Doyle SL, Campbell M, Ozaki E, Salomon RG, Mori A, Kenna PF, Farrar GJ, Kiang AS, Humphries MM, Lavelle EC, O'Neill LAJ, Hollyfield JG, Humphries P (2012) NLRP3 has a protective role in age-related macular degeneration through the

induction of IL-18 by drusen components. Nat Med 18:791–798.

Dunaief JL, Dentchev T, Ying GS, Milam AH (2002) The role of apoptosis in age-related macular degeneration. Arch Ophthalmol 120:1435–1442.

Dunn KC, Aotaki-Keen AE, Putkey FR, Hjelmeland LM (1996) ARPE-19, a human retinal pigment epithelial cell line with differentiated properties. Exp Eye Res 62:155–170.

El-Naga RN, Ahmed HI, Abd Al Haleem EN (2014) Effects of indole-3-carbinol on clonidine-induced neurotoxicity in rats: Impact on oxidative stress, inflammation, apoptosis and monoamine levels. Neurotoxicology 44:48–57.

Elmore MRP, Najafi AR, Koike MA, Dagher NN, Spangenberg EE, Rice RA, Kitazawa M, Matusow B, Nguyen H, West BL, Green KN (2014) Colony-stimulating factor 1 receptor signaling is necessary for microglia viability, unmasking a microglia progenitor cell in the adult brain. Neuron 82:380–397.

Enan E, Matsumura F (1996) Identification of c-Src as the integral component of the cytosolic Ah receptor complex, transducing the signal of 2,3,7,8-tetrachlorodibenzo-p-dioxin (TCDD) through the protein phosphorylation pathway. Biochem Pharmacol 52:1599–1612.

Erblich B, Zhu L, Etgen AM, Dobrenis K, Pollard JW (2011) Absence of colony stimulation factor-1 receptor results in loss of microglia, disrupted brain development and olfactory deficits. PLoS One 6:10.

Erskine L, Herreral E (2015) Connecting the retina to the brain. ASN Neuro 6:26.

Esser C (2016) The aryl hydrocarbon receptor in immunity: Tools and potential. In: Methods in Molecular Biology, Humana Press Inc 1371:239-57.

Esser C, Rannug A (2015) The aryl hydrocarbon receptor in barrier organ physiology, immunology, and toxicology. Pharmacol Rev 67:259–279.

Fauser S, Viebahn U, Muether PS (2015) Intraocular and systemic inflammation-related cytokines during one year of ranibizumab treatment for neovascular age-related macular degeneration. Acta Ophthalmol 93:734–738.

Fernández-Arjona M del M, Grondona JM, Granados-Durán P, Fernández-Llebrez P, López-Ávalos MD (2017) Microglia Morphological Categorization in a Rat Model of Neuroinflammation by Hierarchical Cluster and Principal Components Analysis.

Front Cell Neurosci 11:235.

Fernandez-Salguero P, Pineau T, Hilbert DM, McPhail T, Lee SST, Kimura S, Nebert DW, Rudikoff S, Ward JM, Gonzalez FJ (1995) Immune system impairment and hepatic fibrosis in mice lacking the dioxin-binding Ah receptor. Science (80-) 268:722–726.

Fernandez-Salguero P, Ward JM, Sundberg JP, Gonzalez FJ (1997) Lesions of Aryl-hydrocarbon Receptor-deficient Mice. Vet Pathol 34:605–614.

Ferrer-Martín RM, Martín-Oliva D, Sierra-Martín A, Carrasco M-C, Martín-Estebané M, Calvente R, Martín-Guerrero SM, Marín-Teva JL, Navascués J, Cuadros MA (2015) Microglial Activation Promotes Cell Survival in Organotypic Cultures of Postnatal Mouse Retinal Explants Block ML, ed. PLoS One 10:e0135238.

Fiebich BL, Batista CRA, Saliba SW, Yousif NM, de Oliveira ACP (2018) Role of microglia TLRs in neurodegeneration. Front Cell Neurosci 12:329.

Fletcher EL (2020) Contribution of microglia and monocytes to the development and progression of age related macular degeneration. Ophthalmic Physiol Opt 40:128–139.

Fletcher EL, Jobling AI, Greferath U, Mills SA, Waugh M, Ho T, De Iongh RU, Phipps JA, Vessey KA (2014) Studying age-related macular degeneration using animal models. Optom Vis Sci 91:878–886.

Frericks M, Meissner M, Esser C (2007) Microarray analysis of the AHR system: Tissue-specific flexibility in signal and target genes. Toxicol Appl Pharmacol 220:320–332.

Fritsche LG, Fariss RN, Stambolian D, Abecasis GR, Curcio CA, Swaroop A (2014) Age-Related Macular Degeneration: Genetics and Biology Coming Together. Annu Rev Genomics Hum Genet 15:151–171.

Frost JL, Schafer DP (2016) Microglia: Architects of the Developing Nervous System. Trends Cell Biol 26:587–597.

Fu R, Shen Q, Xu P, Luo JJ, Tang Y (2014) Phagocytosis of microglia in the central nervous system diseases. Mol Neurobiol 49:1422–1434.

Fujii-Kuriyama Y, Kawajiri K (2010) Molecular mechanisms of the physiological functions of the aryl hydrocarbon (dioxin) receptor, a multifunctional regulator that

senses and responds to environmental stimuli. Proc Japan Acad Ser B Phys Biol Sci 86:40–53.

Fukunaga BN, Probst MR, Reisz-Porszasz S, Hankinson O (1995) Identification of functional domains of the aryl hydrocarbon receptor. J Biol Chem 270:29270–29278.

Galloway DA, Phillips AEM, Owen DRJ, Moore CS (2019) Phagocytosis in the brain: Homeostasis and disease. Front Immunol 10:1575.

Gao J, Liu RT, Cao S, Cui JZ, Wang A, To E, Matsubara JA (2015) NLRP3 Inflammasome: Activation and Regulation in Age-Related Macular Degeneration. Mediators Inflamm 2015: 690243.

García-Layana A, Cabrera-López F, García-Arumí J, Arias-Barquet L, Ruiz-Moreno JM (2017) Early and intermediate age-related macular degeneration: Update and clinical review. Clin Interv Aging 12:1579–1587.

Gehrs KM, Anderson DH, Johnson L V., Hageman GS (2006) Age-related macular degeneration—emerging pathogenetic and therapeutic concepts. Ann Med 38:450–471.

Giaimo R Di, Durovic T, Barquin P, Wurst W, Stricker SH, Ninkovic J (2018) The Aryl Hydrocarbon Receptor Pathway Defines the Time Frame for Restorative Neurogenesis. CellReports 25:3241-3251.e5.

Ginhoux F, Lim S, Hoeffel G, Low D, Huber T (2013) Origin and differentiation of microglia. Front Cell Neurosci 7:45.

Ginhoux F, Prinz M (2015) Origin of microglia: Current concepts and past controversies. Cold Spring Harb Perspect Biol 7:a020537.

Golestaneh N, Chu Y, Xiao YY, Stoleru GL, Theos AC (2017) Dysfunctional autophagy in RPE, a contributing factor in age-related macular degeneration. Cell Death Dis 8:e2537–e2537.

Grimm C, Remé CE (2012) Light Damage as a Model of Retinal Degeneration. In: Methods in molecular biology (Clifton, N.J.) Methods Mol Biol. 87–97.

Grimm C, Wenzel A, Stanescu D, Samardzija M, Hotop S, Groszer M, Naash M, Gassmann M, Remé C (2004) Constitutive overexpression of human erythropoietin protects the mouse retina against induced but not inherited retinal

degeneration. J Neurosci 24:5651–5658.

Gupta N, Brown KE, Milam AH (2003) Activated microglia in human retinitis pigmentosa, late-onset retinal degeneration, and age-related macular degeneration. Exp Eye Res 76:463–471.

Gutiérrez-Vázquez C, Quintana FJ (2018) Regulation of the Immune Response by the Aryl Hydrocarbon Receptor. Immunity 48:19–33.

Gutierrez MA, Davis SS, Rosko A, Nguyen SM, Mitchell KP, Mateen S, Neves J, Garcia TY, Mooney S, Perdew GH, Hubbard TD, Lamba DA, Ramanathan A (2016) A novel AhR ligand, 2AI, protects the retina from environmental stress. Sci Rep 6:29025.

Guttenplan K, Blum J, Bennett M (2018) A role for microglia in retinal development. J Neurosci 38:9126–9128.

Hao N, Whitelaw ML (2013) The emerging roles of AhR in physiology and immunity. Biochem Pharmacol 86:561–570.

Harrigan TJ, Abdullaev IF, Jourd'heuil D, Mongin AA (2008) Activation of microglia with zymosan promotes excitatory amino acid release via volume-regulated anion channels: The role of NADPH oxidases. J Neurochem 106:2449–2462.

Hassell JB, Lamoureux EL, Keeffe JE (2006) Impact of age related macular degeneration on quality of life. Br J Ophthalmol 90:593–596.

Heesterbeek TJ, Lorés-Motta L, Hoyng CB, Lechanteur YTE, den Hollander AI (2020a) Risk factors for progression of age-related macular degeneration. Ophthalmic Physiol Opt 40:140–170.

Heesterbeek TJ, Lorés-Motta L, Hoyng CB, Lechanteur YTE, den Hollander AI (2020b) Risk factors for progression of age-related macular degeneration. Ophthalmic Physiol Opt 40:140–170.

Henn A, Lund S, Hedtjärn M, Schrattenholz A, Pörzgen P, Leist M (2009) The suitability of BV2 cells as alternative model system for primary microglia cultures or for animal experiments examining brain inflammation. ALTEX 26:83–94.

Hickman S, Izzy S, Sen P, Morsett L, El Khoury J (2018) Microglia in neurodegeneration. Nat Neurosci 21:1359–1369.

Hoon M, Okawa H, Della Santina L, Wong ROL (2014) Functional architecture of the

retina: Development and disease. Prog Retin Eye Res 42:44–84.

Horie S, Robbie SJ, Liu J, Wu WK, Ali RR, Bainbridge JW, Nicholson LB, Mochizuki M, Dick AD, Copland DA (2013) CD200R signaling inhibits pro-angiogenic gene expression by macrophages and suppresses choroidal neovascularization. Sci Rep 3:1–10.

Hu P et al. (2013) Aryl hydrocarbon receptor deficiency causes dysregulated cellular matrix metabolism and age-related macular degeneration-like pathology. Proc Natl Acad Sci USA 110:E4069–E4078.

Huai W, Zhao R, Song H, Zhao J, Zhang L, Zhang L, Gao C, Han L, Zhao W (2014) Aryl hydrocarbon receptor negatively regulates NLRP3 inflammasome activity by inhibiting NLRP3 transcription. Nat Commun 5:1–9.

Huang L, Xu W, Xu G (2013) Transplantation of CX3CL1-expressing mesenchymal stem cells provides neuroprotective and immunomodulatory effects in a rat model of retinal degeneration. Ocul Immunol Inflamm 21:276–285.

Huang Y, He J, Liang H, Hu K, Jiang S, Yang L, Mei S, Zhu X, Yu J, Kijlstra A, Yang P, Hou S (2018a) Aryl hydrocarbon receptor regulates apoptosis and inflammation in a murine model of experimental autoimmune uveitis. Front Immunol 9:1713.

Huang Y, Xu Z, Xiong S, Qin G, Sun F, Yang J, Yuan TF, Zhao L, Wang K, Liang YX, Fu L, Wu T, So KF, Rao Y, Peng B (2018b) Dual extra-retinal origins of microglia in the model of retinal microglia repopulation. Cell Discov 4:9.

Indaram M, Ma W, Zhao L, Fariss RN, Rodriguez IR, Wong WT (2015) 7-Ketocholesterol Increases Retinal Microglial Migration, Activation, and Angiogenicity: A Potential Pathogenic Mechanism Underlying Age-related Macular Degeneration. Sci Rep 5:1–10.

Jang S, Kelley KW, Johnson RW (2008) Luteolin reduces IL-6 production in microglia by inhibiting JNK phosphorylation and activation of AP-1. Proc Natl Acad Sci USA 105:7534–7539.

Jarrett SG, Boulton ME (2012) Consequences of oxidative stress in age-related macular degeneration. Mol Aspects Med 33:399–417.

Ji Cho M, Yoon SJ, Kim W, Park J, Lee J, Park JG, Cho YL, Hun Kim J, Jang H, Park YJ, Lee SH, Min JK (2019) Oxidative stress-mediated TXNIP loss causes RPE

dysfunction. Exp Mol Med 51:121.

Jiang D, Ryals RC, Huang SJ, Weller KK, Titus HE, Robb BM, Saad FW, Salam RA, Hammad H, Yang P, Marks DL, Pennesi ME (2019) Monomethyl fumarate protects the retina from light-induced retinopathy. Investig Ophthalmol Vis Sci 60:1275–1285.

Jiang J, Kang TB, Shim DW, Oh NH, Kim TJ, Lee KH (2013) Indole-3-carbinol inhibits LPS-induced inflammatory response by blocking TRIF-dependent signaling pathway in macrophages. Food Chem Toxicol 57:256–261.

Jin UH, Park H, Li X, Davidson LA, Allred C, Patil B, Jayaprakasha G, Orr AA, Mao L, Chapkin RS, Jayaraman A, Tamamis P, Safe S (2018) Structure-dependent modulation of aryl hydrocarbon receptor-mediated activities by flavonoids. Toxicol Sci 164:205–217.

Jurgens HA, Johnson RW (2012) Dysregulated neuronal-microglial cross-talk during aging, stress and inflammation. Exp Neurol 233:40–48.

Juricek L, Carcaud J, Pelhaitre A, Riday TT, Chevallier A, Lanzini J, Auzeil N, Laprévote O, Dumont F, Jacques S, Letourneur F, Massaad C, Agulhon C, Barouki R, Beraneck M, Coumoul X (2017) AhR-deficiency as a cause of demyelinating disease and inflammation. Sci Rep 7.

Juricek L, Coumoul X (2018) The aryl hydrocarbon receptor and the nervous system. Int J Mol Sci 19.

Karlstetter M, Lippe E, Walczak Y, Moehle C, Aslanidis A, Mirza M, Langmann T (2011) Curcumin is a potent modulator of microglial gene expression and migration. J Neuroinflammation 8:125.

Karlstetter M, Nothdurfter C, Aslanidis A, Moeller K, Horn F, Scholz R, Neumann H, Weber BHF, Rupprecht R, Langmann T (2014) Translocator protein (18 kDa) (TSPO) is expressed in reactive retinal microglia and modulates microglial inflammation and phagocytosis. J Neuroinflammation 11:3.

Karlstetter M, Scholz R, Rutar M, Wong WT, Provis JM, Langmann T (2015) Retinal microglia: Just bystander or target for therapy? Prog Retin Eye Res 45:30–57.

Kauppinen A, Paterno JJ, Blasiak J, Salminen A, Kaarniranta K (2016) Inflammation and its role in age-related macular degeneration. Cell Mol Life Sci 73:1765–1786.

Kaye J, Piryatinsky V, Birnberg T, Hingaly T, Raymond E, Kashi R, Amit-Romach E, Caballero IS, Towfic F, Ator MA, Rubinstein E, Laifenfeld D, Orbach A, Shinar D, Marantz Y, Grossman I, Knappertz V, Hayden MR, Laufer R (2016) Laquinimod arrests experimental autoimmune encephalomyelitis by activating the aryl hydrocarbon receptor. Proc Natl Acad Sci USA 113:E6145–E6152.

Keeling E, Lotery A, Tumbarello D, Ratnayaka J (2018) Impaired Cargo Clearance in the Retinal Pigment Epithelium (RPE) Underlies Irreversible Blinding Diseases. Cells 7:16.

Kerkvliet NI (2009) AHR-mediated immunomodulation: The role of altered gene transcription. Biochem Pharmacol 77:746–760.

Khan A, Ali T, Rehman SU, Khan MS, Alam SI, Ikram M, Muhammad T, Saeed K, Badshah H, Kim MO (2018) Neuroprotective Effect of Quercetin Against the Detrimental Effects of LPS in the Adult Mouse Brain. Front Pharmacol 9:1383.

Kigerl KA, de Rivero Vaccari JP, Dietrich WD, Popovich PG, Keane RW (2014) Pattern recognition receptors and central nervous system repair. Exp Neurol 258:5–16.

Kim HW, Kim J, Kim J, Lee S, Choi BR, Han JS, Lee KW, Lee HJ (2014a) 3,3'-Diindolylmethane Inhibits Lipopolysaccharide-Induced Microglial Hyperactivation and Attenuates Brain Inflammation. Toxicol Sci 137:158–167.

Kim SY, Chang YS, Chang YS, Kim JW, Brooks M, Chew EY, Wong WT, Fariss RN, Rachel RA, Cogliati T, Qian H, Swaroop A (2014b) Deletion of aryl hydrocarbon receptor AHR in mice leads to subretinal accumulation of microglia and RPE atrophy. Investig Ophthalmol Vis Sci 55:6031–6040.

Klein R, Klein BEK, Moss SE (1998) Relation of smoking to the incidence of age-related maculopathy. The beaver dam eye study. Am J Epidemiol 147:103–110.

Kudo I, Hosaka M, Haga A, Tsuji N, Nagata Y, Okada H, Fukuda K, Kakizaki Y, Okamoto T, Grave E, Itoh H (2018) The regulation mechanisms of AhR by molecular chaperone complex. J Biochem 163:223–232.

Kumar A, Pandey RK, Miller LJ, Singh PK, Kanwar M (2013) Müller glia in retinal innate immunity: A perspective on their roles in endophthalmitis. Crit Rev Immunol 33:119–135.

Lamas B, Natividad JM, Sokol H (2018) Aryl hydrocarbon receptor and intestinal

immunity review-article. Mucosal Immunol 11:1024–1038.

Lamb TD (2013) Evolution of phototransduction, vertebrate photoreceptors and retina. Prog Retin Eye Res 36:52–119.

Lamb TD, Collin SP, Pugh EN (2007) Evolution of the vertebrate eye: Opsins, photoreceptors, retina and eye cup. Nat Rev Neurosci 8:960–976.

Lambert NG, ElShelmani H, Singh MK, Mansergh FC, Wride MA, Padilla M, Keegan D, Hogg RE, Ambati BK (2016) Risk factors and biomarkers of age-related macular degeneration. Prog Retin Eye Res 54:64–102.

Langmann T (2007) Microglia activation in retinal degeneration. J Leukoc Biol 81:1345–1351.

Larigot L, Juricek L, Dairou J, Coumoul X (2018) AhR signaling pathways and regulatory functions. Biochim Open 7:1–9.

Latchney SE, Hein AM, O'Banion MK, Dicicco-Bloom E, Opanashuk LA (2013) Deletion or activation of the aryl hydrocarbon receptor alters adult hippocampal neurogenesis and contextual fear memory. J Neurochem 125:430–445.

Lawson LJ, Perry VH, Dri P, Gordon S (1990) Heterogeneity in the distribution and morphology of microglia in the normal adult mouse brain. Neuroscience 39:151–170.

Lee BB, Martin PR, Grünert U (2010) Retinal connectivity and primate vision. Prog Retin Eye Res 29:622–639.

Lee HU, McPherson ZE, Tan B, Korecka A, Pettersson S (2017) Host-microbiome interactions: the aryl hydrocarbon receptor and the central nervous system. J Mol Med 95:29–39.

Lenz KM, Nelson LH (2018) Microglia and beyond: Innate immune cells as regulators of brain development and behavioral function. Front Immunol 9:1.

Levy O, Calippe B, Lavalette S, Hu SJ, Raoul W, Dominguez E, Housset M, Paques M, Sahel J, Bemelmans A, Combadiere C, Guillonneau X, Sennlaub F (2015) Apolipoprotein E promotes subretinal mononuclear phagocyte survival and chronic inflammation in age-related macular degeneration. EMBO Mol Med 7:211–226.

Liang KJ, Lee JE, Wang YD, Ma W, Fontainhas AM, Fariss RN, Wong WT (2009)

Regulation of dynamic behavior of retinal microglia by CX3CR1 signaling. Investig Ophthalmol Vis Sci 50:4444–4451.

Lim HS, Kim YJ, Kim BY, Park G, Jeong SJ (2018) The anti-neuroinflammatory activity of tectorigenin pretreatment via downregulated NF-κB and ERK/JNK pathways in BV-2 microglial and microglia inactivation in mice with lipopolysaccharide. Front Pharmacol 9:462.

Linnartz-Gerlach B, Mathews M, Neumann H (2014) Sensing the neuronal glycocalyx by glial sialic acid binding immunoglobulin-like lectins. Neuroscience 275:113–124.

Lu X, Ma L, Ruan L, Kong Y, Mou H, Zhang Z, Wang Z, Wang JM, Le Y (2010) Resveratrol differentially modulates inflammatory responses of microglia and astrocytes. J Neuroinflammation 7:46.

Lückoff A, Caramoy A, Scholz R, Prinz M, Kalinke U, Langmann T (2016) Interferon-beta signaling in retinal mononuclear phagocytes attenuates pathological neovascularization. EMBO Mol Med 8:670–678.

Luibl V, Isas JM, Kayed R, Glabe CG, Langen R, Chen J (2006) Drusen deposits associated with aging and age-related macular degeneration contain nonfibrillar amyloid oligomers. J Clin Invest 116:378–385.

Madeira MH, Rashid K, Ambrósio AF, Santiago AR, Langmann T (2018) Blockade of microglial adenosine A2A receptor impacts inflammatory mechanisms, reduces ARPE-19 cell dysfunction and prevents photoreceptor loss in vitro. Sci Rep 8:1–15.

Malek G, Lad EM (2014) Emerging roles for nuclear receptors in the pathogenesis of age-related macular degeneration. Cell Mol Life Sci 71:4617–4636.

Mariathasan S, Weiss DS, Newton K, McBride J, O'Rourke K, Roose-Girma M, Lee WP, Weinrauch Y, Monack DM, Dixit VM (2006) Cryopyrin activates the inflammasome in response to toxins and ATP. Nature 440:228–232.

Marlowe JL, Fan Y, Chang X, Peng L, Knudsen ES, Xia Y, Puga A (2008) The aryl hydrocarbon receptor binds to E2F1 and inhibits E2F1-induced apoptosis. Mol Biol Cell 19:3263–3271.

Martin DF, Maguire MG, Fine SL, Ying GS, Jaffe GJ, Grunwald JE, Toth C, Redford

M, Ferris FL (2012) Ranibizumab and bevacizumab for treatment of neovascular age-related macular degeneration: Two-year results. Ophthalmology 119:1388–1398.

Masland RH (2001) Neuronal diversity in the retina. Curr Opin Neurobiol 11:431–436.

Masland RH (2011) Cell populations of the retina: The proctor lecture. Investig Ophthalmol Vis Sci 52:4581–4591.

Masland RH (2012) The Neuronal Organization of the Retina. Neuron 76:266–280.

Matcovitch-Natan O et al. (2016) Microglia development follows a stepwise program to regulate brain homeostasis. Science 80:353.

Mazaheri F, Breus O, Durdu S, Haas P, Wittbrodt J, Gilmour D, Peri F (2014) Distinct roles for BAI1 and TIM-4 in the engulfment of dying neurons by microglia. Nat Commun 5:1–11.

Mazaheri F, Snaidero N, Kleinberger G, Madore C, Daria A, Werner G, Krasemann S, Capell A, Trümbach D, Wurst W, Brunner B, Bultmann S, Tahirovic S, Kerschensteiner M, Misgeld T, Butovsky O, Haass C (2017) TREM 2 deficiency impairs chemotaxis and microglial responses to neuronal injury. EMBO Rep 18:1186–1198.

McCarthy CA, Widdop RE, Deliyanti D, Wilkinson-Berka JL (2013) Brain and retinal microglia in health and disease: An unrecognized target of the renin-angiotensin system. Clin Exp Pharmacol Physiol 40:571–579.

McMenamin PG, Saban DR, Dando SJ (2019) Immune cells in the retina and choroid: Two different tissue environments that require different defenses and surveillance. Prog Retin Eye Res 70:85–98.

Meyer BK, Perdew GH (1999) Characterization of the AhR-hsp90-XAP2 core complex and the role of the immunophilin-related protein XAP2 in AhR stabilization. Biochemistry 38:8907–8917.

Michalska-Małecka K, Kabiesz A, Nowak M, Śpiewak D (2015) Age related macular degeneration - Challenge for future: Pathogenesis and new perspectives for the treatment. Eur Geriatr Med 6:69–75.

Mitchell J, Bradley C (2006) Quality of life in age-related macular degeneration: A review of the literature. Health Qual Life Outcomes 4:97.

Mohammadi-Bardbori A, Bengtsson J, Rannug U, Rannug A, Wincent E (2012) Quercetin, resveratrol, and curcumin are indirect activators of the aryl hydrocarbon receptor (AHR). Chem Res Toxicol 25:1878–1884.

Molday RS, Moritz OL (2015) Photoreceptors at a glance. J Cell Sci 128:4039–4045.

Mulfaul K, Ozaki E, Fernando N, Brennan K, Chirco KR, Connolly E, Greene C, Maminishkis A, Salomon RG, Linetsky M, Natoli R, Mullins RF, Campbell M, Doyle SL (2020) Toll-like Receptor 2 Facilitates Oxidative Damage-Induced Retinal Degeneration. Cell Rep 30:2209-2224.e5.

Myers CE, Klein BEK, Gangnon R, Sivakumaran TA, Iyengar SK, Klein R (2014) Cigarette smoking and the natural history of age-related macular degeneration: The beaver dam eye study. Ophthalmology 121:1949–1955.

Nam HY, Nam JH, Yoon G, Lee JY, Nam Y, Kang HJ, Cho HJ, Kim J, Hoe HS (2018) Ibrutinib suppresses LPS-induced neuroinflammatory responses in BV2 microglial cells and wild-type mice. J Neuroinflammation 15:271.

Napoli I, Neumann H (2009) Microglial clearance function in health and disease. Neuroscience 158:1030–1038.

Natoli R, Fernando N, Jiao H, Racic T, Madigan M, Barnett NL, Chu-Tan JA, Valter K, Provis J, Rutar M (2017) Retinal macrophages synthesize C3 and activate complement in AMD and in models of focal retinal degeneration. Investig Ophthalmol Vis Sci 58:2977–2990.

Nebel C, Aslanidis A, Rashid K, Langmann T (2017) Activated microglia trigger inflammasome activation and lysosomal destabilization in human RPE cells. Biochem Biophys Res Commun 484:681–686.

Nozaki M, Raisler BJ, Sakurai E, Sarma JV, Barnum SR, Lambris JD, Chen Y, Zhang K, Ambati BK, Baffi JZ, Ambati J (2006) Drusen complement components C3a and C5a promote choroidal neovascularization. Proc Natl Acad Sci 103:2328–2333.

Obert E, Strauss R, Brandon C, Grek C, Ghatnekar G, Gourdie R, Rohrer B (2017) Targeting the tight junction protein, zonula occludens-1, with the connexin43 mimetic peptide, αCT1, reduces VEGF-dependent RPE pathophysiology. J Mol Med 95:535–552.

Organisciak DT, Vaughan DK (2010) Retinal light damage: Mechanisms and protection. Prog Retin Eye Res 29:113–134.

Owsley C, McGwin G (2008) Driving and Age-Related Macular Degeneration. J Vis Impair Blind 102:621–635.

Paliwal P, Chauhan G, Gautam D, Dash D, Patne SCU, Krishnamurthy S (2018) Indole-3-carbinol improves neurobehavioral symptoms in a cerebral ischemic stroke model. Naunyn Schmiedebergs Arch Pharmacol 391:613–625.

Paolicelli RC, Ferretti MT (2017) Function and dysfunction of microglia during brain development: Consequences for synapses and neural circuits. Front Synaptic Neurosci 9:71.

Pattamatta U, McPherson Z, White A (2016) A mouse retinal explant model for use in studying neuroprotection in glaucoma. Exp Eye Res 151:38–44.

Paul D, Achouri S, Yoon YZ, Herre J, Bryant CE, Cicuta P (2013) Phagocytosis dynamics depends on target shape. Biophys J 105:1143–1150.

Pennesi ME, Neuringer M, Courtney RJ (2012) Animal models of age related macular degeneration. Mol Aspects Med 33:487–509.

Prinz M, Jung S, Priller J (2019) Microglia Biology: One Century of Evolving Concepts. Cell 179:292–311.

Puga A, Ma C, Marlowe JL (2009) The aryl hydrocarbon receptor cross-talks with multiple signal transduction pathways. Biochem Pharmacol 77:713–722.

Puga A, Marlowe J, Barnes S, Chang CY, Maier A, Tan Z, Kerzee JK, Chang X, Strobeck M, Knudsen ES (2002) Role of the aryl hydrocarbon receptor in cell cycle regulation. Toxicology 181-182:171-177.

Puigdellívol M, Allendorf DH, Brown GC (2020) Sialylation and Galectin-3 in Microglia-Mediated Neuroinflammation and Neurodegeneration. Front Cell Neurosci 14:162.

Ramirez AI, de Hoz R, Salobrar-Garcia E, Salazar JJ, Rojas B, Ajoy D, López-Cuenca I, Rojas P, Triviño A, Ramírez JM (2017) The role of microglia in retinal neurodegeneration: Alzheimer's disease, Parkinson, and glaucoma. Front Aging Neurosci 9:214.

Ramkumar HL, Zhang J, Chan CC (2010) Retinal ultrastructure of murine models of

dry age-related macular degeneration (AMD). Prog Retin Eye Res 29:169–190.

Raoul W, Auvynet C, Camelo S, Guillonneau X, Feumi C, Combadière C, Sennlaub F (2010) CCL2/CCR2 and CX3CL1/CX3CR1 chemokine axes and their possible involvement in age-related macular degeneration. J Neuroinflammation 7:1–7.

Rashid K, Akhtar-Schaefer I, Langmann T (2019) Microglia in retinal degeneration. Front Immunol 10:1975.

Rashid K, Verhoyen M, Taiwo M, Langmann T (2020) Translocator protein (18 kDa) (TSPO) ligands activate Nrf2 signaling and attenuate inflammatory responses and oxidative stress in human retinal pigment epithelial cells. Biochem Biophys Res Commun 528:261–268.

Rashid K, Wolf A, Langmann T (2018) Microglia activation and immunomodulatory therapies for retinal degenerations. Front Cell Neurosci 12:201.

Rathnasamy G, Foulds WS, Ling EA, Kaur C (2019) Retinal microglia – A key player in healthy and diseased retina. Prog Neurobiol 173:18–40.

Réu P, Khosravi A, Bernard S, Mold JE, Salehpour M, Alkass K, Perl S, Tisdale J, Possnert G, Druid H, Frisén J (2017) The Lifespan and Turnover of Microglia in the Human Brain. Cell Rep 20:779–784.

Romero-Sandoval EA, Horvath R, Landry RP, DeLeo JA (2009) Cannabinoid receptor type 2 activation induces a microglial anti-inflammatory phenotype and reduces migration via MKP induction and ERK dephosphorylation. Mol Pain 5:25.

Rothhammer V et al. (2016) Type i interferons and microbial metabolites of tryptophan modulate astrocyte activity and central nervous system inflammation via the aryl hydrocarbon receptor. Nat Med 22:586–597.

Rothhammer V et al. (2018) Microglial control of astrocytes in response to microbial metabolites. Nature 557:724–728.

Rothhammer V, Quintana FJ (2019) The aryl hydrocarbon receptor: an environmental sensor integrating immune responses in health and disease. Nat Rev Immunol 19:184–197.

Rouse M, Singh NP, Nagarkatti PS, Nagarkatti M (2013) Indoles mitigate the development of experimental autoimmune encephalomyelitis by induction of reciprocal differentiation of regulatory T cells and Th17 cells. Br J Pharmacol

169:1305–1321.

Roztocil E, Hammond CL, Gonzalez MO, Feldon SE, Woeller CF (2020) The aryl hydrocarbon receptor pathway controls matrix metalloproteinase-1 and collagen levels in human orbital fibroblasts. Sci Rep 10:1–16.

Rutar M, Natoli R, Provis JM (2012) Small interfering RNA-mediated suppression of Ccl2 in Müller cells attenuates microglial recruitment and photoreceptor death following retinal degeneration. J Neuroinflammation 9:221.

Rutar M, Natoli R, Valter K, Provis JM (2011) Early focal expression of the chemokine Ccl2 by Müller cells during exposure to damage-inducing bright continuous light. Investig Ophthalmol Vis Sci 52:2379–2388.

Saccà SC, Vagge A, Pulliero A, Izzotti A (2014) Helicobacter pylori infection and eye diseases: A systematic review. Med (United States) 93:e216.

Safe S, Han H, Goldsby J, Mohankumar K, Chapkin RS (2018) Aryl hydrocarbon receptor (AhR) ligands as selective AhR modulators: Genomic studies. Curr Opin Toxicol 11–12:10–20.

Saini N, Akhtar A, Chauhan M, Dhingra N, Pilkhwal Sah S (2020) Protective effect of Indole-3-carbinol, an NF-κB inhibitor in experimental paradigm of Parkinson's disease: In silico and in vivo studies. Brain Behav Immun 90:108-137.

Sakurai S, Shimizu T, Ohto U (2017) The crystal structure of the AhRR–ARNT heterodimer reveals the structural basis of the repression of AhR-mediated transcription. J Biol Chem 292:17609–17616.

Sato T, Takeuchi M, Karasawa Y, Takayama K, Enoki T (2019) Comprehensive expression patterns of inflammatory cytokines in aqueous humor of patients with neovascular age-related macular degeneration. Sci Rep 9:1–13.

Sayyad Z, Sirohi K, Radha V, Swarup G (2017) 661W is a retinal ganglion precursor-like cell line in which glaucoma-associated optineurin mutants induce cell death selectively. Sci Rep 7:1–13.

Schick T, Steinhauer M, Aslanidis A, Altay L, Karlstetter M, Langmann T, Kirschfink M, Fauser S (2017) Local complement activation in aqueous humor in patients with age-related macular degeneration. Eye 31:810–813.

Schnekenburger M, Peng L, Puga A (2007) HDAC1 bound to the Cyp1a1 promoter

blocks histone acetylation associated with Ah receptor-mediated trans-activation. Biochim Biophys Acta - Gene Struct Expr 1769:569–578.

Schnichels S, Paquet-Durand F, Löscher M, Tsai T, Hurst J, Joachim SC, Klettner A (2020) Retina in a dish: Cell cultures, retinal explants and animal models for common diseases of the retina. Prog Retin Eye Res:100880.

Scholz R, Caramoy A, Bhuckory MB, Rashid K, Chen M, Xu H, Grimm C, Langmann T (2015a) Targeting translocator protein (18 kDa) (TSPO) dampens pro-inflammatory microglia reactivity in the retina and protects from degeneration. J Neuroinflammation 12:201.

Scholz R, Sobotka M, Caramoy A, Stempfl T, Moehle C, Langmann T (2015b) Minocycline counter-regulates pro-inflammatory microglia responses in the retina and protects from degeneration. J Neuroinflammation 12:209.

Schwarzer P, Kokona D, Ebneter A, Zinkernagel MS (2020) Effect of Inhibition of Colony-Stimulating Factor 1 Receptor on Choroidal Neovascularization in Mice. Am J Pathol 190:412–425.

Seddon JM, Reynolds R, Yu Y, Daly MJ, Rosner B (2011) Risk models for progression to advanced age-related macular degeneration using demographic, environmental, genetic, and ocular factors. Ophthalmology 118:2203–2211.

Sennlaub F et al. (2013) CCR2+ monocytes infiltrate atrophic lesions in age-related macular disease and mediate photoreceptor degeneration in experimental subretinal inflammation in Cx3cr1 deficient mice. EMBO Mol Med 5:1775–1793.

Shinde R, McGaha TL (2018) The Aryl Hydrocarbon Receptor: Connecting Immunity to the Microenvironment. Trends Immunol 39:1005–1020.

Sierra A, Encinas JM, Deudero JJP, Chancey JH, Enikolopov G, Overstreet-Wadiche LS, Tsirka SE, Maletic-Savatic M (2010) Microglia shape adult hippocampal neurogenesis through apoptosis-coupled phagocytosis. Cell Stem Cell 7:483–495.

Silverman SM, Wong WT (2018) Microglia in the Retina: Roles in Development, Maturity, and Disease. Annu Rev Vis Sci 4:45–77.

Slakter JS, Stur M (2005) Quality of life in patients with age-related macular degeneration: Impact of the condition and benefits of treatment. Surv Ophthalmol

50:263–273.

Smith ME, Van Maesen K Der, Somera FP, Sobel RA (1998) Effects of phorbol myristate acetate (PMA) on functions of macrophages and microglia in vitro. Neurochem Res 23:427–434.

Sousa C, Biber K, Michelucci A (2017) Cellular and molecular characterization of microglia: A unique immune cell population. Front Immunol 8:198.

Spindler J, Zandi S, Pfister IB, Gerhardt C, Garweg JG (2018) Cytokine profiles in the aqueous humor and serum of patients with dry and treated wet age-related macular degeneration Jablonski MM, ed. PLoS One 13:e0203337.

Squarzoni P, Oller G, Hoeffel G, Pont-Lezica L, Rostaing P, Low D, Bessis A, Ginhoux F, Garel S (2014) Microglia Modulate Wiring of the Embryonic Forebrain. Cell Rep 8:1271–1279.

Stansley B, Post J, Hensley K (2012) A comparative review of cell culture systems for the study of microglial biology in Alzheimer's disease. J Neuroinflammation 9:577.

Stejskalova L, Vecerova L, Peréz LM, Vrzal R, Dvorak Z, Nachtigal P, Pavek P (2011) Aryl hydrocarbon receptor and aryl hydrocarbon nuclear translocator expression in human and rat placentas and transcription activity in human trophoblast cultures. Toxicol Sci 123:26–36.

Stockinger B, Meglio P Di, Gialitakis M, Duarte JH (2014) The Aryl Hydrocarbon Receptor: Multitasking in the Immune System. Annu Rev Immunol 32:403–432.

Stratoulias V, Venero JL, Tremblay M, Joseph B (2019) Microglial subtypes: diversity within the microglial community. EMBO J 2:38.

Sun GY, Chen Z, Jasmer KJ, Chuang DY, Gu Z, Hannink M, Simonyi A (2015) Quercetin Attenuates Inflammatory Responses in BV-2 Microglial Cells: Role of MAPKs on the Nrf2 Pathway and Induction of Heme Oxygenase-1. PLoS One 10:e0141509.

Suñer IJ, Espinosa-Heidmann DG, Marin-Castano ME, Hernandez EP, Pereira-Simon S, Cousins SW (2004) Nicotine Increases Size and Severity of Experimental Choroidal Neovascularization. Investig Ophthalmol Vis Sci 45:311–317.

Sung CH, Chuang JZ (2010) The cell biology of vision. J Cell Biol 190:953–963.

Sunness JS, Gonzalez-Baron J, Applegate CA, Bressler NM, Tian Y, Hawkins B,

Barron Y, Bergman A (1999) Enlargement of atrophy and visual acuity loss in the geographic atrophy form of age-related macular degeneration. Ophthalmology 106:1768–1779.

Takeuchi A, Takeuchi M, Oikawa K, Sonoda KH, Usui Y, Okunuki Y, Takeda A, Oshima Y, Yoshida K, Usui M, Goto H, Kuroda M (2009) Effects of dioxin on vascular endothelial growth factor (VEGF) production in the retina associated with choroidal neovascularization. Investig Ophthalmol Vis Sci 50:3410–3416.

Tan E, Ding XQ, Saadi A, Agarwal N, Naash MI, Al-Ubaidi MR (2004) Expression of cone-photoreceptor-specific antigens in a cell line derived from retinal tumors in transgenic mice. Investig Ophthalmol Vis Sci 45:764–768.

Tao X, Li N, Liu F, Hu Y, Liu J, Zhang YM (2018) In vitro examination of microglia-neuron crosstalk with BV2 cells, and primary cultures of glia and hypothalamic neurons. Heliyon 4:e00730.

Tappenden DM, Hwang HJ, Yang L, Thomas RS, Lapres JJ (2013) The aryl-hydrocarbon receptor protein interaction network (AHR-PIN) as identified by tandem affinity purification (TAP) and mass spectrometry. J Toxicol 2013:12.

Tay TL, Savage JC, Hui CW, Bisht K, Tremblay MÈ (2017) Microglia across the lifespan: from origin to function in brain development, plasticity and cognition. J Physiol 595:1929–1945.

Taylor DJ, Hobby AE, Binns AM, Crabb DP (2016) How does age-related macular degeneration affect real-world visual ability and quality of life? A systematic review. BMJ Open 6:e011504.

Thornton J, Edwards R, Mitchell P, Harrison RA, Buchan I, Kelly SP (2005) Smoking and age-related macular degeneration: A review of association. Eye 19:935–944.

Tisi A, Passacantando M, Ciancaglini M, Maccarone R (2019) Nanoceria neuroprotective effects in the light-damaged retina: A focus on retinal function and microglia activation. Exp Eye Res 188:107797.

Tomany SC, Wang JJ, Van Leeuwen R, Klein R, Mitchell P, Vingerling JR, Klein BEK, Smith W, De Jong PTVM (2004) Risk factors for incident age-related macular degeneration: Pooled findings from 3 continents. Ophthalmology 111:1280–1287.

Toomey CB, Johnson L V., Bowes Rickman C (2018) Complement factor H in AMD:

Bridging genetic associations and pathobiology. Prog Retin Eye Res 62:38–57.

Tsai CH, Lee Y, Li CH, Cheng YW, Kang JJ (2020) Down-regulation of aryl hydrocarbon receptor intensifies carcinogen-induced retinal lesion via SOCS3-STAT3 signaling. Cell Biol Toxicol 36:223–242.

Velagapudi R, El-Bakoush A, Olajide OA (2018) Activation of Nrf2 Pathway Contributes to Neuroprotection by the Dietary Flavonoid Tiliroside. Mol Neurobiol 55:8103–8123.

Walker DG, Lue LF (2013) Understanding the neurobiology of CD200 and the CD200 receptor: A therapeutic target for controlling inflammation in human brains? Future Neurol 8:321–332.

Wang M, Wong WT (2014) Microglia-Müller cell interactions in the retina. Adv Exp Med Biol 801:333–338.

Wang S, Cheng L, Liu Y, Wang J, Jiang W (2016a) Indole-3-Carbinol (I3C) and its Major Derivatives: Their Pharmacokinetics and Important Roles in Hepatic Protection. Curr Drug Metab 17:401–409.

Wang SK, Xue Y, Rana P, Hong CM, Cepko CL (2019) Soluble CX3CL1 gene therapy improves cone survival and function in mouse models of retinitis pigmentosa. Proc Natl Acad Sci USA 116:10140–10149.

Wang X, Zhao L, Zhang J, Fariss RN, Ma W, Kretschmer F, Wang M, Qian HH, Badea TC, Diamond JS, Gan WB, Roger JE, Wong WT (2016b) Requirement for microglia for the maintenance of synaptic function and integrity in the mature retina. J Neurosci 36:2827–2842.

Wässle H (2004) Parallel processing in the mammalian retina. Nat Rev Neurosci 5:747–757.

Weng JR, Tsai CH, Kulp SK, Chen CS (2008) Indole-3-carbinol as a chemopreventive and anti-cancer agent. Cancer Lett 262:153–163.

Wenzel A, Grimm C, Samardzija M, Remé CE (2005) Molecular mechanisms of light-induced photoreceptor apoptosis and neuroprotection for retinal degeneration. Prog Retin Eye Res 24:275–306.

Wheeler MA, Rothhammer V, Quintana FJ (2017) Control of immune-mediated pathology via the aryl hydrocarbon receptor. J Biol Chem 292:12383–12389.

Wheway G, Nazlamova L, Turner D, Cross S (2019) 661W Photoreceptor Cell Line as a Cell Model for Studying Retinal Ciliopathies. Front Genet 10:308.

Wiedemann J, Rashid K, Langmann T (2018) Resveratrol induces dynamic changes to the microglia transcriptome, inhibiting inflammatory pathways and protecting against microglia-mediated photoreceptor apoptosis. Biochem Biophys Res Commun 501:239–245.

Winans B, Nagari A, Chae M, Post CM, Ko C-I, Puga A, Kraus WL, Lawrence BP (2015) Linking the Aryl Hydrocarbon Receptor with Altered DNA Methylation Patterns and Developmentally Induced Aberrant Antiviral CD8 + T Cell Responses. J Immunol 194:4446–4457.

Woeller CF, Roztocil E, Hammond CL, Feldon SE, Phipps RP (2016) The Aryl Hydrocarbon Receptor and Its Ligands Inhibit Myofibroblast Formation and Activation: Implications for Thyroid Eye Disease. Am J Pathol 186:3189–3202.

Wolf A, Herb M, Schramm M, Langmann T (2020) The TSPO-NOX1 axis controls phagocyte-triggered pathological angiogenesis in the eye. Nat Commun 11:2709.

Wong WL, Su X, Li X, Cheung CMG, Klein R, Cheng CY, Wong TY (2014) Global prevalence of age-related macular degeneration and disease burden projection for 2020 and 2040: A systematic review and meta-analysis. Lancet Glob Heal 2:e106–e116.

Xu H, Chen M, Forrester J V (2009) Para-inflammation in the aging retina. Prog Retin Eye Res 28:348–368.

Yang I, Han SJ, Kaur G, Crane C, Parsa AT (2010) The role of microglia in central nervous system immunity and glioma immunology. J Clin Neurosci 17:6–10.

Yin J, Valin KL, Dixon ML, Leavenworth JW (2017) The Role of Microglia and Macrophages in CNS Homeostasis, Autoimmunity, and Cancer. J Immunol Res 2017.e5150678.

Zele AJ, Cao D (2015) Vision under mesopic and scotopic illumination. Front Psychol 5:1594.

Zeng HY, Green WR, Tso MOM (2008) Microglial activation in human diabetic retinopathy. Arch Ophthalmol 126:227–232.

Zhang S, Qin C, Safe SH (2003) Flavonoids as aryl hydrocarbon receptor

agonists/antagonists: Effects of structure and cell context. Environ Health Perspect 111:1877–1882.

Zhang Y, Zhao L, Wang X, Ma W, Lazere A, Qian HH, Zhang J, Abu-Asab M, Fariss RN, Roger JE, Wong WT (2018) Repopulating retinal microglia restore endogenous organization and function under CX3CL1-CX3CR1 regulation. Sci Adv 4:8492.

Zhao L, Zabel MK, Wang X, Ma W, Shah P, Fariss RN, Qian H, Parkhurst CN, Gan W, Wong WT (2015) Microglial phagocytosis of living photoreceptors contributes to inherited retinal degeneration. EMBO Mol Med 7:1179–1197.

Zhou Y, Li S, Huang L, Yang Y, Zhang L, Yang M, Liu W, Ramasamy K, Jiang Z, Sundaresan P, Zhu X, Yang Z (2018) A splicing mutation in aryl hydrocarbon receptor associated with retinitis pigmentosa. Hum Mol Genet 27:2563–2572.

Zhu J, Luo L, Tian L, Yin S, Ma X, Cheng S, Tang W, Yu J, Ma W, Zhou X, Fan X, Yang X, Yan J, Xu X, Lv C, Liang H (2018) Aryl hydrocarbon receptor promotes IL-10 expression in inflammatory macrophages through Src-STAT3 signaling pathway. Front Immunol 9:2033.

Zhu K, Meng Q, Zhang Z, Yi T, He Y, Zheng J, Lei W (2019) Aryl hydrocarbon receptor pathway: Role, regulation and intervention in atherosclerosis therapy (Review). Mol Med Rep 20:4763–4773.

7 Acknowledgments

Foremost, I would like to express my sincere gratitude to Prof. Dr. Thomas Langmann, Chair of Experimental Immunology of the Eye, for providing me this opportunity to complete my PhD in his laboratory. I sincerely thank him for his invaluable guidance, which contributed significantly to improve and complete my research. My deepest appreciations is to his patience and enthusiasm because he helped me with his immense knowledge. Thanks for being a very nice and a brilliant supervisor. You have a big contribution in my scientific career.

I also thank Prof. Dr. Elena Rugarli for being a second reviewer. Thank you very much for accepting my request to be a reviewer.

I would also like to thank my tutor PD. Dr. Benjamin Altenhein for his suggestions and discussions about my project and accepting my request for taking minutes during examination session. I also want to thank Prof. Dr. Mario Fabri for being my second tutor. I am also thankful to Prof. Dr. Stanilav Kopriva for chairing my PhD examination session.

I also want to thank my present laboratory colleagues as well as former lab members. It was nice to work with you all.

I would like to thank Dr. Isabell Witt, the scientific coordinator for Graduate school for helping me in project-related matters for completion of this project.

I want to special thank my family members, my mother who is always a big support for me throughout my life. My sister Guria and brother Naveed, they always helped me, strengthen me and motivated me to finish my goals. I am grateful to khala Samina for her support and encouragement. I also want to thank Sana and Kashfa for their suggestions. I would like to thank my love Tahera and my son Danyal for their care, support, and love.

Words cannot explain how highly grateful I am to all of you. Thanks once again from the core of my heart.

8 Erklärung

Ich versichere, dass ich die von mir vorgelegte Dissertation selbständig angefertigt, die benutzten Quellen und Hilfsmittel vollständig angegeben und die Stellen der Arbeit − einschließlich Tabellen, Karten und Abbildungen −, die anderen Werken im Wortlaut oder dem Sinn nach entnommen sind, in jedem Einzelfall als Entlehnung kenntlich gemacht habe; dass diese Dissertation noch keiner anderen Fakultät oder Universität zur Prüfung vorgelegen hat; dass sie − abgesehen von unten angegebenen Teilpublikationen − noch nicht veröffentlicht worden ist, sowie, dass ich eine solche Veröffentlichung vor Abschluss des Promotionsverfahrens nicht vornehmen werde. Die Bestimmungen der Promotionsordnung sind mir bekannt. Die von mir vorgelegte Dissertation ist von (Prof. Dr. Thomas Langmann) betreut worden.

Teilpublikationen:

Khan, A.S., Langmann, T. Indole-3-carbinol regulates microglia homeostasis and protects the retina from degeneration. *J Neuroinflammation* **17,** 327 (2020). https://doi.org/10.1186/s12974-020-01999-8

Köln, 02 November 2020 Amir Saeed Khan

9 Curriculum vitae

This page only appears on the printed version of the thesis.